AD-773 178

APPLICATIONS OF ACTIVE COOLING TO NOSE CONES

Victor Zakkay, et al

New York University

Prepared for:

Aerospace Research Laboratories

November 1973

AD-773 178

UNCLASSIFIED
Security Classification

DOCUMENT CONTROL DATA - R & D

(Security classification of title, body of abstract and indexing annotation must be entered when the overall report is classified)

1 ORIGINATING ACTIVITY *(Corporate author)*
New York University
School of Engineering and Science
University Heights, Bronx, New York 10453

2a. REPORT SECURITY CLASSIFICATION
Unclassified

2b. GROUP

3 REPORT TITLE

APPLICATIONS OF ACTIVE COOLING TO NOSE CONES

4 DESCRIPTIVE NOTES *(Type of report and inclusive dates)*
Scientific. Final.

5 AUTHOR(S) *(First name, middle initial, last name)*
Victor Zakkay
Chi Rong Wang

6 REPORT DATE	7a. TOTAL NO. OF PAGES	7b. NO. OF REFS
November 1973	120	23

8a. CONTRACT OR GRANT NO	9a. ORIGINATOR'S REPORT NUMBER(S)
F33615-72-C-1370	
b. PROJECT NO. 70650263	ARL 73-0143
c. DoD Element 61102F	9b. OTHER REPORT NO(S) *(Any other numbers that may be assigned this report)*
d. DoD Subelement 681307	

10 DISTRIBUTION STATEMENT
Approved for public release; distribution unlimited.

11 SUPPLEMENTARY NOTES	12. SPONSORING MILITARY ACTIVITY
TECH OTHER	Fluid Dynamics Research Laboratory Aerospace Research Laboratories (AFSC) Wright-Patterson AFB, Ohio 45433

13 ABSTRACT The use of film cooling for protecting a nose cone in a hypersonic Mach 6 freestream was investigated experimentally. Tests were performed in a Mach 6 wind tunnel with a contoured axisymmetric nozzle. Downstream and upstream tangential slot injections were applied to investigate the film cooling effectiveness on the surface of a nose cone Multiple tangential downstream slot injections were used to cool the surface of the blunt nose cone while tangential upstream slot injections were used for the surface cooling of a sharp nose cone. Air at a stagnation temperature of 530°R was used as an injectant. Surface distributions of the heat transfer rates and static pressures were measured for different injection mass flow rates. Results of the present downstream injection experiments have shown that a reduction in the effectiveness due to a decrease in the slot heights was significant when the boundary layer was thin at the injection slot. A 30% increase in the cooling length was obtained when multiple slot injection was employed, and an improvement in the film cooling effectiveness downstream from the injection slot was found. Comparison with the existing results of Mach 6 experiments shows that film cooling is more effective in high Mach number flows than in a low Mach number flow. Approximate theoretical results have shown that the film cooling effectiveness was predominated by the stagnation properties of the injectant. Experiments of the upstream slot injection indicated that film cooling was more effective in a high Reynolds number flow, and an increase in the step size of the forward facing step increased the effectiveness.

DD FORM 1 NOV 65 1473

UNCLASSIFIED
Security Classification

14 KEY WORDS	LINK A		LINK B		LINK C	
	ROLE	WT	ROLE	WT	ROLE	WT
film cooling						
hypersonic						
cones						
heat transfer						

☆U.S.Government Printing Office: 1973 — 758-429/287

NOTICES

When Government drawings, specifications, or other data are used for any purpose other than in connection with a definitely related Government procurement operation, the United States Government thereby incurs no responsibility nor any obligation whatsoever; and the fact that the Government may have formulated, furnished, or in any way supplied the said drawings, specifications, or other data, is not to be regarded by implication or otherwise as in any manner licensing the holder or any other person or corporation, or conveying any rights or permission to manufacture, use, or sell any patented invention that may in any way be related thereto.

Organizations or individuals receiving reports via Aerospace Research Laboratories automatic mailing lists should refer to the ARL number of the report received when corresponding about change of address or cancellation. Such changes should be directed to the specific laboratory originating the report. Do not return this copy; retain or destroy.

Reports are not stocked by the Aerospace Research Laboratories. Copies may be obtained from:

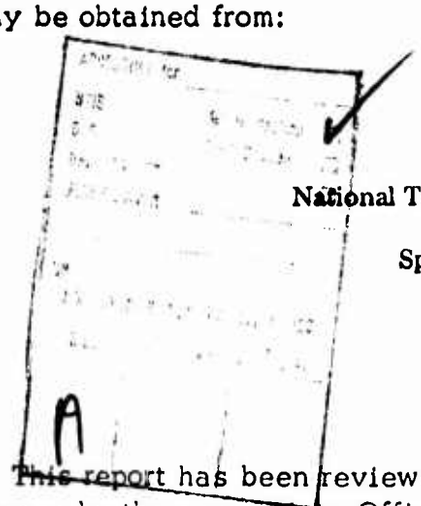

National Technical Information Services
Clearinghouse
Springfield, VA 22151

This report has been reviewed and cleared for open publication and public release by the appropriate Office of Information in accordance with AFR 190-12 and DODD 5230.0. There is no objection to unlimited distribution of this report to the public at large, or by DDC to the National Technical Information Service.

AIR FORCE/56780/4 December 1973 – 300

ARL 73-0143

APPLICATIONS OF ACTIVE COOLING TO NOSE CONES

VICTOR ZAKKAY
CHI RONG WANG

NEW YORK UNIVERSITY
UNIVERSITY HEIGHTS
BRONX, NEW YORK 10453

NOVEMBER 1973

CONTRACT NO. F-33615-72-C-1370
PROJECT NO. 7065

AEROSPACE RESEARCH LABORATORIES
AIR FORCE SYSTEMS COMMAND
UNITED STATES AIR FORCE
WRIGHT–PATTERSON AIR FORCE BASE, OHIO 45433

ic

FOREWORD

This final report was prepared by Dr. Victor Zakkay, Assistant Director of the Aerospace Laboratory and Professor of Aeronautics and Astronautics, and Chi Rong Wang, Research Assistant, New York University Aerospace Laboratory.

The report presents research carried out from November 22, 1971 to November 22, 1972 under Contract F33615-72-C-1370, "Applications of Active Cooling to Nose Cones," under Project No. 7065. This contract was technically monitored by Kenneth F. Stetson, Fluid Dynamics Facilities Research Laboratory, Aerospace Research Laboratories (AFSC), Wright-Patterson AF Base, Ohio.

ABSTRACT

The use of film cooling for protecting a nose cone in a hypersonic Mach 6 freestream was investigated experimentally. Tests were performed in a Mach 6 wind tunnel with a contoured axisymmetric nozzle. Downstream and upstream tangential slot injections were applied to investigate the film cooling effectiveness on the surface of a nose cone. Multiple tangential downstream slot injections were used to cool the surface of the blunt nose cone while tangential upstream slot injections were used for the surface cooling of a sharp nose cone. Air at a stagnation temperature of 530°R was used as an injectant. Surface distributions of the heat transfer rates and static pressures were measured for different injection mass flow rates. Different tunnel stagnation conditions were also used to investigate the freestream Reynolds number effect on the film cooling effectiveness of upstream injection. The local adiabatic wall temperature was not measured directly. Theories of turbulent boundary layer and wall jet were used to obtain the adiabatic wall temperature from the heat transfer measurements. Correlations of the present experimental film cooling effectiveness were found. Results from the approximate theoretical analysis were also compared with those from the experiments. Results of the present downstream injection experiments have shown that a reduction in the effectiveness due to a decrease in the slot heights was significant when the boundary layer was thin at the injection slot. A 30% increase in the cooling length was obtained when multiple slot injection was employed, and an improvement in the film cooling effectiveness downstream from the injection slot was found. Comparison with the existing results of Mach 6 experiments shows that film cooling is more effective in high Mach number flows than in a low Mach number flow. Approximate theoretical results have shown that the film cooling effectiveness was predominated by the stagnation properties of the injectant. Experiments of the upstream slot injection indicated that film cooling was more effective in a high Reynolds number flow, and an increase in the step size of the forward facing step increased the effectiveness.

TABLE OF CONTENTS

LIST OF ILLUSTRATIONS

LIST OF ILLUSTRATIONS (Cont'd)

LIST OF ILLUSTRATIONS (Cont'd)

LIST OF ILLUSTRATIONS (Cont'd)

LIST OF ILLUSTRATIONS (Cont'd)

LIST OF ILLUSTRATIONS (Cont'd)

LIST OF ILLUSTRATIONS (Cont'd)

NOMENCLATURE

a	sonic speed
C_f	skin friction coefficient
C_p	specific heat at constant pressure
H	stagnation enthalpy
h	local heat transfer coefficient
K	coefficient of thermal conductivity
k	proportional constant used in the modified Oseen approximation
ℓ	stepsize of the forward facing step of the upstream injection slot
M	Mach number
N_{Nu}	local Nusselt number based on reference enthalpy state, $Q_w C_{p,ref} x_o / K_{ref} (H_{aw,o} - H_w)$
N_R	local Reynolds number based on reference enthalpy state, $\rho_{ref} u_e x_o / \mu_{ref}$
P	dimensionless quantity, $(M_e / (1+(\frac{\gamma-1}{2}) M_e^2))^4$
Pr	Prandtl number
p	pressure
Q	local heat transfer rate at the wall
Re	Reynolds number
s	slot height
St	Stanton number
T	temperature
u	velocity component parallel to the body surface
X	transform coordinate along the body surface, $(\int_o^{x_o} P\, dx)/P$
x	distance along the conical body surface from the injection slot

x_o distance along the conical body surface from cone tip

x_1 distance between slots in the two slot downstream injection, or the distance between the first slot and last slot in the three slot injection

x_2 distance between the second and third slots in the three slot downstream injection

α angle of attack

γ ratio of specific heats, 1.4

δ local boundary layer thickness

ϵ film cooling effectiveness, $(T_{aw,i} - T_{o\infty})/(T_{oj} - T_{o\infty})$

ζ transformed coordinate in the x_o direction $\int_o^{\bar{x}} \bar{\rho}_e \bar{\mu}_e \bar{u}_e \bar{r}^2 \, d\bar{x}$

θ local boundary layer momentum thickness

λ summation of the injection mass flow rates

λ_m upstream injection mass flow rate, $\rho_j u_j / \rho_{\infty 2} u_{\infty 2}$

$\lambda_{i,m}$ downstream injection mass flow rate, $\rho_j u_j / \rho_{\infty 1} u_{\infty 1}$

$\lambda_{i,me}$ local downstream injection mass flow rate, $\rho_j u_j / \rho_e u_e$

μ absolute viscosity

ν kinematic viscosity

ξ transformed coordinate in the x_o direction $\int_o^{\zeta} (\rho \mu u / \rho_e \mu_e u_e) \, d\zeta$

ρ density

ψ transformed coordinate normal to the body surface, $\bar{\rho}_e \bar{u}_e \bar{r} \int_o^{\bar{y}} (\frac{\rho u}{\rho_e u_e}) \, d\bar{y}$

φ_1 parameter represents first slot injection, $x_1/s_1 \; \lambda_{1,me}^{0.8}$

φ_2 parameter represents second slot injection, $x_2/s_2 \; \lambda_{2,me}^{0.8}$

Subscripts

oe	main stream stagnation condition after normal or oblique shock
o_∞	free stream stagnation condition
oj	stagnation condition of the injectant
aw,o	adiabatic wall condition without injection
aw,i	adiabatic wall condition with injection
ej	the edge condition of the boundary layer of the injectant
ref	condition evaluated at the reference temperature
e	boundary layer edge condition of the mixing flow
i=1,2,3	number of the downstream injection slot
j	condition at the exit of injection slot
n	condition downstream of the nth injection slot
s	static condition
w	wall condition
∞_1	free stream condition before shock
∞_2	main stream local condition after shock
-	dimensionless quantity

SECTION I

INTRODUCTION

Various possible surface heating protection schemes have been proposed to maintain a surface structure capable of withstanding the large heating loads at high velocity. One technique which provided a promising utilization is surface film cooling. In general, film cooling involves the introduction of a coolant fluid through discrete slots, positioned along the surface to be cooled, to insulate thermally the surface from the hot stream.

Experimental investigations of the film cooling due to tangential slot injection, employing low-speed subsonic flow in both primary and secondary streams, can be found in Refs. 1 to 5. The distribution of adiabatic wall temperature downstream from a discrete tangential slot was measured, and the film cooling effectiveness, in terms of dimensionless adiabatic wall temperature, was computed. Correlations of the film cooling effectiveness were also found. Existing empirical correlations of film cooling effectiveness due to single downstream tangential slot injection are reviewed in Ref. 6. Due to the lack of data of film cooling to a high Mach number flow, results extrapolated from low Mach number flow data indicate an unfavorable effect. Recently, experiments of film cooling effectiveness to a Mach 6 hypersonic turbulent flow,[7] using gaseous helium, hydrogen, argon, and air, indicated that a substantial gain in film cooling effectiveness was obtained, and that extrapolation of low speed data was erroneous. In addition, it indicated that film cooling resulted in skin friction reduction of up to 40%. By measuring the local adiabatic wall temperature,[8] experimental results indicated that the film cooling effectiveness could be correlated in the form of

$$\epsilon = (T_{aw,i} - T_{\infty})/(T_{oj} - T_{\infty}) = 6.1\ (x/s\ \lambda_{i,me}^{0.8})^{-0.39}$$

for single tangential slot injection to a Mach 6 free stream.

The same correlation parameter was used [9] to correlate experimental data of downstream slot injection, except for a difference in the power of decay. These investigations indicated a substantial gain over film cooling at low speeds. Recently, the effect of adverse pressure gradient on film cooling due to tangential slot injection was investigated experimentally [10]. Upon comparison with available data of zero pressure gradient, it was concluded that better effectiveness could be obtained for the same injection mass flow rate when an adverse pressure gradient was present.

Film cooling due to multiple slot configuration in a two-dimensional case can be found in Ref. 5. An increase in effectiveness for succeeding slot was found significant. A model, with three downstream tangential slots, was used to investigate the film cooling effectiveness to Mach 6 hypersonic turbulent flow, [11] Based on some analogies with jet mixing phenomena, turbulent slot injection was analyzed. Results from experiments and theory were also compared.

An alternative scheme of film cooling employing upstream slot injection to a wedge in Mach 6 flow has been performed [12]. Coolant was injected with a two-dimensional tangential injection slot, located at the base of the wedge with a forward facing step. Boundary layer theory was used to predict the experiments. Correlation of film cooling effectiveness was obtained from a limited amount of experimental data.

In the present work, experiments of the downstream and upstream injection film cooling to blunt and sharp nose cones are described. Tests were performed in a Mach 6 wind tunnel. Film cooling effectiveness of downstream injection with single and multiple slot injections was determined. Correlations of the film cooling effectiveness were found. Analytical film cooling

effectiveness, obtained from the approximate solution to the boundary layer energy equation, was compared with experiments. Upstream injection film cooling effectiveness, due to tangential slot with a forward-facing step, was also determined from experiments. Their correlations were found. Different slots were used in the tests.

For the downstream slot injection, stagnation temperature and stagnation pressure of the tunnel were approximately $900^{\circ}R$ and 1900 psia. Two different tunnel stagnation pressures, 1000 psia and 1900 psia, were used for the upstream injection experiments. Air at a stagnation temperature of $530^{\circ}R$ was used as injectant for all tests. Distributions of wall heat transfer rates and of static pressure were measured with various injection mass flow rates. Experimental film cooling effectiveness, $\epsilon = (T_{aw,i} - T_{o\infty})/(T_{oj} - T_{o\infty})$, was determined from these measurements. The local adiabatic wall temperature was not measured directly. It was inferred from the heat transfer measurements with the aid of the theories of turbulent boundary layer and wall jet.

A large amount of data was obtained from the experiments. For the downstream slot injection, the effects of the dimension of the injection slot, the boundary layer thickness at the injection slot, and angle of attack on the surface film cooling effectiveness were discussed. The effects of single and multiple slot downstream injections on film cooling effectiveness were compared. Approximate analytical and experimental results were also compared at zero angle of attack. From the results of the upstream slot injection experiments, effects of the free stream Reynolds number, size of the injection slot to the heat transfer rates, wall static pressure, and the film cooling effectiveness were investigated.

SECTION II

EXPERIMENTS

1. Testing Models

Two stainless steel models were designed for the present experiments. A blunt nose cone was used in the downstream film cooling tests, while a sharp nose cone was used in the upstream film cooling experiments.

a. Downstream Injection Model

A schematic drawing of the blunt nose cone is shown in Fig. 1. The cone half angle was 7.5°. The nose radius was 0.4 inch and base diameter was approximately 5 inches. Based on the correlation for cooling lengths given in Ref. 7, three downstream axial symmetric tangential injection slots were located along the cone surface at x_o = 1.2 inches, 5.6 inches, and 10.8 inches respectively. These slots were made separately and threaded onto the main frame of the conical body. They could be rotated around the centerline of the blunt nose cone so that different injection slot heights between 0.0 and 0.025 inch could be obtained. Thin steel shimstock was used and special efforts were taken to smooth out the body surface when any slot was closed. Coolant air was supplied independently. Injection mass flow rates were measured with three venturi tubes.

Chromel-alumel thermocouples, attached to the steel shimstock 0.01 inch in thickness, were located along the plane of symmetry for heat transfer measurements. Pressure taps, 0.02 inch in diameter, drilled normal to the surface, were used to measure the wall static pressure.

b. Upstream Injection Model

The model consisted of a sharp nose cone and an axial symmetric upstream injection slot with a forward facing step, Fig. 2. The outside surfaces near the base of the cone and the inner surface of the forward facing step were used to form the axial symmetric upstream injection slot. The nose radius

was 0.031 inch with a half angle of 7.5°. The wall thickness was 0.020 inch. The forward facing step was exchangeable to give different injection slot heights. Rings could be fitted on the outer surface of the step to increase the step size, ℓ . A venturi tube, 0.125 inch in diameter, was used to measure the injection mass flow rates. Chromel-alumel thermocouples and pressure taps, 0.02 inch in diameter, drilled normal to the surface, were also used to measure the distributions of the heat transfer rates and the wall static pressures.

2. Testing Facility

All tests were performed in the Aerospace Laboratory in the New York university blowdown type tunnel equipped with a Mach 6 axisymmetric contoured nozzle. The facility consisted of a 2200 psia air supply, a regenerative type heater capable of delivering 900°R air with a mass flux of up to 60 lbs/sec. The test section was 1 feet in diameter with a uniform flow 9 inches in diameter and 3 feet in length. The tunnel was capable of supplying nominally constant stagnation temperature flow up to 40 seconds of running time. The temperature time record from the response of the thermocouples and pressure readings from the pressure taps were recorded with a visicorder. Details of the equipment can be found in Ref. 13. For the presently described tests, models were mounted on a moveable support in line with the center of the contoured nozzle.

3 Testing Conditions

Downstream Injection

The blunt nose cone was used for the experiments of downstream injection. The stagnation temperature, $T_{o\infty}$, and stagnation pressure, $p_{o\infty}$, of the wind tunnel were approximately 900°R and 1900 psia. These resulted in a Mach 5.85 freestream with a Reynolds number, Re_{∞}, 3.8×10^7 per foot in the test section.

Two different injection slot heights, s = 0.015 inch and 0.025 inch, were used. Air at a stagnation temperature of 530°R was used as the injectant. Measurements were taken for the following different injection slot arrangements with the injection mass rates indicated:

(1) Single Slot injection

(a) First Slot Injection, $0.49 \leq \lambda_{1,m} \leq 1.75$

(b) Second Slot Injection, $0.22 \leq \lambda_{2,m} \leq 1.38$

(c) Third Slot Injection, $0.16 \leq \lambda_{3,m} \leq 1.89$

(2) Combinations of Two-Slot Injections

(a) Combinations of 1st and 2nd slot injection

$$0.224 \leq \lambda_{2,m} \leq 1.34$$

$$100 \leq \varphi_1 \leq 320$$

(b) Combinations of 1st and 3rd slot injection

$$0.302 \leq \lambda_{3,m} \leq 1.07$$

$$260 \leq \varphi_1 \leq 730$$

(c) Combinations of three slot injection

$$0.31 \leq \lambda_{3,m} \leq 1.85$$

$$200 \leq \varphi_1 \leq 580$$

$$200 \leq \varphi_2 \leq 590$$

A major portion of the present tests were concentrated on the case when the model was at zero angle of attack. Some tests were done to take the measurements on the windward and leeward sides when the model was at an 8°

angle of attack. Additional tests were performed to measure the distributions of surface heat transfer and static pressure without slot injection.

Upstream Injection

The sharp nose cone was used for the experiments of surface film cooling due to upstream slot injection. Tests were also performed in a Mach 5.85 freestream. The injection slot height, s, was 0.03 inch. Two step sizes, ℓ = 0.2 inch, and 0.36 inch were used. Tests were conducted with a freestream stagnation temperature, $T_{o\infty}$ = 900°R, but with two different stagnation pressures, $p_{o\infty}$ = 1900 psia, and 1000 psia. Two corresponding freestream Reynolds numbers, Re_∞, 3.8×10^7 per foot, and 1.9×10^7 per foot, were obtained. Air at a stagnation temperature of 530°R was injected tangentially in the upstream direction. Measurements were taken for the following injection conditions at zero andle of attack:

(1) s = 0.03 inches, ℓ = 0.36 inches, $p_{o\infty}$ = 1900 psia

$0.0 \leq \lambda_m \leq 1.10$

(2) s = 0.03 inches, ℓ = 0.36 inches, $p_{o\infty}$ = 1000 psia

$0.0 \leq \lambda_m \leq 0.98$

(3) s = 0.03 inches, ℓ = 0.20 inches, $p_{o\infty}$ = 1900 psia

$0.0 \leq \lambda_m \leq 0.72$

4. Results of Experiments

The local thin-skin technique[7] was used to evaluate the heat transfer rate from the slope of the temperature time record of the thermocouples on the model. Surface pressure and the injection mass flow rates were measured with the pressure taps and the venturi tubes. Thermocouples, pressure taps, and venturi

tubes were calibrated before all tests. Experimental results of the downstream injection at zero angle of attack are presented in Figs. 3 to 23. Results at an 8° angle of attack are shown in Figs. 24 to 30. Results of the upstream slot injection are shown in Figs. 31 to 36.

SECTION III

FILM COOLING EFFECTIVENESS

In the investigation of surface film cooling, the effectiveness, defined as $\epsilon = (T_{aw,i} - T_o)/(T_{oj} - T_o)$, was used to estimate the film cooling efficiency. In previous investigations[6], the local adiabatic wall temperature was measured directly. However, in recent investigations[7,8,12], the local adiabatic wall temperature was inferred from the transient heat transfer measurements, and the corresponding film cooling effectiveness was obtained. This technique has been found satisfactory[9]. The same method was used here to obtain the local adiabatic wall temperature. Reynolds analogy of the turbulent boundary layer was used for the downstream slot injection at zero angle of attack. For the case of an 8° angle of attack, approximate estimations of the film cooling effectiveness were made with the assumption that the local heat transfer coefficient was the same with and without injection. The wall jet theory[14,15] was applied to compute the local adiabatic wall temperature for the upstream slot injection experiments.

1. Downstream Injection at Zero Angle of Attack

a. Experimental Approach

In order to insure that turbulent boundary layers developed along the body surface, existing theory[16] was used to investigate the experimental measurements for the case of zero injection. Neglecting the effect of entropy swallowing across the detached shock caused by the bluntness of the blunt nose cone, a modified Newtonian approximation was used to estimate the edge conditions of the boundary layer along the nose part. The boundary layer thickness at the location of the first injection slot was obtained with the following equation given in Ref. 17.

$$\delta = 0.37 \times R_{ex}^{-0.2}$$

where $Re_x = \rho_e u_e x / \mu_e$, $x = \left(\int_o^{xo} P dx'\right)/P$, with $P = \left(Me/\left(1+\frac{\gamma-1}{2} Me^2\right)\right)^4$.

The corresponding boundary layer momentum thickness was estimated by assuming $\theta/\delta = 0.065$[18]. This momentum thickness, $\theta = 0.0015$ inch, was used as an input of an existing numerical program to compute the theoretical surface heat transfer rates[16], without the effect of injectant. Theoretical results were compared with the measurements in Figs. 37 and 38. In the investigation[19], the flat plate reference enthalpy method was found to give quite accurate predictions of fully developed turbulent heat transfer rates. The basic formula for the relation between Nusselt and Reynolds number of a turbulent flow was given as:

$$N_{Nu} = 0.030\ Pr^{1/3}\ (N_R)^{4/5}$$

This formula was used to verify the present experiments and the results are shown in Fig. 39. From the comparisons between these existing theories and experiments, it could be concluded that turbulent flow was established along the body surface of the nose cone.

For these tests of downstream slot injection with large injection mass flow rates it was assumed that an inner turbulent boundary layer, dominated by the properties of the injectant, originated at the injection slot. The local skin friction was determined from the development of this turbulent boundary layer. For a cone at zero angle of attack, the surface skin friction factor, C_f, has been found[16], to be

$$C_f = 0.102\ (Me_j\ a_{oj}\ x/\nu_{oj})^{-0.22}\ (T_{ej}/\ T_{ref})^{0.571}\ (T_{oj}/T_{ej})^{0.452}$$

and the Stanton number, St, was also given as

$$St = 0.051\ C_f\ Pr^{-2/3}$$

where the reference temperature, T_{ref}, was found from

$$T_{ref}/T_{ej} = 0.5\ (T_w/T_{ej} + 1) + 0.22\ (T_{aw,i}/Te_j - 1)$$

and was a function of the unknown adiabatic wall temperature, $T_{aw,i}$, when coc ant was injected.

The effect of the external flow on the film cooling was through the static pressure which was imposed on the inner layer. It has been found from these experiments that the wall pressure distribution was independent of the presence of the injectant. The local Mach number M_{ej} external to the inner layer, was determined from the wall static pressure, p_s, and the stagnation pressure of the injectant, p_{oj}, with the isentropic relations. The local heat transfer rates. Q , was obtained by

$$Q = (St)\ \rho_{ej}\ u_{ej}\ C_p\ (T_{aw,i} - T_w)$$

Numerically, trial and error was used to obtain the local adiabatic wall temperature which gave a heat transfer rate within 95% of the experimental value. This adiabatic wall temperature was used to define the experimental film cooling effectiveness of the downstream slot injection at zero angle of attack.

b. Analytical Approach

Experimental and theoretical investigations of multiple slot downstream film cooling on a cylindrical axialsymmetric body can be found in Ref. 11. This theoretical analysis was extended to predict present experimental effectiveness.

Consider the boundary layer energy equation, written in terms of the dimensionless stagnation enthalpy, for constant C_p and unit Prandtl number. Introducing the Von Mises transformation[20] one simplified the boundary layer energy equatior to the following form:

$$\frac{\partial}{\partial \zeta} \bar{H} = \frac{\partial}{\partial \psi} \left[\frac{\rho \mu u}{\rho_e \mu_e u_e} \frac{\partial \bar{H}}{\partial \psi} \right] \tag{1}$$

with $\bar{H} = H/H_e$,

$$\zeta = \int_o^{\ddot{x}} \bar{\rho}_e \, \bar{\mu}_e \, \bar{u}_e \, \bar{r}^2 \, dx'$$

$$\psi = \bar{\rho}_e \, \bar{u}_e \, \bar{r} \int_o^{\dot{y}} \left(\frac{\rho u}{\rho_e u_e} \right) dy'$$

The dimensionless quantities $\bar{\rho}_e$, $\bar{u}_e$, $\bar{\mu}_e$ and $\bar{r}$ are defined by

$$\bar{\rho}_e = \rho_e/\rho_\infty, \; \bar{u}_e = u_e/u_\infty, \; \bar{r} = r/s, \text{ and } \bar{\mu}_e = \mu_e/\rho_\infty \, u_\infty s$$

Employing the modified Oseen approximation in the form

$$\rho \, \mu \, u = k \, \rho_{ref} \, \mu_{ref} \, u_{ref}$$

with k as a proportional constant,

let $\xi = \int_o^{\zeta} \left(\frac{\rho \mu u}{\rho_e \mu_e u_e} \right) d\zeta = \int_o^{\zeta} f(\zeta) \, d\zeta$.

Equation (1) becomes

$$\frac{\partial \bar{H}}{\partial \xi} = \frac{\partial^2 \bar{H}}{\partial \psi^2} \tag{2}$$

subjected to the following initial and boundary conditions:

$$\begin{aligned} &\text{at } \xi = 0, && \bar{H}(\psi) = \bar{H}_o, \text{ initial} \\ &\text{at } \psi = 0, && \left(\frac{\partial \bar{H}}{\partial \psi}\right)_{(\xi, o)} = 0 \\ &\text{at } \psi = \infty, && \bar{H}(\xi, \psi) = \bar{H}_{oe} \end{aligned} \tag{3}$$

Approximate and exact solutions to the governing equation (Eq. (2)), with the initial and boundary conditions of Eq. (3) are described in Ref. 11. However, approximate solutions predicted satisfactorily the two-dimensional experimental results, and will be used in the present work.

In terms of the Von Mises coordinate, we define the edge of the slot where $y = s$ as $\psi_n = \psi_{jn}$. Then the equivalent initial profile can be described by

$$\bar{H}_o = \bar{H}_{oj}, \qquad \text{for } 0 < \psi_n < \psi_{jn}$$

$$\bar{H}_{o\,av,n-1} \qquad \text{for } \psi_{jn} < \psi_n < \psi_{av,n-1} + \psi_{jn}$$

$$\bar{H}_{oe} \qquad \text{for } \psi_{av,n-1} + \psi_{jn} < \psi_n$$

where we have subscripted the independent variable ψ so that the correspondence to the particular slot is apparent. In any new setup, $\psi_{av,n-1}$ is defined as the value of ψ_{n-1} where $\bar{H}_{o,n-1} / \bar{H}_{o,e} = 0.99$ and $\bar{H}_{o\,av,n-1}$ is defined by

$$\bar{H}_{oav,n-1} = (1/\psi_{av,n-1}) \int_0^{\psi_{av,n-1}} \bar{H}_o \, d\psi_{n-1}$$

when the integral is taken at $\xi = \xi_n$ for the (n-1) slot. The solution to the governing equation (Eq (2)) can be found in Ref. 12. The results are:

$$(\bar{H}_{on} - \bar{H}_{o\infty})/(\bar{H}_{oj} - \bar{H}_{o\infty}) = (T_{on} - T_{o\infty})/(T_{oj} - T_{o\infty})$$

$$= 1/2 \left(\frac{T_{oj} - T_{oav,n-1}}{T_{oj} - T_{o\infty}}\right) \left[\mathrm{Erf} \left(\frac{\psi_n + \psi_{jn}}{2\sqrt{\xi}}\right) - \mathrm{Erf} \left(\frac{\psi_n - \psi_{jn}}{2\sqrt{\xi}}\right) \right]$$

$$+ 1/2 \left(\frac{T_{oav,n-1} - T_{o\infty}}{T_{oj} - T_{o\infty}}\right) \left[\mathrm{Erf} \left(\frac{\psi_n + \hat{\psi}_n}{2\sqrt{\xi}}\right) - \mathrm{Erf} \left(\frac{\psi_n - \hat{\psi}_n}{2\sqrt{\xi}}\right) \right] \qquad (4)$$

with $\hat{\psi}_n = \psi_{\partial n} + \psi_{av,n-1}$.

The film cooling effectiveness, ϵ_n, for $\xi \geq \xi_n$, can be obtained by setting $\psi_n = 0$ in Eq. (4),

$$\epsilon_n = (T_{aw,n} - T_{o\infty})/(T_{oj} - T_{o\infty})$$

$$= \left(\frac{T_{oj} - T_{o,av,n-1}}{T_{oj} - T_{o\infty}}\right) \text{Erf}\left(\frac{\psi_{jn}}{2\sqrt{\xi}}\right) + \left(\frac{T_{oav,n-1} - T_{o\infty}}{T_{oj} - T_{o\infty}}\right)$$

$$\text{Erf}\left(\frac{\psi_{jn} + \psi_{av,n-1}}{2\sqrt{\xi}}\right) \tag{5}$$

For the present case of thin boundary layer thickness, the effect of $\psi_{av,n-1}$ was neglected, and the film cooling effectiveness was found to be

$$\epsilon_n = \text{Erf}\left(\frac{\psi_{jn}}{2\sqrt{\xi}}\right) \tag{6}$$

The reference properties were the main stream fluid properties evaluated at the reference temperature defined by

$$T_{ref} = 0.5\ (T_w + T_e) + 0.22\ \ (T_{o\infty} - T_e)$$

The temperature, T_e, of the freestream was obtained by neglecting the effect of the entropy swallowing across the detached shock wave. Total pressure was assumed constant at the edge of the boundary layer.

In the evaluation of the Von Mises coordinate, ψ_{jn}, at the edge of the injection slot, assumption of the profiles of the coolant properties should be made. Details in this respect can be found in Ref. 11. In the present investigations, a linear variation of $\rho_j u_j$ at the slot exit was assumed, i.e.,

$(\rho_j u_j)/(\rho_j n_j)_{y=s} = y/s$. The injectant properties, ρ_j and u_j at y = s, were evaluated from the injectant stagnation conditions with the assumption that the coolant air was injected at sonic velocity, i.e. $M_j = 1.0$.

2. Downstream Injection at An Angle of Attack

In these tests, the blunt nose cone was set at an 8° angle of attack. An appropriate estimation of the effectiveness of the surface film cooling along the plane of symmetry on the windward side and leeward side was considered. The following assumptions were made:

A. Due to the existence of the cross flow, the effect of the film coolant on the local heat transfer coefficient, h, was insignificant. The local heat transfer rate was related to the local adiabatic wall temperature by

$$Q_o = h\ (T_{aw,o} - T_w), \quad \lambda_{i,m} = 0 \tag{7}$$

$$Q_i = h\ (T_{aw,i} - T_w), \quad \lambda_{i,m} > 0 \tag{8}$$

B. The local adiabatic wall temperature with zero injection, $T_{aw,o}$, was given by

$$T_{aw,o} = T_e \left(1 + \frac{\gamma-1}{2} M_e^2 \times 0.9 \right)$$

where a recovery factor, 0.9, was assumed.

C. The effect of entropy swallowing across the detached shock was neglected. Isentropic relations were valid for the estimation of the free stream conditions with constant stagnation pressure after a normal shock in $M_\infty = 5.85$ freestream.

From Eq. 7, the local heat transfer coefficient can be found with the aid of the heat transfer measurements with zero injection effect. Using this local heat transfer coefficient, we computed the local adiabatic wall temperature with

injection, $T_{aw,i}$, from the corresponding measured heat transfer rate according to Eq (8). This adiabatic wall temperature was used to evaluate the local film cooling effectiveness at an angle of attack.

3. Upstream Injection

Experimental and theoretical investigations of single upstream slot injection film cooling on the surface of the wedge in a Mach 6 freestream can be found in Ref. 12. It was concluded that the turbulent boundary layer was separated due to the presence of the forward facing step. A dead air region was created near the forward facing step. However, turbulent boundary layer analysis was assumed valid and Reynolds analogy was used to determine the local adiabatic wall temperature from the heat transfer measurements at various injection mass flow rates. Corresponding film cooling effectiveness due to the upstream slot injection was computed. Limited data were used to define a correlation of the film cooling effectiveness.

A different approach was used to estimate the local adiabatic wall temperature from the heat transfer rate in the present studies. It was assumed that the boundary layer along the conical surface was separated due to the presence of the forward facing step. A dead air region was created around most part of the conical body. A flowfield similar to the wall jet existed when the coolant air was injected.

For the case of cylindrical wall jets, heat transfer rates and velocity profile survey were presented in Ref. 14. Experimental results were also correlated. Velocity and temperature profiles in plane wall jets, can be found in Ref. 15. Colburn analogy was used to relate the local heat transfer rate and skin friction coefficient. The following relation is also given in

Ref. 15,

$$h/\rho u_j C_p = 0.184 \, (x/s)^{-0.60} \left(\frac{u_j s}{\nu} \right)^{-0.25} \tag{9}$$

with $h = Q/(T_{aw,i} - T_w)$

It has been found [14] that under similar conditions the Stanton number values for a cylindrical wall jet are as much as 1.7 times that of a plane wall jet. Therefore, for a cylindrical wall jet, Eq. (9) becomes

$$h/\rho u_j C_p = 0.313 \, (x/s)^{-0.60} \left(\frac{u_j s}{\nu} \right)^{-0.25} \tag{10}$$

Equations (9) and (10), were used to evaluate the coefficient of heat transfer h, for the present upstream injection experiments. With the aid of the measured heat transfer rate, the local adiabatic wall temperature, $T_{aw,i}$, at different upstream injection mass flow rates, was computed. The corresponding experimental film cooling effectiveness, defined as $\epsilon = (T_{aw,i} - T_{o\infty})/(T_{oj} - T_{o\infty})$, was found.

SECTION IV

CORRELATIONS OF EXPERIMENTAL FILM COOLING EFFECTIVENESS

Studies of the film cooling effectiveness correlation have been a major consideration in the single slot film cooling investigations. For downstream injection theoretical correlations derived from different boundary layer models of surface film cooling have been reviewed in Ref. 6. Film cooling effectiveness of a single downstream tangential slot injection to a Mach 6 high speed mainstream is presented in Refs. 7 and 8. Simple correlation of the effectiveness, in terms of the geometric parameter x/s, and the injection mass flow rate, $\lambda_{me} = \rho_j u_j / \rho_e u_e$, was obtained. The same correlation parameters were also used in Ref. 9. Satisfactory correlations were obtained. For upstream slot injection film cooling[12], limited amounts of experimental data were used to obtain a correlation for surface film cooling in a two-dimensional hypersonic flow.

In the present work, the parameter, x/s, and the injection mass flow rates $\lambda_{i,me}$, and λ_m were used to correlate the film cooling effectiveness of the downstream and upstream slot injection. Results were summed up as follows:

1. Downstream Injection at Zero Angle of Attack

   a. Single Slot Injection

Experimental film cooling effectiveness due to single slot downstream injection are plotted in terms of the correlation parameters in Figs. 40 to 42. Correlation of the film cooling effectiveness was obtained for each case and they are given as follows:

(1) First Slot Injection (Fig. 40)

$$\eta = 4.01 \, (x/s_1 \, \lambda_{1,me}^{0.8})^{-0.384} \quad \text{for } s_1 = 0.015 \text{ in.}$$

$$\eta = 3.90 \, (x/s_1 \, \lambda_{1,me}^{0.8})^{-0.364} \quad \text{for } s_1 = 0.025 \text{ in.}$$

(2) Second Slot Injection (Fig. 41)

$$\mathfrak{e} = 4.62\ (x/s_2\ \lambda_{2,me}^{0.8})^{-0.374}, \quad \text{for } s_2 = 0.015 \text{ in}$$

$$\mathfrak{e} = 4.25\ (x/s_2\ \lambda_{2,me}^{0.8})^{-0.370}, \quad \text{for } s_2 = 0.025 \text{ in}$$

(3) Third Slot Injection (Fig. 42)

$$\mathfrak{e} = 2.12\ (x/s_3\ \lambda_{3,me}^{0.8})^{-0.222}, \quad \text{for } s_3 = 0.015 \text{ in}$$

$$\mathfrak{e} = 2.68\ (x/s_3\ \lambda_{3,me}^{0.8})^{-0.279}, \quad \text{for } s_3 = 0.025 \text{ in}$$

b. Combination of Two Slot Injection

The film cooling effectiveness, at a distance x downstream from the 2nd injection slot, was correlated in terms of the dimensionless distance parameter, x/s_i, and the injection mass flow rate, $\lambda_{i,me}$, of the 2nd slot. A parameter, $\phi_1 = x_1/s_1\ \lambda_{1,me}^{0.8}$, was used to represent the injection of the preceding slot.

(1) Simultaneous Injection of the First and Secont Slots

From the results of experiments, Fig. 43, two correlations were obtained for two different ranges of the injection mass flow rates of the preceding injection slot. These correlations are:

$$\mathfrak{e} = 3.15\ (x/s_2\ \lambda_{2,me}^{0.8})^{-0.277}, \quad s_2 = 0.015 \text{ in and } \varphi_1 > 200$$

$$\mathfrak{e} = 3.15\ (x/s_2\ \lambda_{2,me}^{0.8})^{-0.277}, \quad s_2 = 0.015 \text{ in}, \ \varphi_1 < 200 \text{ and } x/s_2\ \lambda_{2,me}^{0.8} < 150$$

$$\mathfrak{e} = 7.50\ (x/s_2\ \lambda_{2,me}^{0.8})^{-0.45}, \quad s_2 = 0.015 \text{ in}, \ \varphi_1 < 200 \text{ and } x/s_2\ \lambda_{2,me}^{0.8} > 150$$

(2) Simultaneous Injection of the First and Third Slots

In this case, one correlation was obtained from the present experiments, Fig. 44, The correlation was

$$\epsilon = 2.73\ (x/s_3\ \lambda_{3,me}^{0.8})^{-0.278},\quad s_3 = 0.015 \text{ in, and } \varphi_1 > 250$$

c. Three Slot Injection

Simple correlation was obtained for the film cooling effectiveness downstream from the third injection slot, Fig. 45. Two parameters, $\varphi_1 = x_1/s_1\ \lambda_{1,me}^{0.8}$ and $\varphi = x_2/s_2\ \lambda_{2,me}^{0.8}$, were used to represent the injection of the two preceding slots. Correlations were found to be

$$\epsilon = 2.45\ (x/s_3\ \lambda_{3,me}^{0.8})^{-0.242},\quad \text{for } s_1 = s_2 = s_3 = 0.015 \text{ in.}$$

with $\varphi_1 > 200$ and $\varphi_2 > 100$, and

$$\epsilon = 2.93\ (x/s_3\ \lambda_{3,me}^{0.8})^{-0.282},\quad \text{for } s_1 = s_2 = s_3 = 0.025 \text{ in}$$

with $\varphi_1 > 268$, and $\varphi_2 > 140$

2. Downstream Injection at an Angle of Attack

The film cooling effectiveness of the blunt nosed cone at an 8° angle of attack, obtained from the method described in Section III-2, was correlated in a form similar to that of the results of the cone at zero angle of attack. Correlations of the film cooling effectiveness in the plane of symmetry on both the windward side and leeward side, with an injection slot height of s = 0.015 in., are shown in Figs. 47 to 52 and are given in the following way.

a. Effectiveness Correlations on the Windward Side

1. Single Slot Injection, Fig. 47,

Effectiveness correlation due to single first slot injection was given here only

$$\epsilon = 38.2\ (x/s_1\ \lambda_{1,me}^{0.8})^{-0.933}, \quad \text{for } s_1 = 0.015 \text{ in.}$$

2. Combinations of Two Slot Injection

Film cooling effectiveness was correlated in the way similar to that of the cone at zero angle of attack, with parameters, $\varphi_1 = x_1/s_1\ \lambda_{1,me}^{0.8}$, $\varphi_2 = x_2/s_2\ \lambda_{2,me}^{0.8}$ to represent the injection of the preceeding injection slots:

(a) Simultaneous Injection of the First and Second Slots, Fig. 48

$$\epsilon = 6.4\ (x/s_2\ \lambda_{2,me}^{0.8})^{-0.536}, \quad \text{for } s_1 = s_2 = 0.015 \text{ in.}$$
$$\text{and } 160 < \varphi_1 < 230.$$

(b) Simultaneous Injection of the First and Third Slots, Fig. 49

$$\epsilon = 21.4\ (x/s_3\ \lambda_{3,me}^{0.8})^{-0.8}, \quad \text{for } s_1 = s_3 = 0.015 \text{ in}$$
$$\text{and } 370 < \varphi_1 < 700$$

3. Three Slot Injection, Fig. 50

$$\epsilon = 11.1\ (x/s_3\ \lambda_{3,me}^{0.8})^{-0.637}, \quad \text{for } s_1 = s_2 = s_3 = 0.015 \text{ in.}$$
$$\text{and } \varphi_1 > 450,\ \varphi_2 > 340$$

b. Effectiveness Correlations on the Leeward Side

A limited amount of present work was done toward the measurements of the heat transfer rates on the leeward side where the blunt nose cone was set at an

8° angle of attack. Correlations of the film cooling effectiveness of the present experiments are shown in Fig. 51-52 and given in the following:

(1) Single Slot Injection Due to the First Injection Slot

$$\eta = 750\ (x/s_1\ \lambda_{1,me}^{0.8})^{-1.66}\ ,\ \text{for}\ s_1 = 0.015\ \text{in. and}\ x/s_1\ \lambda_{1,me}^{0.8} > 54$$

(2) Simultaneous Injection of Two Injection Slots

From the present experimental results, the film cooling effectiveness due to simultaneous injection of the first and second slots and the film cooling effectiveness due to simultaneous injection of the first and third slots were found to be correlated in a single correlation given by

$$\eta = 21.4\ (x_i/s_i\ \lambda_{i,me}^{0.8})^{-0.855}\ ,\ \text{with}\ i = 2,\ \text{and}\ 3$$

$$\text{For}\ s_1 = s_2 = s_3 = 0.015\text{", and}\ x_i/s_i\ \lambda_{i,me}^{0.8} > 36,\ i = 1,2$$

3. Upstream Injection

Experimental film cooling effectiveness of the present upstream film cooling is shown in Figs. 53 to 56. Correlations obtained from different testing conditions are presented in the following:

a. Based on the plane wall jet, Eq. (9), Figs. 53 and 54

(1) for $s = 0.03$ in, $\ell = 0.36$ in., $Re_\infty = 1.9 \times 10^7$ per foot,

$$\eta = 5.9\ (x/s\ \lambda_m)^{-0.521}$$

(2) for $s = 0.03$ in. $\ell = 0.36$ in., and $Re_\infty = 3.8 \times 10^7$ per foot

$$\eta = 4.45\ (x/s\ \lambda_m)^{-0.420}$$

c) for s = 0.03 in., ℓ = 0.20 in., and Re_∞ = 3.8 x 10^7 per foot

$$\epsilon = 3.21\ (x/s\lambda_m)^{-0.36}$$

b. Based on the cylindrical wall jet, Eq. 10, Figs. 55 and 56.

a) For s = 0.03 in., ℓ = 0.36 in., and Re_∞ = 1.9 x 10^7 per foot

$$\epsilon = 2.81\ (x/s\lambda_m)^{-0.315}$$

b) For s = 0.03 in., ℓ = 0.36 in., and Re_∞ = 3.8 x 10^7 per foot

$$\epsilon = 2.78\ (x/s\lambda_m)^{-0.286}$$

c) For s = 0.03 in., ℓ = 0.20 in., and Re_∞ = 3.8 x 10^7 per foot

$$\epsilon = 2.35\ (x/s\lambda_m)^{-0.268}$$

SECTION V

DISCUSSIONS AND CONCLUSIONS

The measurements of the present tests, the assumptions made in the analysis of the experimental data, and the results obtained are discussed in the following paragraphs.

1. Downstream Injection at Zero Angle of Attack

a. Measurements of the local heat transfer rates, without the effect of slot injection, were compared with the results of the existing turbulent boundary layer theory [16]. As can be seen in Fig. 39, smaller values were obtained in the experiments. However, the pertinent parameter of the theoretical results is the initial boundary layer momentum thickness at the first injection slot. The difference may be due to its effect and the assumptions of the existing theory. The local Stanton number and Reynolds number were also computed from these measurements. They were compared with the results of the Flat Plate Reference Enthalpy Method [19]. In Fig. 39. Present experimental results indicate that turbulent flow existed along the surface of the blunt nose cone.

b. Measurements of the wall static pressure with different arrangements of the slot injection have shown that the difference in the wall static pressure between the cases, with and without injection, was insignificant within the accuracy of the measurements. Similar resu'ts have been found in the previous investigation of the film cooling to a Mach 6 hypersonic turbulent flow [7-10]. The change in heat transfer due to the static pressure variation was small.

c. The injection mass flow rate, $\lambda_{i,me} = \rho_j u_j / \rho_e u_e$, used to correlate the film cooling effectiveness, was based on the free stream properties, ρ_e, u_e, external to the boundary layer at the location of the specific injection slot. The effect of the entropy swallowing was neglected, and the total pressure across

the normal shock at $M_\infty = 5.85$ was used to determine the free stream conditions with the aid of the measured wall static pressure. From the numerical solution of the turbulent boundary layer, the mass flow rate in the boundary layer at a location, $x_o = 15$ inches, was computed according to the theoretical momentum thickness obtained. Free stream, $M_\infty = 5.85$, in a stream tube of a cross-sectional area of 0.14 inch in radius contained the equivalent mass flow rate. The shock shape, constructed according to the shape equation given in Ref. 23, was found predominated by the normal shock in a region of 0.14 in. in radius. This indicated that the entropy swallowing effect could be neglected in the determination of the free stream conditions at the edge of the boundary layer. The stagnation pressure across a normal shock in a Mach 5.85 free stream could be used to determine local free stream conditions.

d) In the determination of the local adiabatic wall temperature with slot injection, Reynolds analogy between skin friction and heat transfer rates was used. It has been assumed that an inner turbulent boundary layer, dominated by the stagnation properties of the injectant, originated at the injection slot. The local skin friction factor, C_f, was obtained by using the existing theory Ref. 16, for flow along a conical body surface. It has been found that large injection mass flow rates, $\lambda_{i,me}$, were used in these tests. Film cooling to the stagnation reg on of a blunt body has been analyzed for the laminar case.[21] This theoretical analysis concluded that, at high injection mass flow rates, the boundary layer can be divided into two layers, a thick inner layer of constant shear, constant temperature, and constant composition fluid and a thin outer layer in which the fluid properties adjust themselves rapidly to the external flow values. The present assumption is consistent with this theory. Similar techniques, used in the previous

investigation[7] with the assumption that the skin friction can be determined from a turbulent boundary layer originating at the tip of the nose were also used to evaluate the local skin friction factor for the experiments The corresponding local adiabatic wall temperature was computed. A difference of 5% in the adiabatic wall temperature was found. Its effect on the cooling effectiveness was insignificant. However, the previous investigations were for the case of surface film cooling to a thick turbulent boundary layer with smaller injection mass flow rates. The injectant thickened the turbulent boundary layer and decreased the local skin friction.

e) The experimental film cooling effectiveness was found capable of being correlated in a way similar to that of film cooling to a cylindrical body in a Mach 6 hypersonic main stream[7]. However, a different rate of decay of the correlation was obtained. This was due to the three-dimensional effect. From the comparisons of the correlations of the single slot injection with that of the two-dimensional case[8], the single slot injection due to the third slot injection is seen to show strong similarity to the two-dimensional case, Fig. 42. An approximate Mach 3 free stream external to the present conical body was obtained. Smaller effectiveness was obtained from the present experiments. This indicated that surface film cooling was more effective in a high Mach number main stream than in a low Mach number flow.

f) In order to investigate the effect of the boundary layer thickness at the injection slot on the surface film cooling effectiveness, results of the experiments of single slot injection with the same injection mass flow rate $\lambda_{i,m} \approx 0.50$ and different slot heights, s = 0.015", 0.025", are shown in Fig. 57. A large reduction in the film cooling effectiveness of the first

slot injection due to a decrease in the slot height is shown. However, there was no significant reduction in the effectiveness due to reduction of the slot height for single slot injection due to the second slot or the third slot. Thus, it has been concluded that a reduction in the effectiveness due to a decrease in the slot height was significant only when the system was operated with a thinner boundary layer at the location of the injection slot. The effect of the boundary layer thickness on the film cooling effectiveness in a low Mach number flow can be found in Ref. 22. It is concluded that when the system was operated with thick boundary layer at the injection slot and with a 0.25 inch slot, there was but a minor reduction in the effectiveness at large distance downstream. A greater reduction existed with a 0.125 inch slot and with the 0.063 inch slot. The present results of single slot injection were found in agreement with their statement.

g) Correlations of the film cooling effectiveness due to single slot injection have shown that the cooling length, the distance downstream from the injection slot in which $\epsilon = 1.0$, was similar when the boundary layer was thin at the injection slot. The effect of the boundary layer thickness on the cooling length was insignificant when a large injection slot was used. These results can be seen in Fig. 58.

h) From the comparisons of the effectiveness downstream of the injection slot between single and multiple slot injections, as shown in Fig. 46, a 23% increase in the cooling length was obtained for the case of two slot injection while a 37% increase in the cooling length was found in the case of three slot injection.

i) With the same injection mass flow rates, comparisons of the experimental film cooling effectiveness between single and multiple slot injection are

shown in Figs. 59 to 61. Multiple slot injection improved the effectiveness far downstream from the nose region with significant decreasing in the effectiveness near the nose part.

j) For the case of simultaneous first and second slot downstream injection at zero angle of attack, two different correlations were found when $x_1/s_1 \lambda_{1,me}^{0.8}$ was less than 200, Fig. 43. An increase in the effectiveness due to the preceding slot was significant when the mass flow rate of the second slot, $\lambda_{2,m}$, was less than 0.50. When the injection mass flow of the second slot was greater than 0.50, correlation of film cooling effectiveness similar to that of the single second slot injection was obtained. This indicates that when a large mass flow was injection through the second slot, effect of the surface film cooling was predominated by this slot and the effect of the preceding slot injection was insignificant. Similar results of film cooling with multiple slots in a two-dimensional case can be found in Ref. 5.

k) Approximate analytical results of the film cooling effectiveness were compared with those of the experiments in Figs. 62 to 67. Two values of the proportional constant, k = 1.0 and 2.0, were used in the modified Oseen approximation. Most parts of the analytical results indicated that higher film cooling effectiveness was obtained. This was due to the fact that the analytical results of the film cooling were dominated by the properties of the injectant.[20]

2. Downstream Injection at an Angle of Attack

In the evaluation of the film cooling effectiveness from the measurements for the blunt nose cone at an 8° angle of attack, the effect of the coolant

injection to the local heat transfer coefficient, h, was assumed insignificant. Though the effect of angle of attack has not been thoroughly investigated, significant results were found. Results on the windward and leeward side were discussed separately and compared with the results of zero angle of attack.

a) Film cooling Effectiveness on the Windward Side

1) The correlation parameter used in the case of zero angle of attack, was found capable of correlating the present experimental film cooling effectiveness at eight degree angle of attack. Simple correlations were also obtained from the present experimental data.

2) A comparison of film cooling effectiveness between the cases with and without angle of attack has been made for the first slot injection and is shown in Fig. 51 . Here, the adiabatic wall temperature at zero angle of attack was obtained in the same way as that with angle of attack.
For same injection mass flow rates, $\lambda_{1,m}$, higher film cooling effectiveness was obtained at zero angle of attack. The cross flow effect on the reduction in the effectiveness was significant far downstream from the injectant slot. The film cooling effectiveness at zero angle of attack with $\lambda_{1,m} = 1.08$, obtained from the method of Section III-1, is also shown. Higher film cooling effectiveness was obtained from that method.

3) Comparisons of the film cooling effectiveness due to multiple slot injection between the cases with angle of attack and without angle of attack are shown in Figs. 48 - 50. Large reduction in the effectiveness was found at an angle of attack.

b) Film Cooling Effectiveness on the Leeward Side

1) Single correlation of the film cooling effectiveness, presented in Section IV-3, was found inadequate to correlate the present experimental data

near the injection slot, Figs. 51 - 52. Separate correlations, as is discussed in Ref. 5, must be used. It is also indicated in Ref. 5 that the film cooling effectiveness due to multiple slot injection can be correlated into a single curve. The present results of multiple slot injection, Fig. 47, have shown the similar tendency. The effect of the distance between the injection slot on the cooling effectiveness downstream from the last injection slot has not been found.

2) The wall static pressure distribution on the leeward side was very small compared with that on the windward side or with the results at the zero angle of attack. With the same mass flow rate of the injectant, a large value of the injection mass flow rate, $\lambda_{i,me}$, was obtained on the leeward side. This might contribute to the particular results of the correlation of the film cooling effectiveness. However, a comparison of the film cooling effectiveness among the cases of downstream injection with and without angle of attack, with the same injection mass flow rate, $\lambda_{i,m} \approx 1.10$, is shown in Fig. 68 Significant increase in the effectiveness near the injection slot was found along the leeward side.

3. Upstream Injection

General review of the flow field produced by a jet issuing into a counter mainstream has been described in Ref. 12. The mainstream has to overcome the obstacle presented by the jet and the forward-facing step. Its boundary layer separate because of the adverse pressure gradient. The large separated region of the mainstream exchanges momentum by mixing with the injection flow, which is also separated near the stagnation point. In the present work, results of wall jet theory, (Eqs (9) and (10) of Refs. 14 and 15), were used to compute the local adiabatic wall temperature when the coolant was injected. The local skin

friction coefficient was determined from the velocity profiles by a semi-logarithmic representation of the value near the wall. Verification of the validity of using these equations to determine the heat transfer coefficient, h, for these tests required further investigations of the velocity profile measurements near the injection slot. However, the following results were found.

a) The wall static pressure measurements, at zero injection mass flow rate, indicate that the value of the static pressure increased gradually from that at a conical surface at the tip to more than twice that value, at the location of the forward facing step. When the upstream injection was applied, oscillating pressure distributions were found with a step size, ℓ = 0.36 inch. But gradual increasing in the static pressure was found when the upstream injection was applied with a step size, ℓ = 0.20 inch. A variation in the injection mass flow rate also changed the distribution of the wall static pressure.

b) Without upstream injection, higher heat transfer rates were obtained when a larger forward facing step was used. Heat transfer rates increased with an increasing in the free stream Reynolds number. A large decrease in the heat transfer rate was found when coolant was injected. An increase in the heat transfer rate near the tip region was also found, especially when the smaller forward facing step, ℓ = 0.20 inch, was used. Higher penetration of the injectant could be obtained with a large forward facing step.

c) From the correlations of the film cooling effectiveness obtained in the present studies, the following results were obtained.

1) With the same geometry of the upstream injectant slot, film cooling

was more effective in a high Reynolds number flow than in a low Reynolds number flow, Figs. 54 and 56.

2) An increase in the dimensionless quantity, ℓ/s, resulted in an increase of film cooling effectiveness, Fig. 53.

3) Comparisons between the correlations, obtained from the plane wall jet and cylindrical jet theory, are shown in Fig. 69. Higher film cooling effectiveness was obtained from the cylindrical jet theory.

SECTION VI

SUMMARY

Experimental investigation of the turbulent slot film cooling to the surface of a nose cone has been performed. Two models were designed and used for the experiments in a Mach 6 axial-symmetric wind tunnel. Multiple tangential downstream slot injection was used to investigate the film cooling effectiveness to the surface downstream of the shoulder of a blunt nose cone. Upstream injection from a tangential injection slot, located at the base of a sharp nose cone, was used to investigate the upstream film cooling to the surface of a sharp nose cone.

Tests of the downstream slot injection were conducted with a tunnel stagnation condition of 1900 psia, and 900°R. A high free stream Reynolds number 3.8×10^7 per foot, was obtained to insure turbulent conditions. Air at a stagnation temperature of 530°R was used as injectant. For the upstream slot injection, tests were performed with two different tunnel stagnation pressures, 1000 psia and 1900 psia. Air at a stagnation temperature of 530°R was also used as an injectant.

Pressure taps and the transient thin wall technique were used to measure the wall static pressure and heat transfer rates with different injection mass flow rates. A large amount of data was obtained to analyze the surface film cooling effectiveness. The local adiabatic wall temperature was not directly measured but was inferred from the heat transfer measurements. Film cooling effectiveness, $\epsilon = (T_{aw,i} - T_{o\infty})/(T_{oj} - T_{o\infty})$, was found from this local adiabatic wall temperature. Correlations of the film cooling effectiveness due to single and multiple slot injection were obtained. The effects of the slot height and the boundary layer thickness at the injection slot on the downstream film cooling effectiveness were also investigated. A minor amount of the present work has been

done at an 8° angle of attack.

These experiments indicated that downstream film cooling was more effective in high Mach numbers than in a low Mach number flow. A reduction in the effectiveness due to a decrease in the slot heights was significant when a thinner boundary layer existed at the injection slot; a 30% increase in the cooling length was obtained when multiple slot injection was employed; improvement in the film cooling effectiveness downstream from the injection slot was also found. Large reduction in the effectiveness on the windward side was found with the same injection mass flow rate as that for an angle of attack. The cross flow effect on the film cooling effectiveness was significant.

Approximate theoretical analysis, to predict the downstream film cooling effectiveness, has shown that higher effectiveness was obtained from the theory than from the experiments. The analytical film cooling effectiveness was dominated by the stagnation properties of the injectant.

In the upstream injection, the main flow separated from the surface of the sharp nose cone due to the existence of the forward facing step. Coolant was injected upstream into the dead air near the injection slot. In contrast to the results of the experimental measurements of the downstream injection, distribution of the surface pressure was found to be a function of the injection mass flow rate. The coefficient of heat transfer rate, obtained from existing theory of wall jet, was used to compute the local adiabatic wall temperature from the heat transfer measurement. Film cooling effectiveness was also found. Results indicate that upstream film cooling was more effective in a high Reynolds number flow than it was in a low Reynolds number flow. An increase in the size of the forward facing step increased the film cooling effectiveness. However, the validity of employing the wall jet theory to estimate the local

adiabatic wall temperature required detailed experimental investigation of the velocity profiles of the flow field.

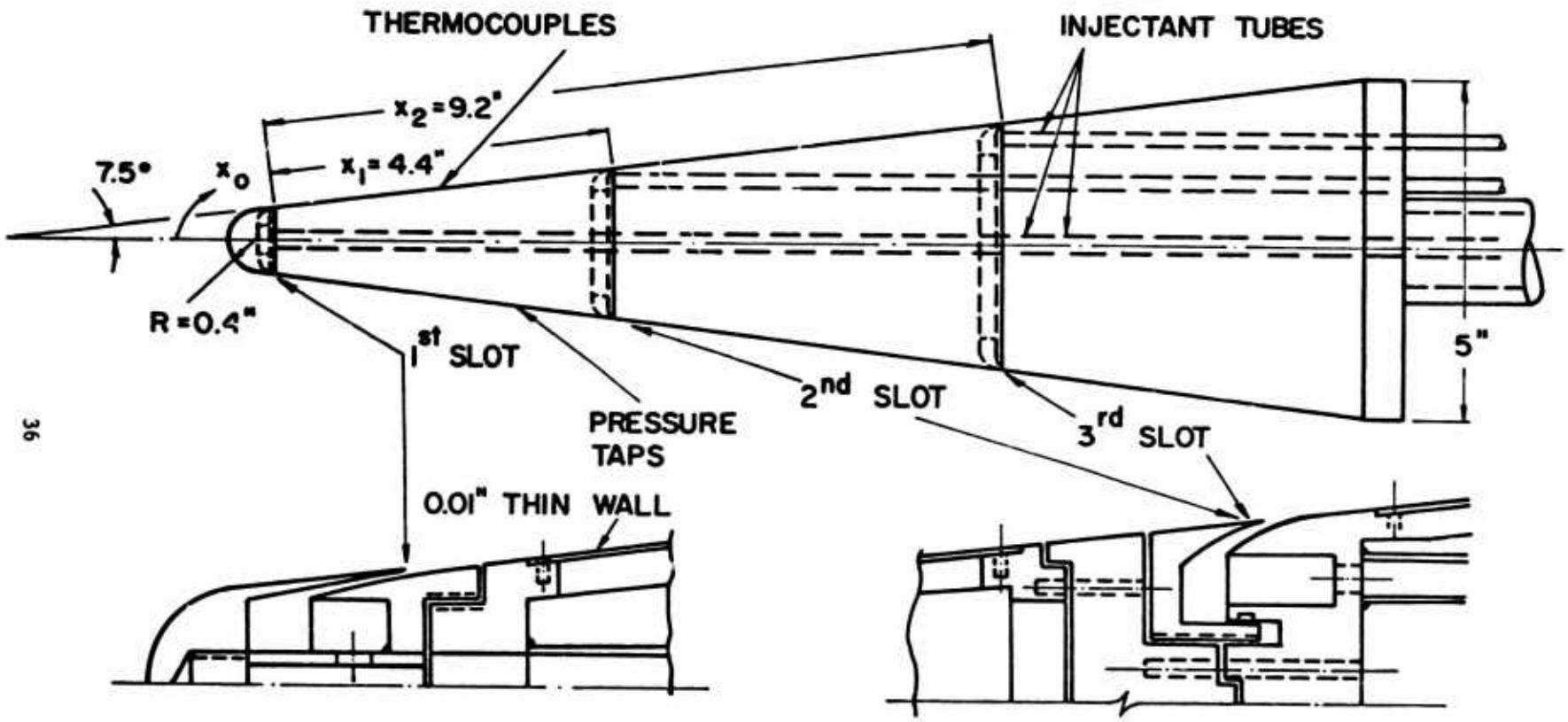

Fig. 1 Schematic drawing of the downstream injection model

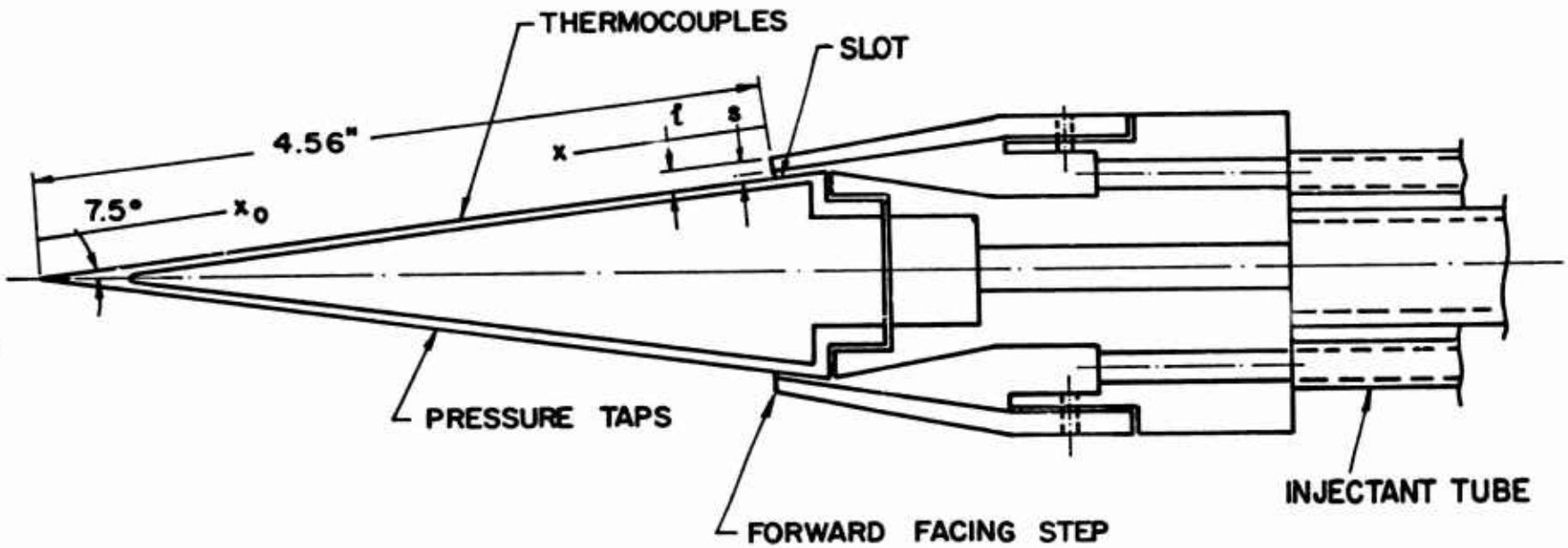

Fig. 2 Schematic drawing of the upstream injection model

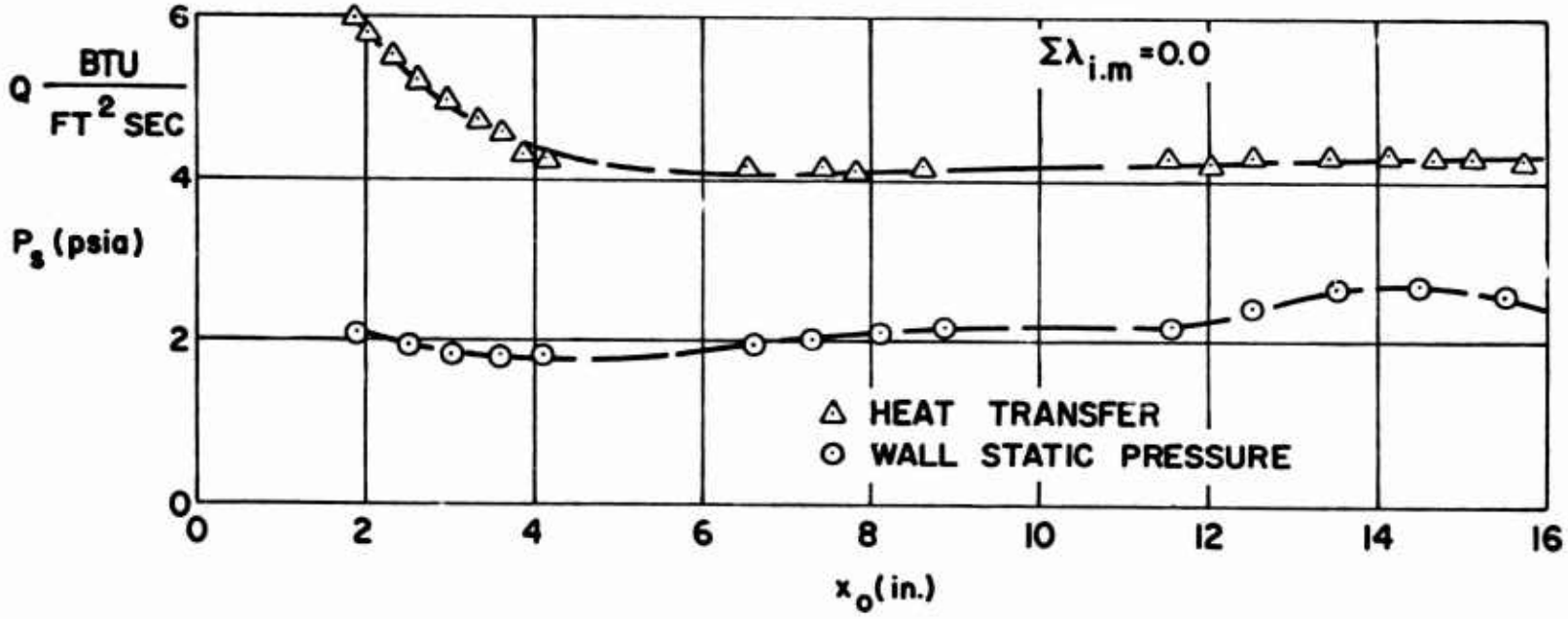

Fig. 3 Distributions of the surface pressure and heat transfer rate without injection, downstream injection model

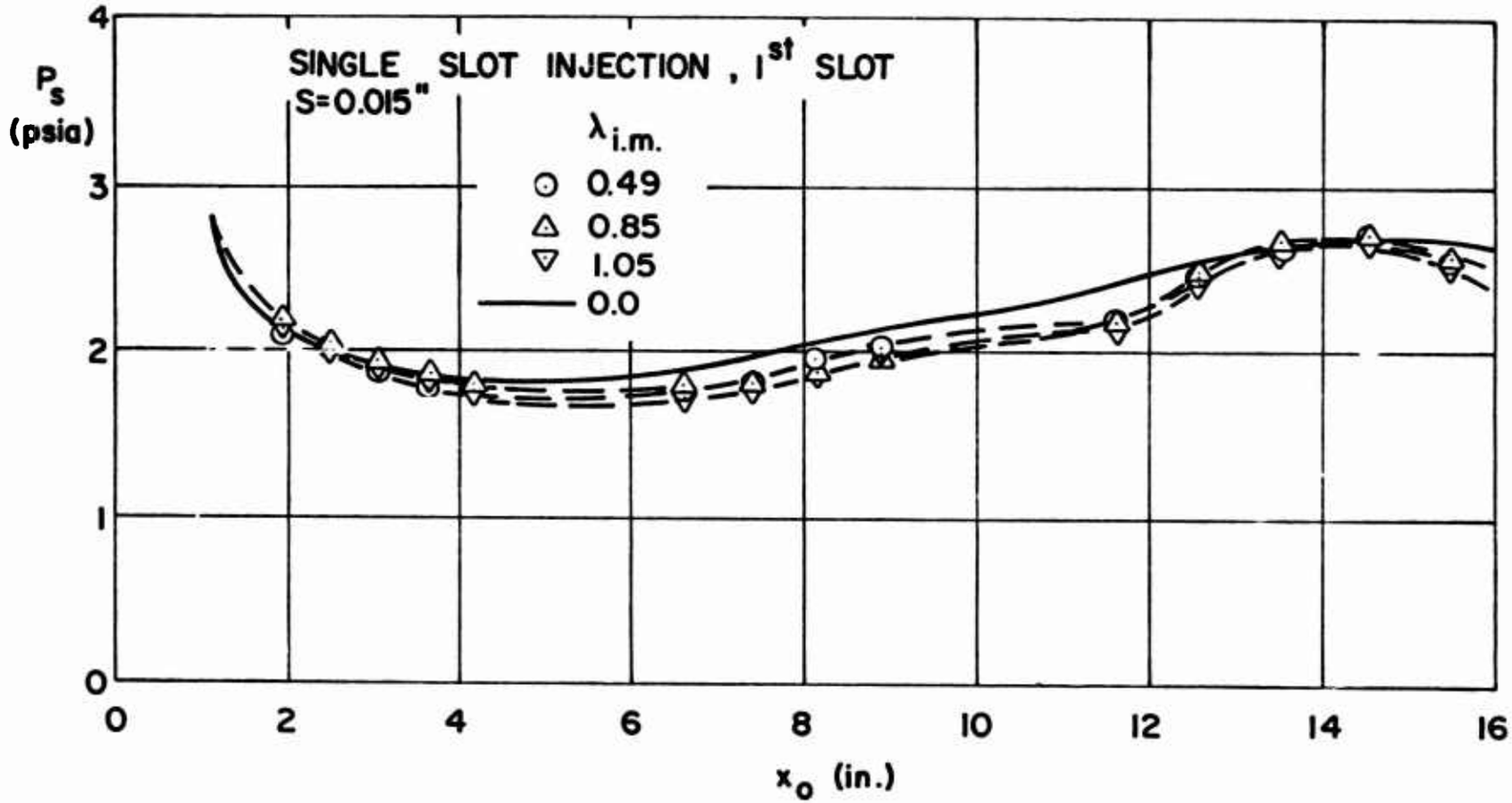

Fig. 4 Distribution of the surface pressure, 1st slot downstream injection, s = 0.015 in., $\alpha = 0^\circ$

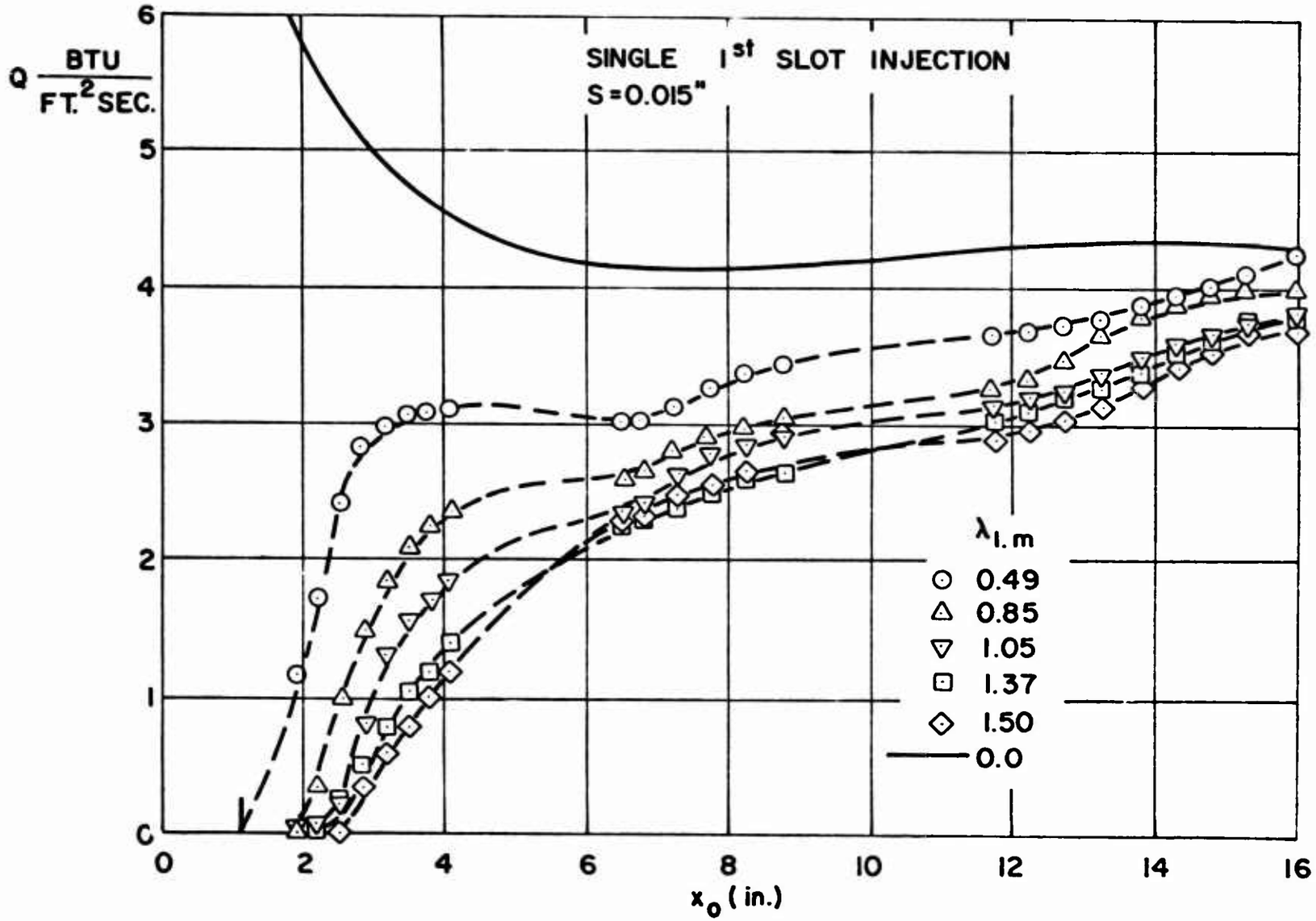

Fig. 5 Distributions of the surface heat transfer rate, 1st slot downstream injection, $s = 0.015$ in., $\alpha = 0^{\circ}$

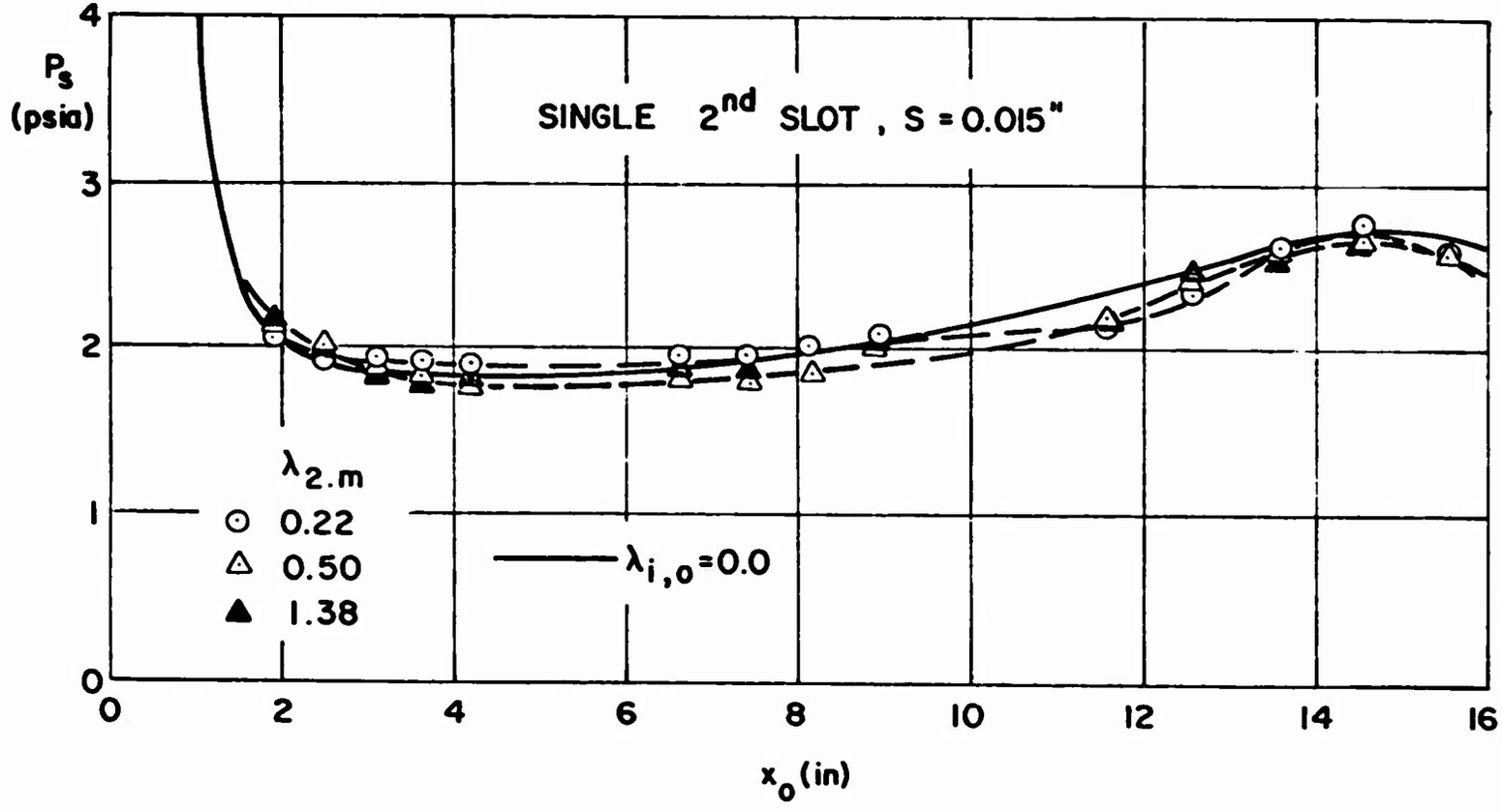

Fig. 6 Distributions of the surface pressure, 2nd slot downstream injection, s = 0.015 in., $\alpha = 0^{\circ}$

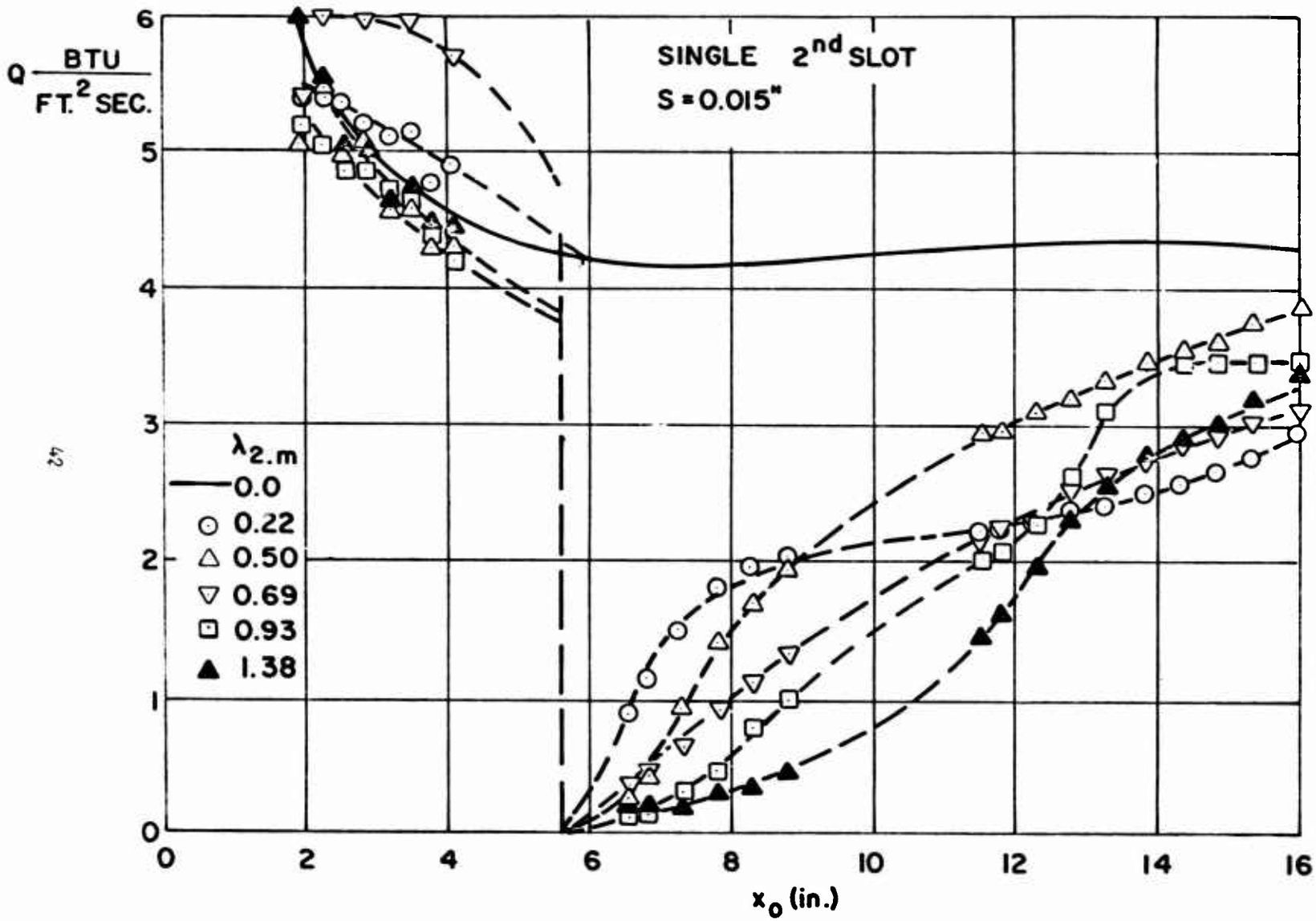

Fig. 7 Distributions of the surface heat transfer rate, 2nd slot downstream injection, s = 0.015 in., $\alpha = 0^{\circ}$

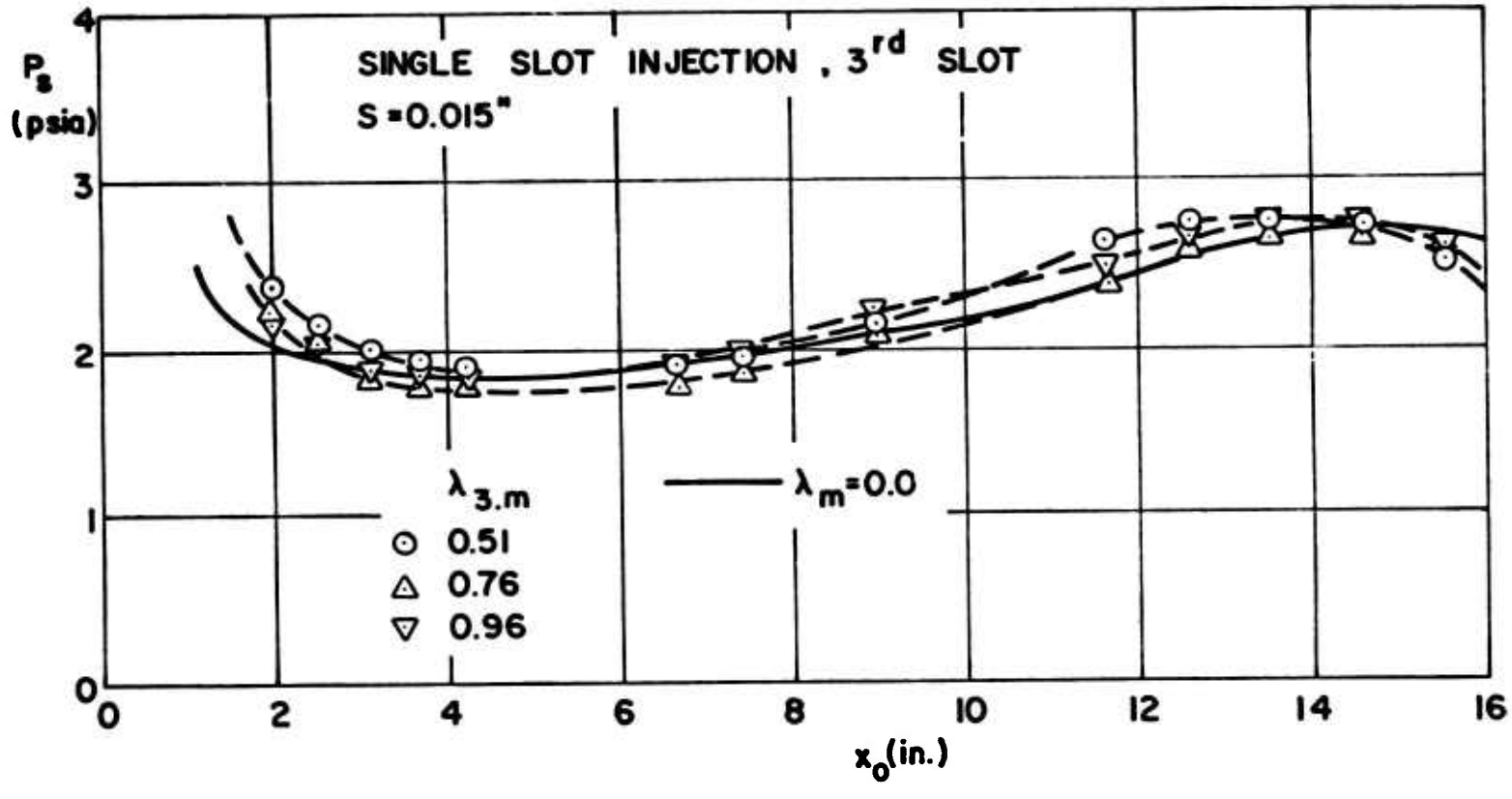

Fig. 8 Distributions of the surface pressure, 3rd slot downstream injection, s = 0.015 in., $\alpha = 0^\circ$

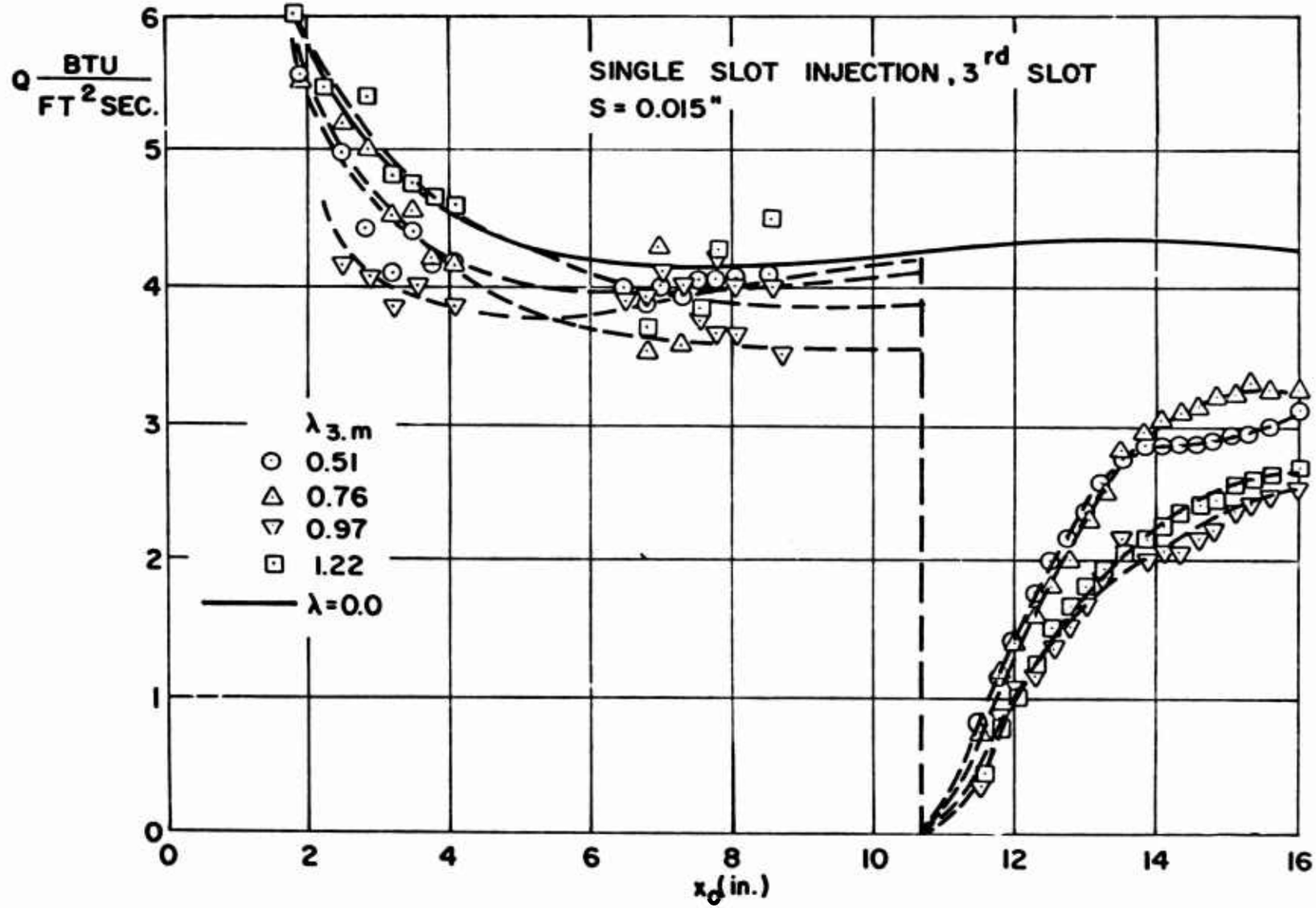

Fig. 9 Distributions of the surface heat transfer rate, 3rd slot injection, s = 0.015 in., $\alpha = 0^{\circ}$

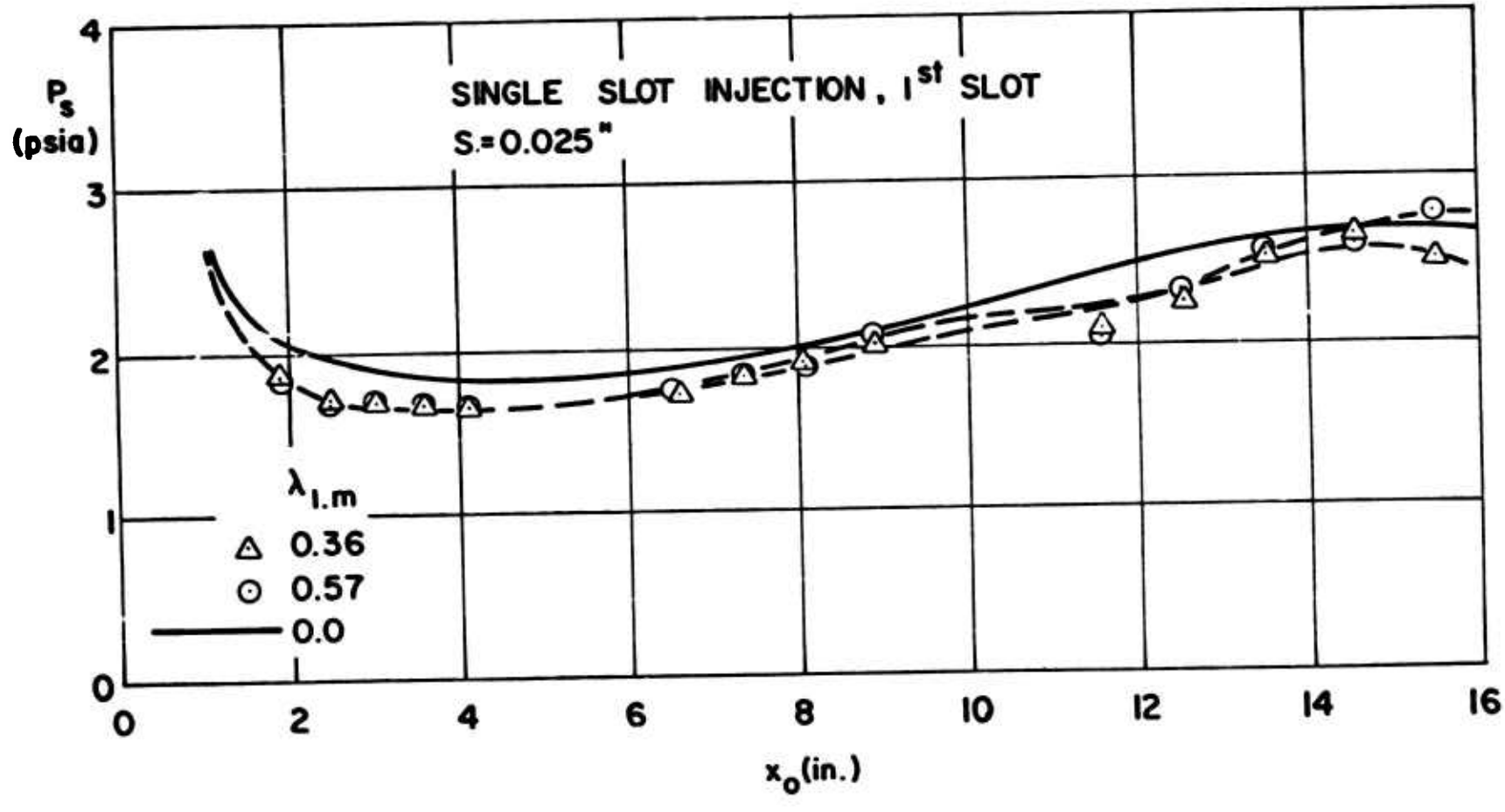

Fig. 10 Distributions of the surface pressure, 1st slot downstream injection, s = 0.025 in., $\alpha = 0^c$

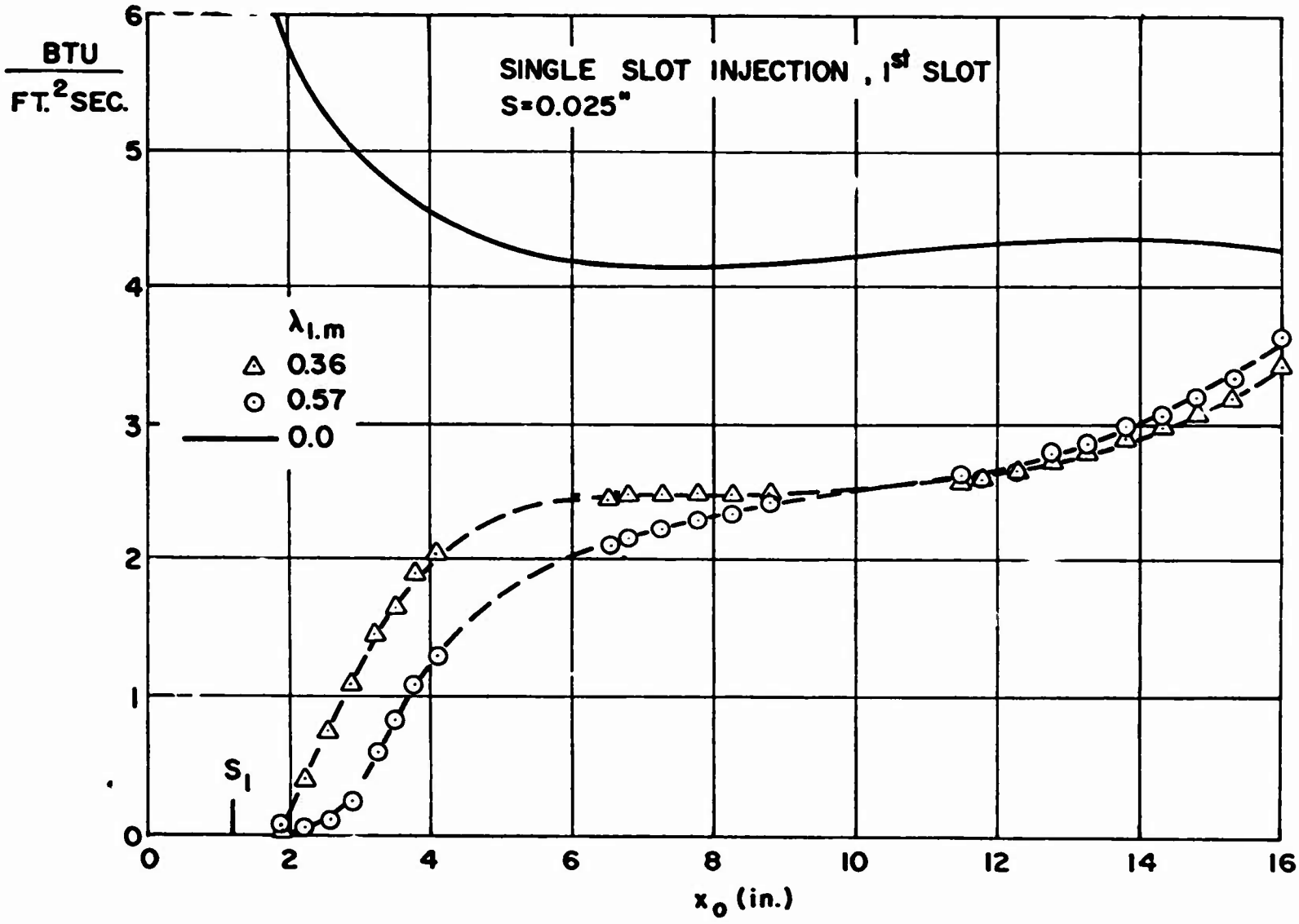

Fig. 11 Distributions of the surface heat transfer rate, 1st slot downstream injection s= 0.025 in., $\alpha = 0^{\circ}$

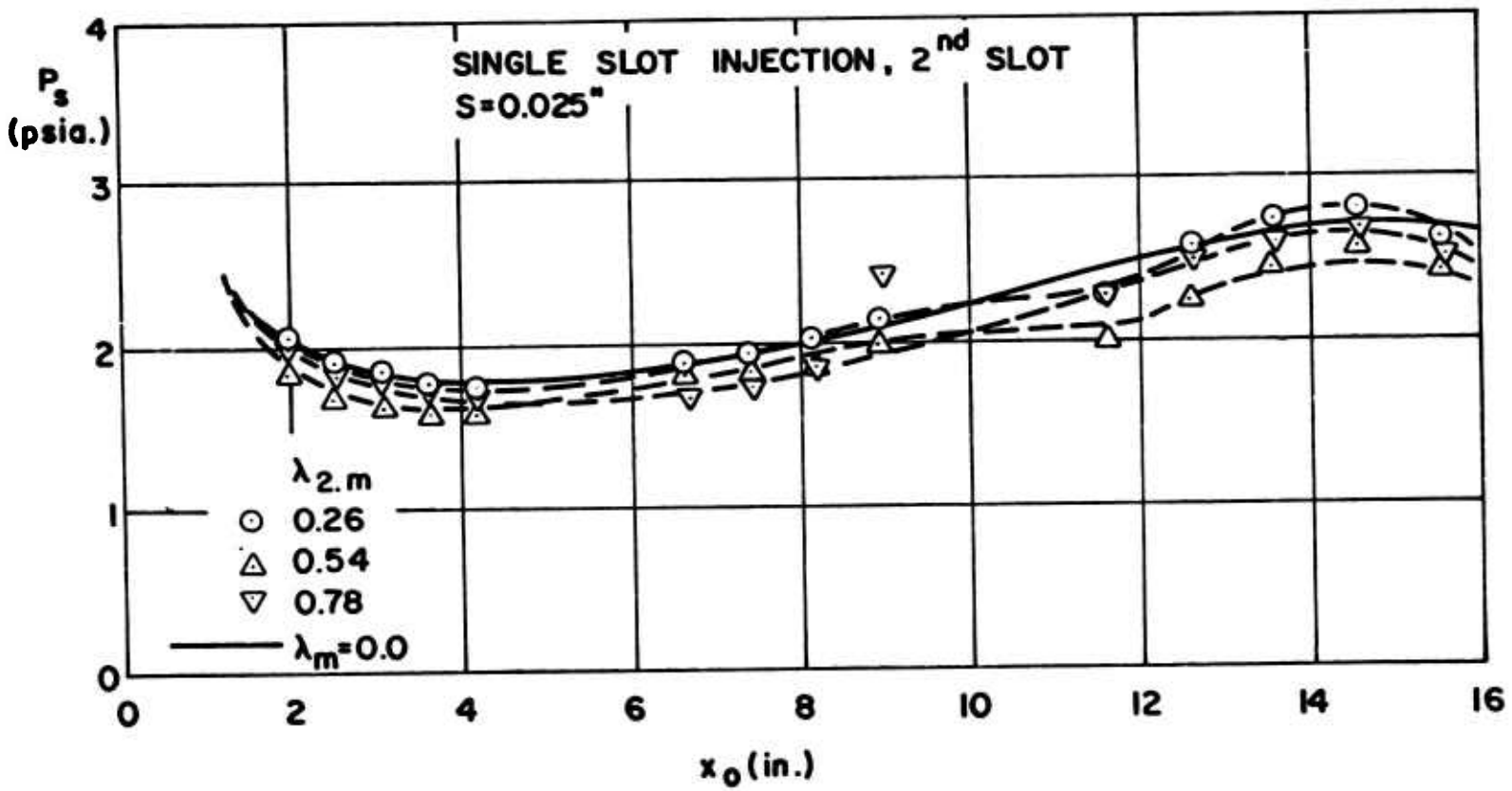

Fig. 12 Distributions of the surface pressure, 2nd slot downstream injection, s = 0.025 in., $\alpha = 0^o$

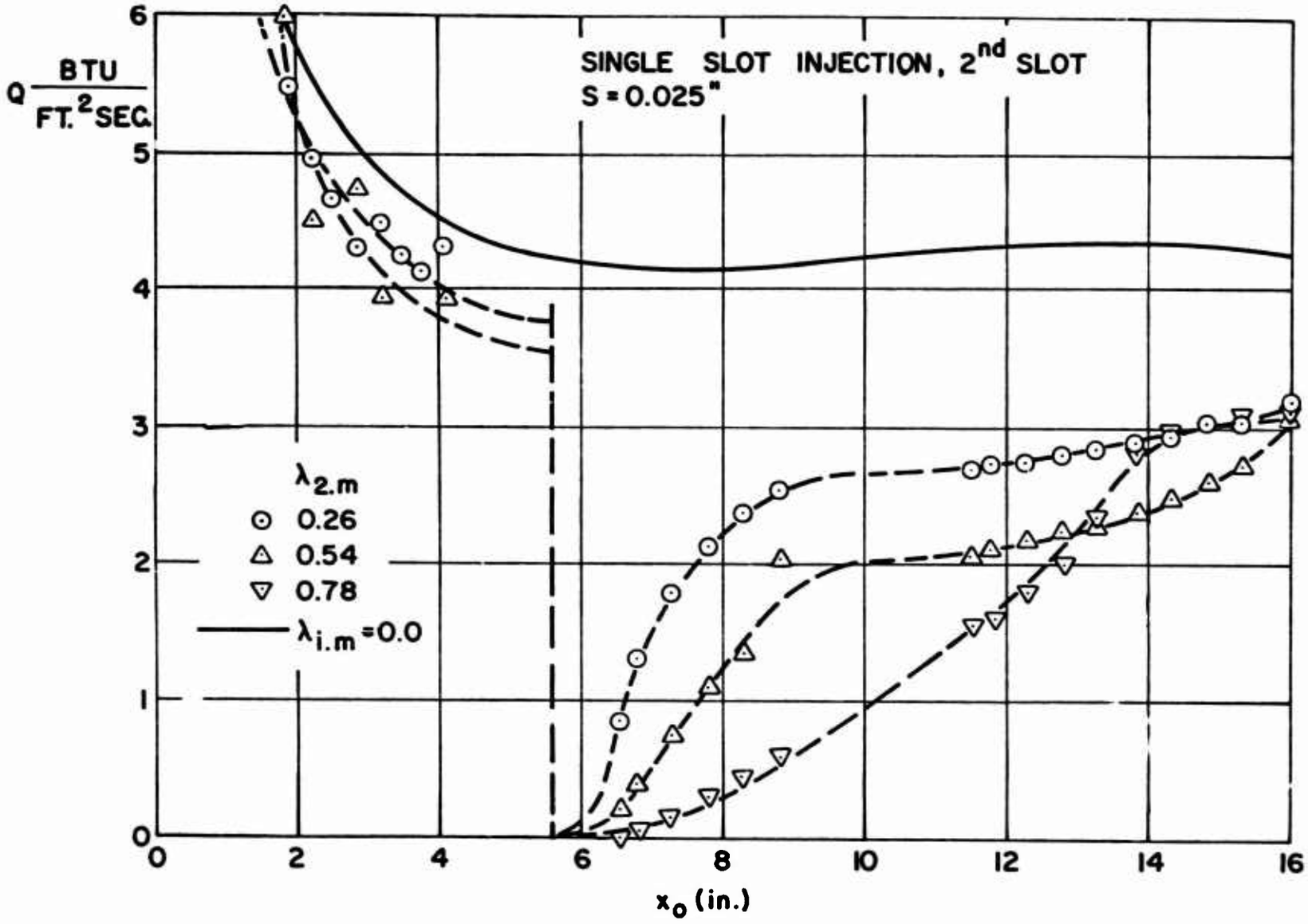

Fig. 13 Distributions of the surface heat transfer rate, 2nd slot downstream injection, s = 0.025 in., $\alpha = 0^{\circ}$

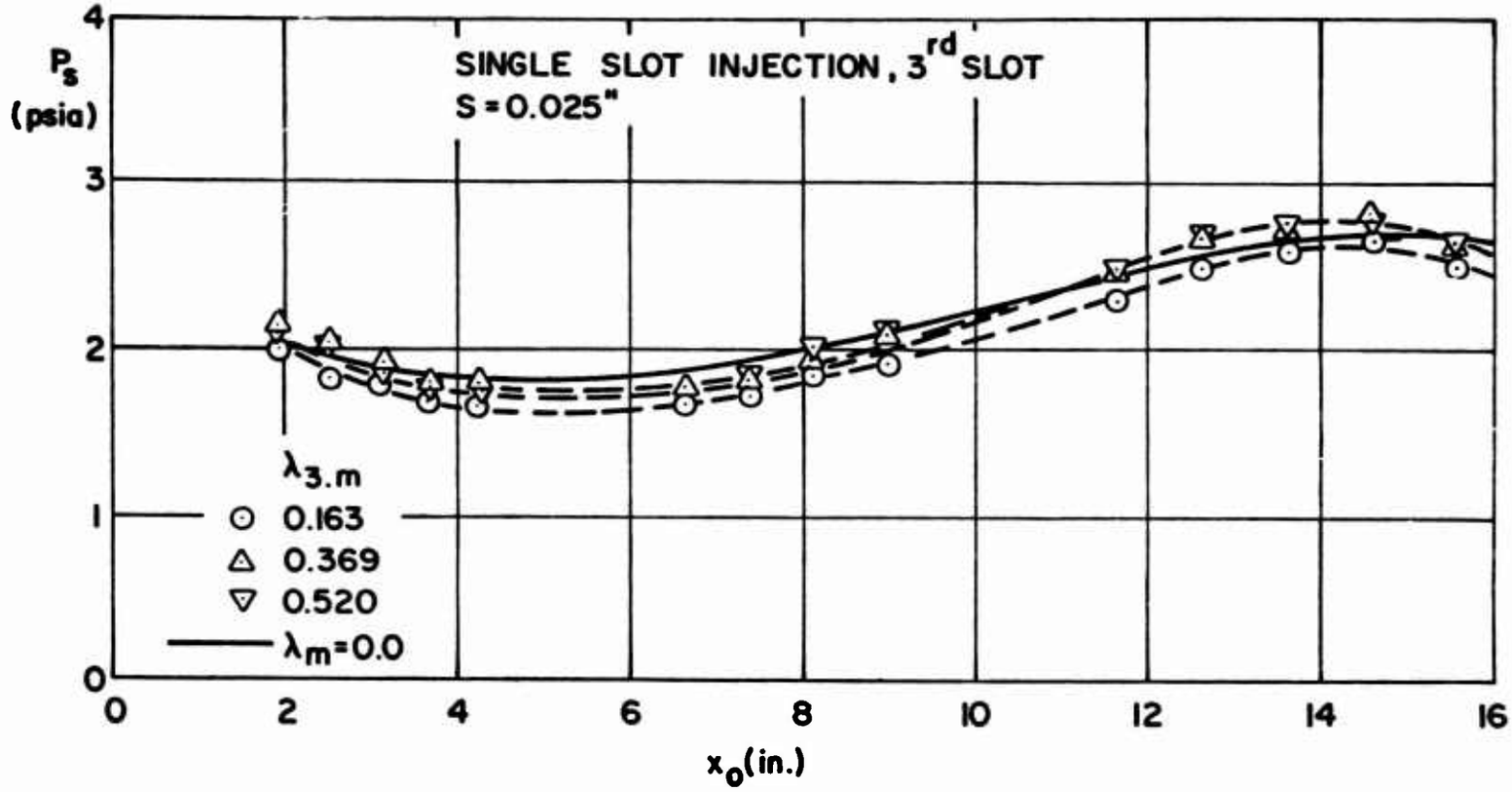

Fig. 14 Distributions of the surface pressure, 3rd slot downstream injection, s = 0.025 in., $\alpha = 0^\circ$

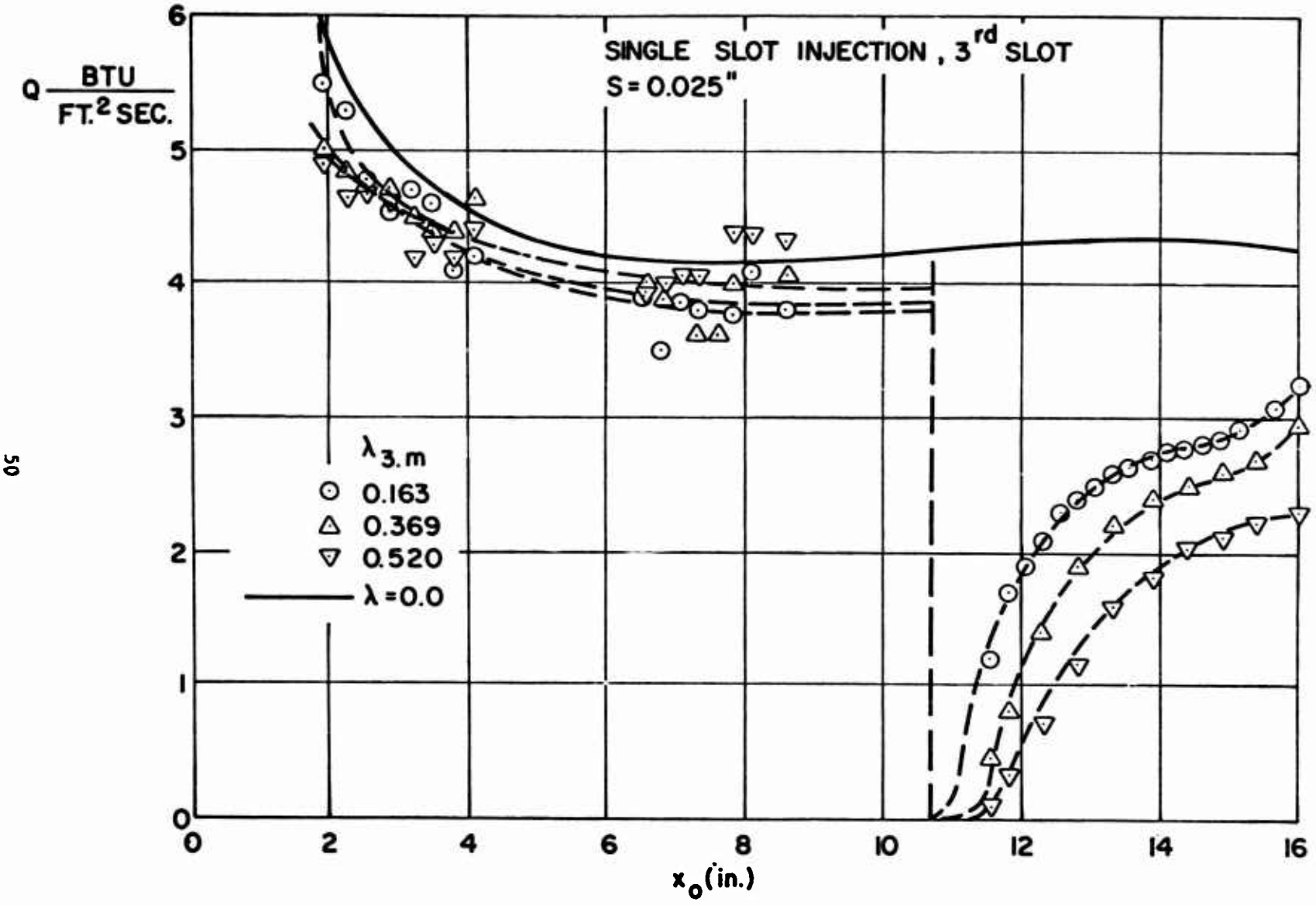

Fig. 15 Distributions of the surface heat transfer rate, 3rd slot downstream injection, s = 0.025 in., $\alpha = 0^{o}$

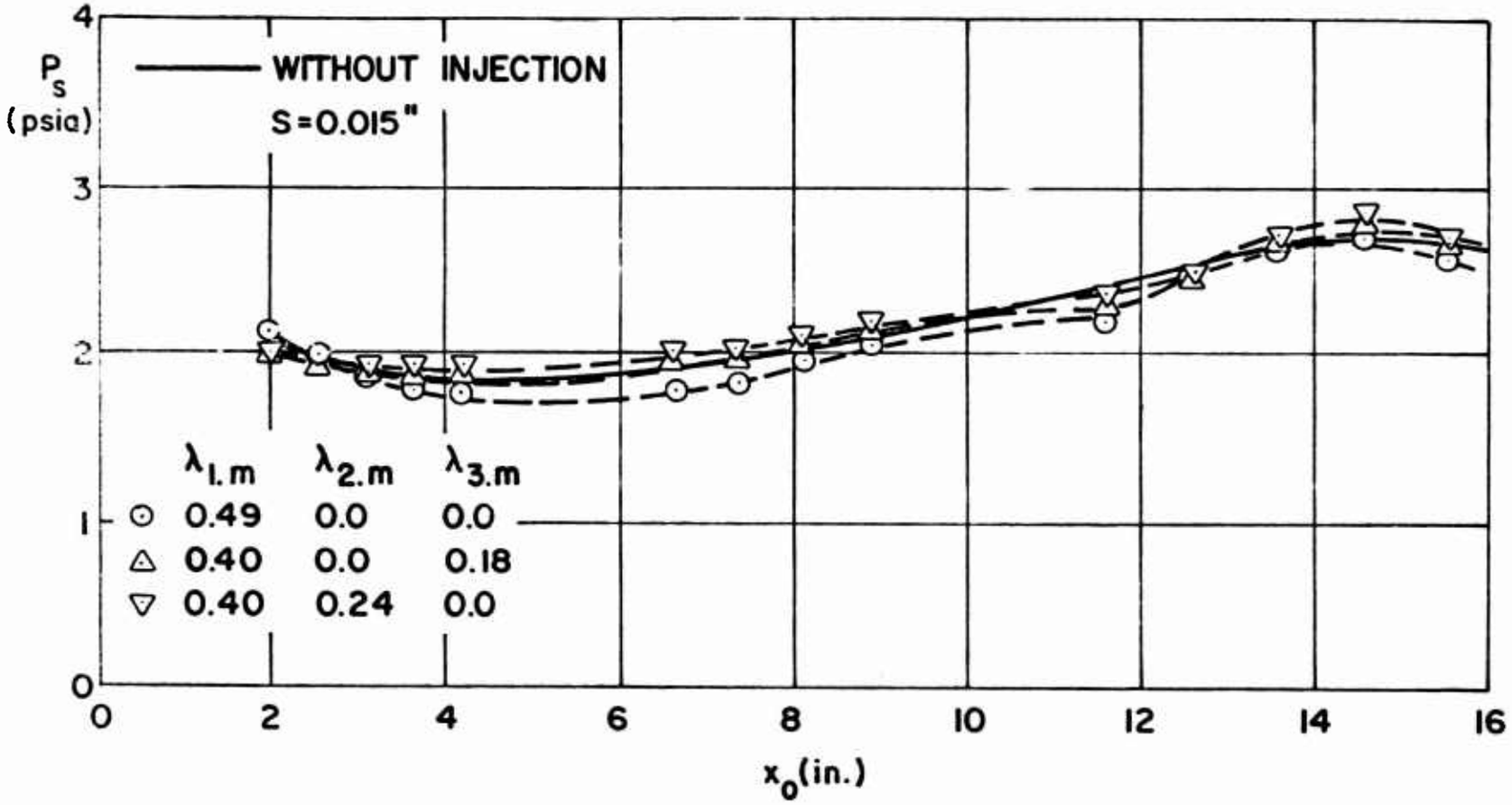

Fig. 16 Distributions of the surface pressure, 2 and 3 slots downstream injection, $s = 0.015$ in., $\alpha = 0^{\circ}$

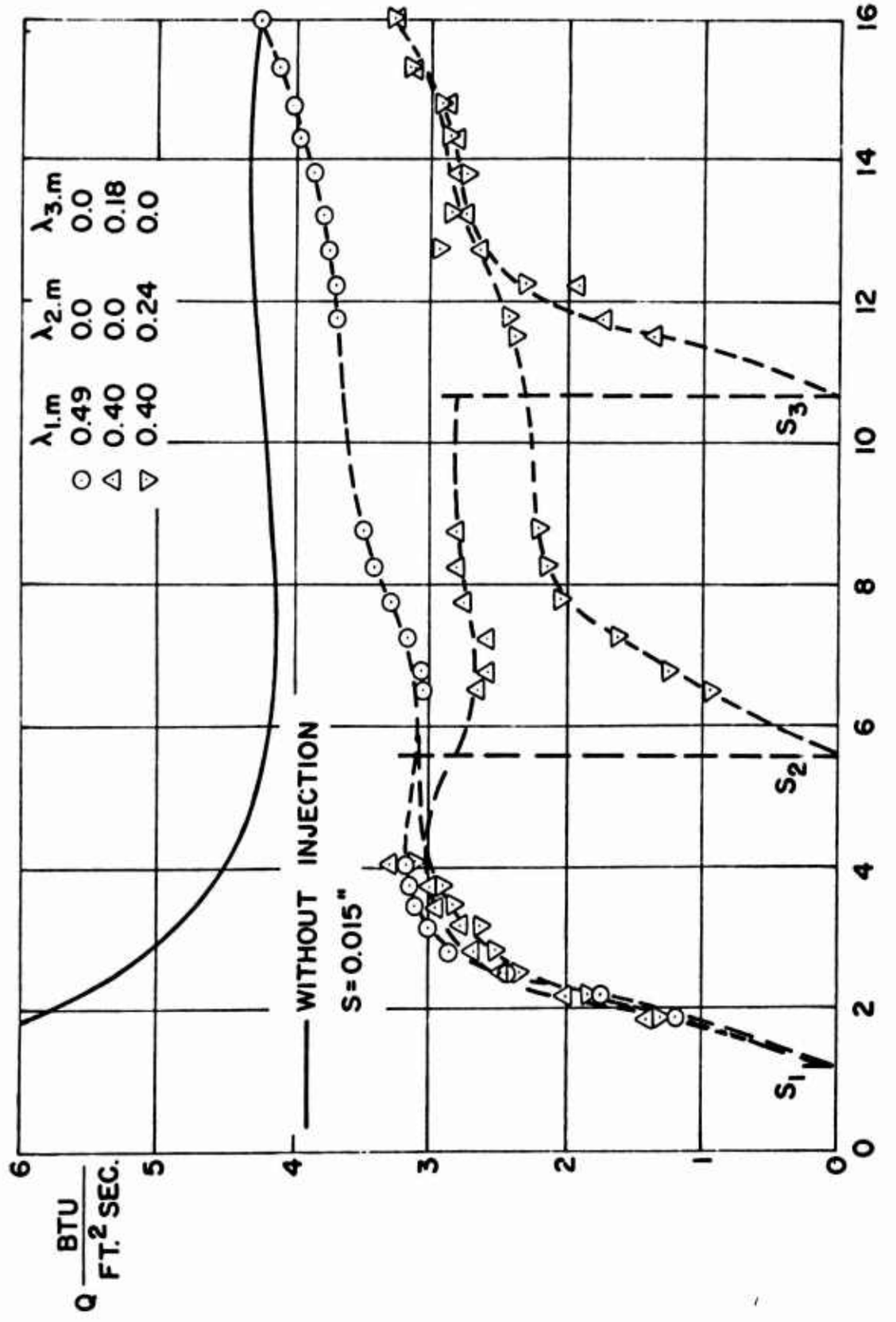

Fig. 17 Distributions of the surface heat transfer rate, 2 and 3 slots downstream injection, $s = 0.015$ in., $\alpha = 0^\circ$

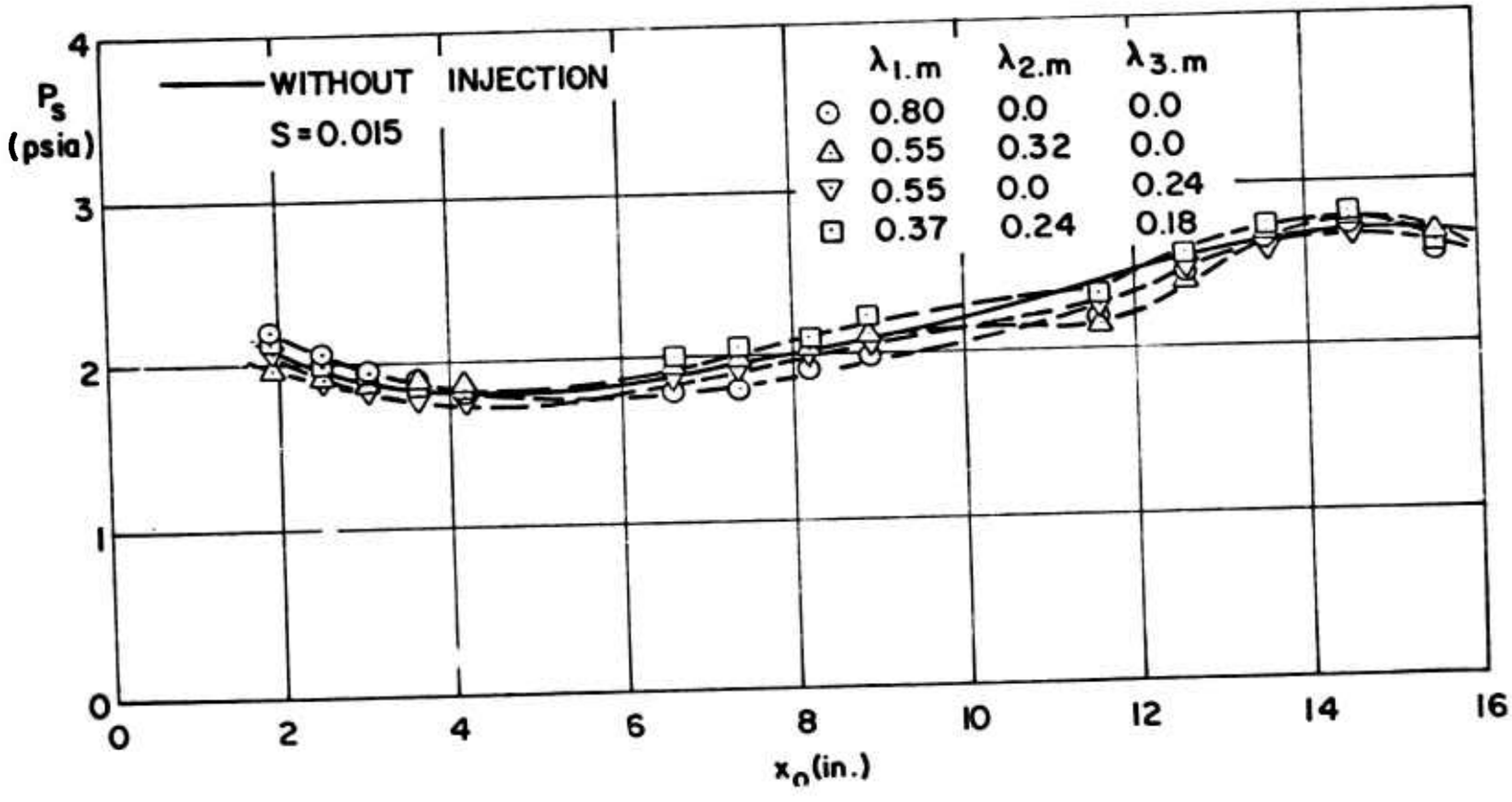

Fig. 18 Distributions of the surface pressure, 2 and 3 slots downstream injection, $s = 0.015$ in., $\alpha = 0^{o}$

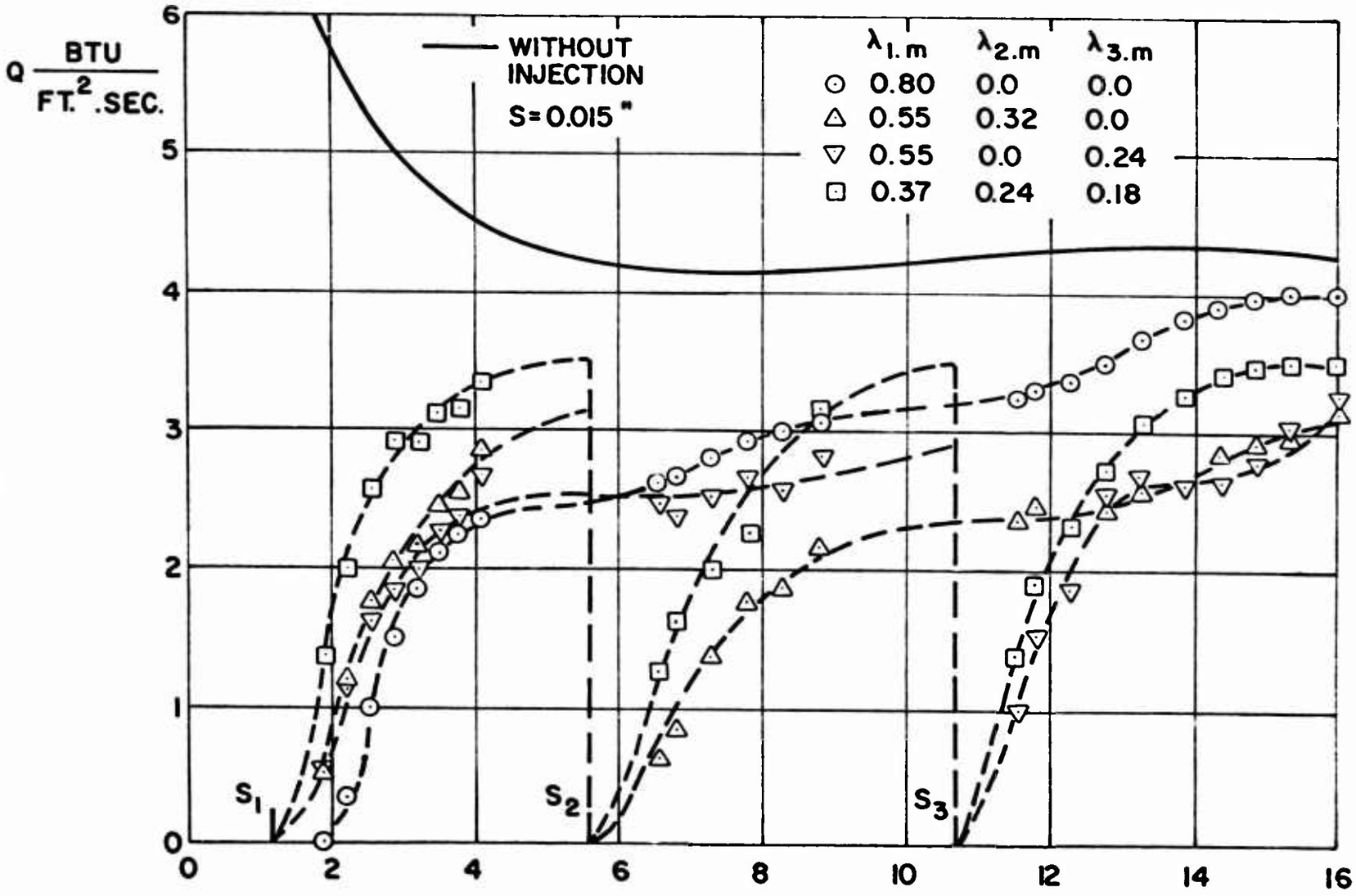

Fig. 19 Distributions of the surface heat transfer rate, 2 and 3 slots downstream injection, $s = 0.015$ in., $\alpha = 0^{\circ}$

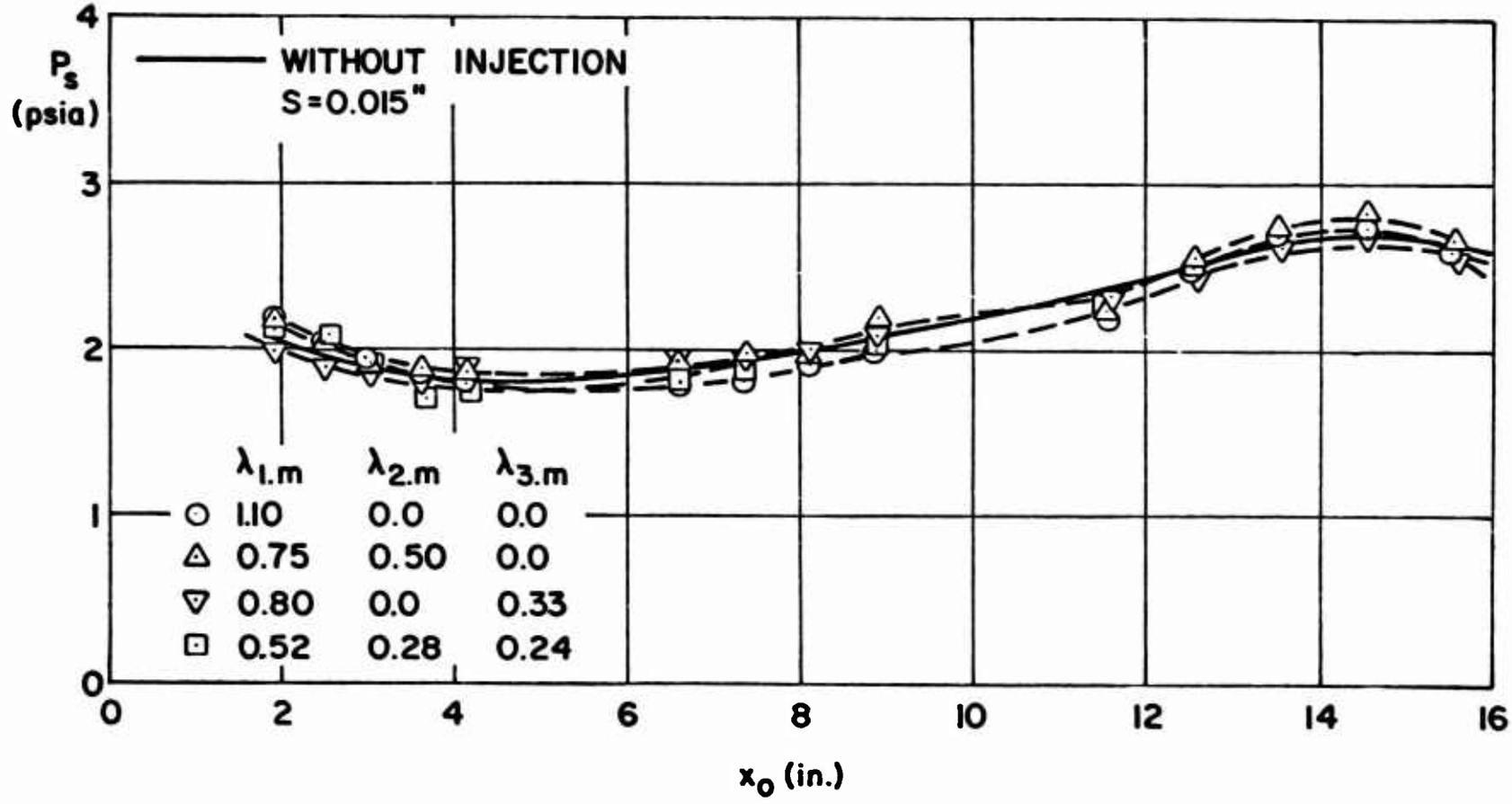

Fig. 20 Distributions of the surface pressure, 2 and 3 slots downstream injection, $\alpha = 0^{\circ}$

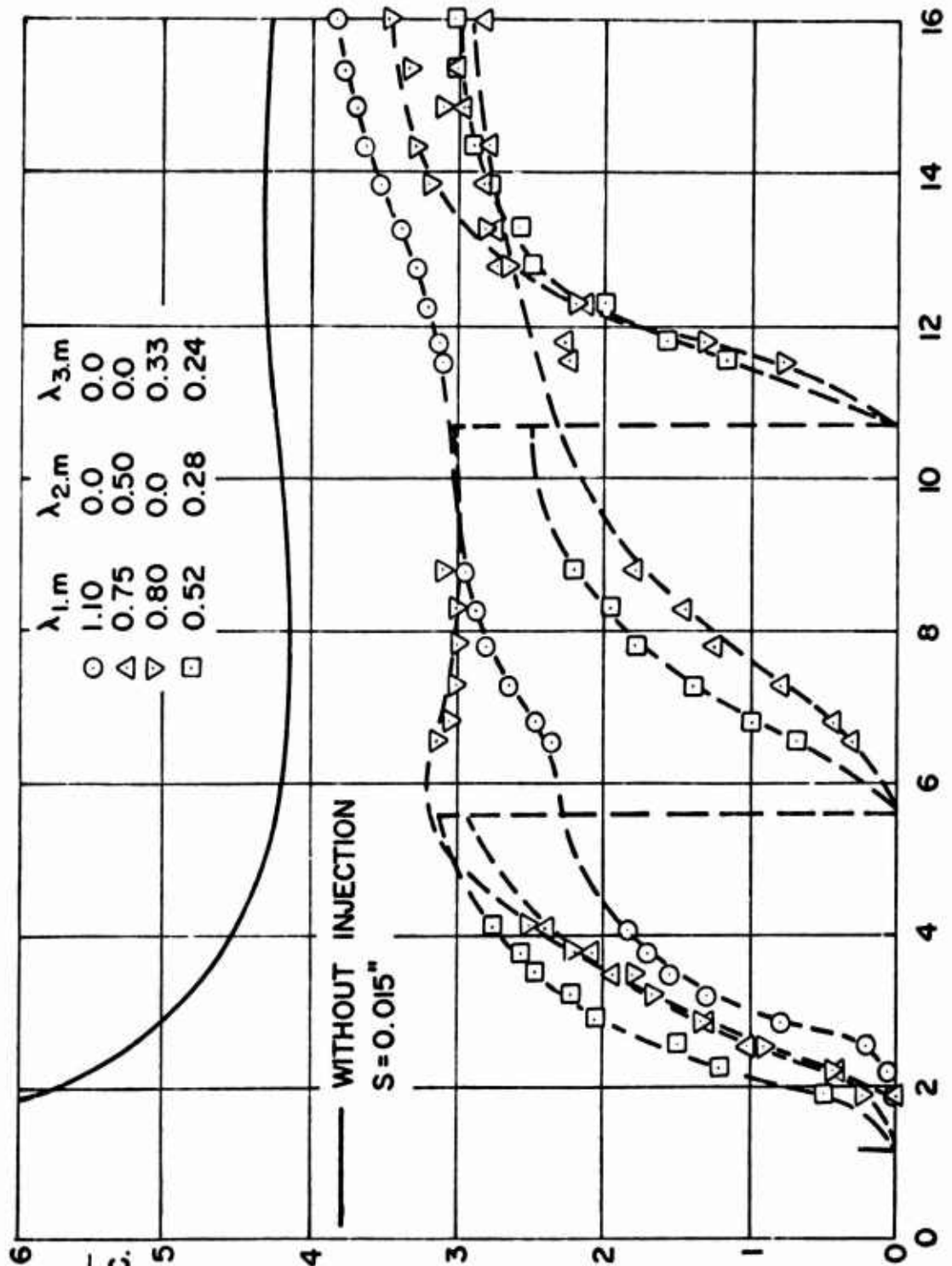

Fig. 21 Distributions of the surface heat transfer rate, 2 and 3 slots downstream injection, $s = 0.015$ in., $\alpha = 0^{\circ}$

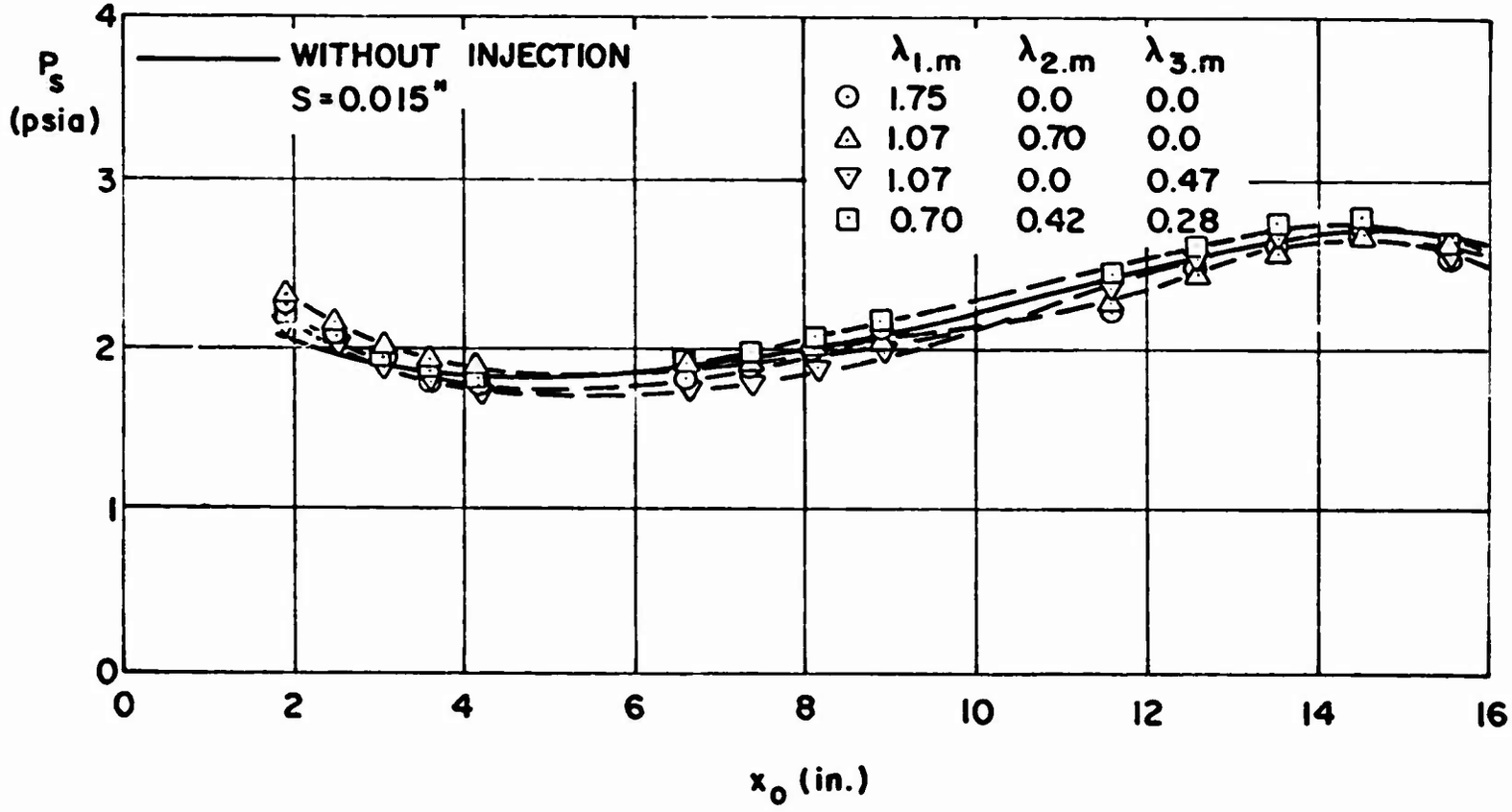

Fig. 22 Distributions of the surface pressure, 2 and 3 slots downstream injection, $s = 0.015$ in., $\alpha = 0^{\circ}$

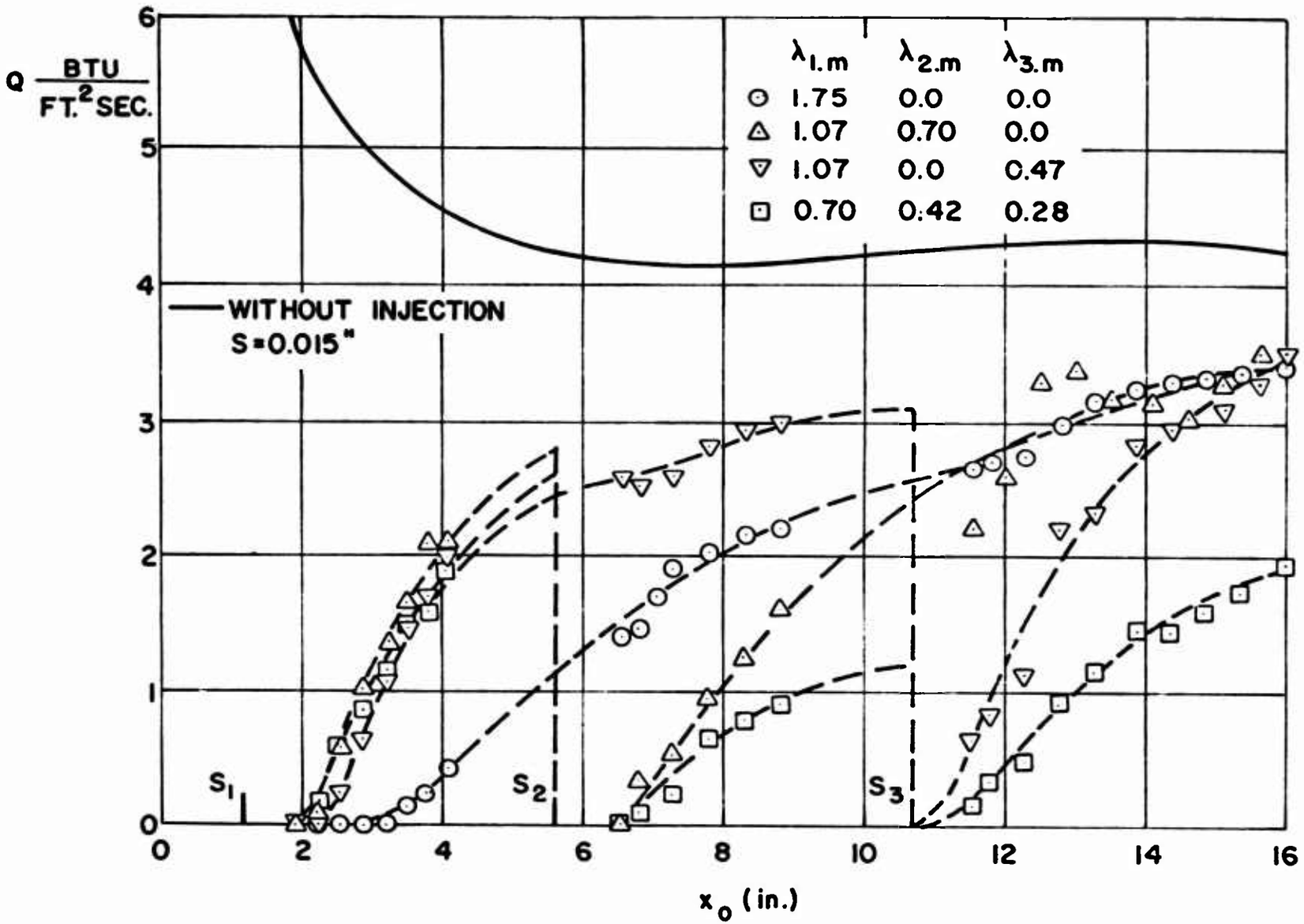

Fig. 23 Distributions of the surface heat transfer, 2 and 3 slots downstream injection, $\alpha = 0^{\circ}$

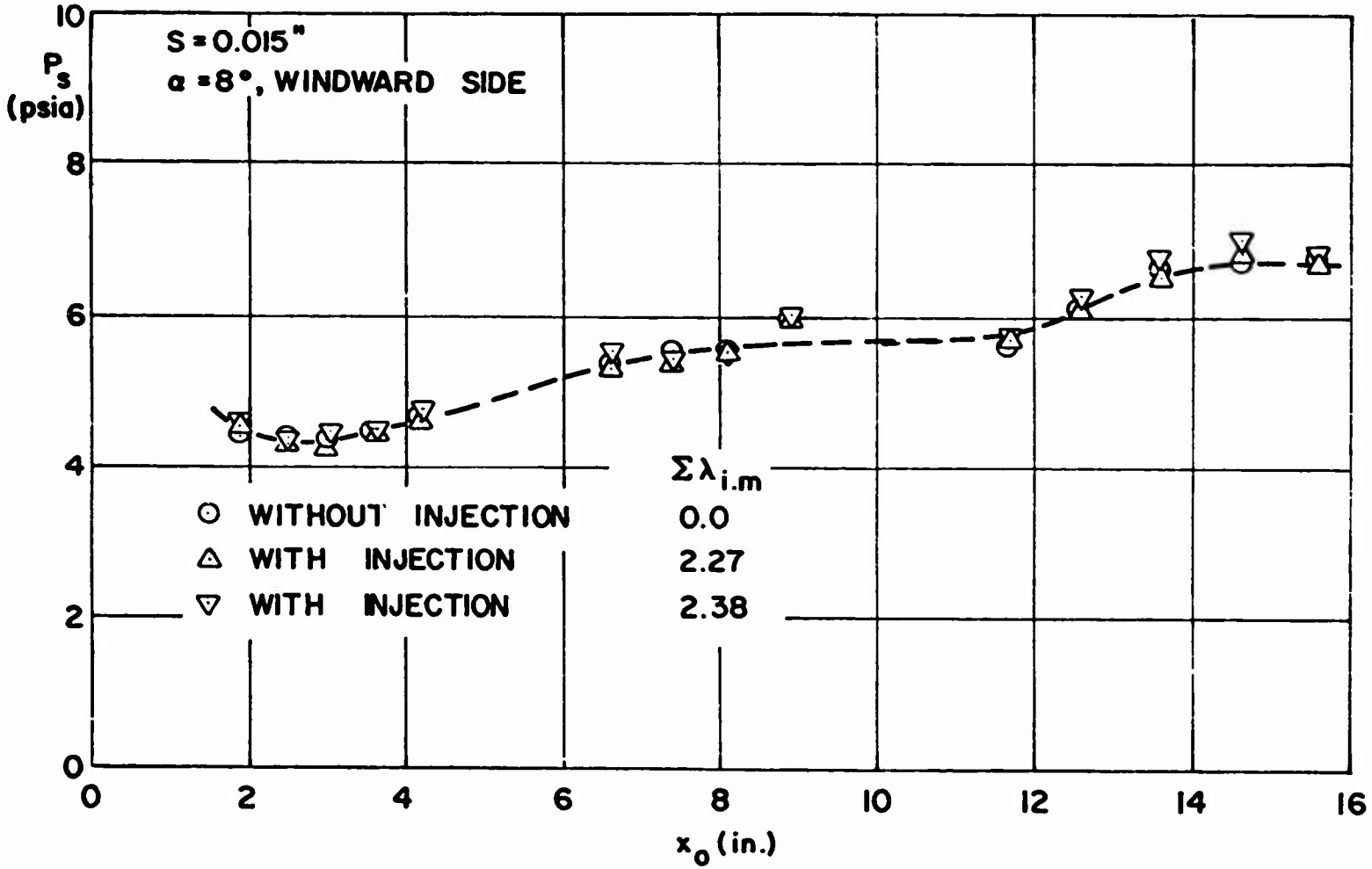

Fig. 24 Distributions of the surface pressure on the windward side at $\alpha = 8^{\circ}$

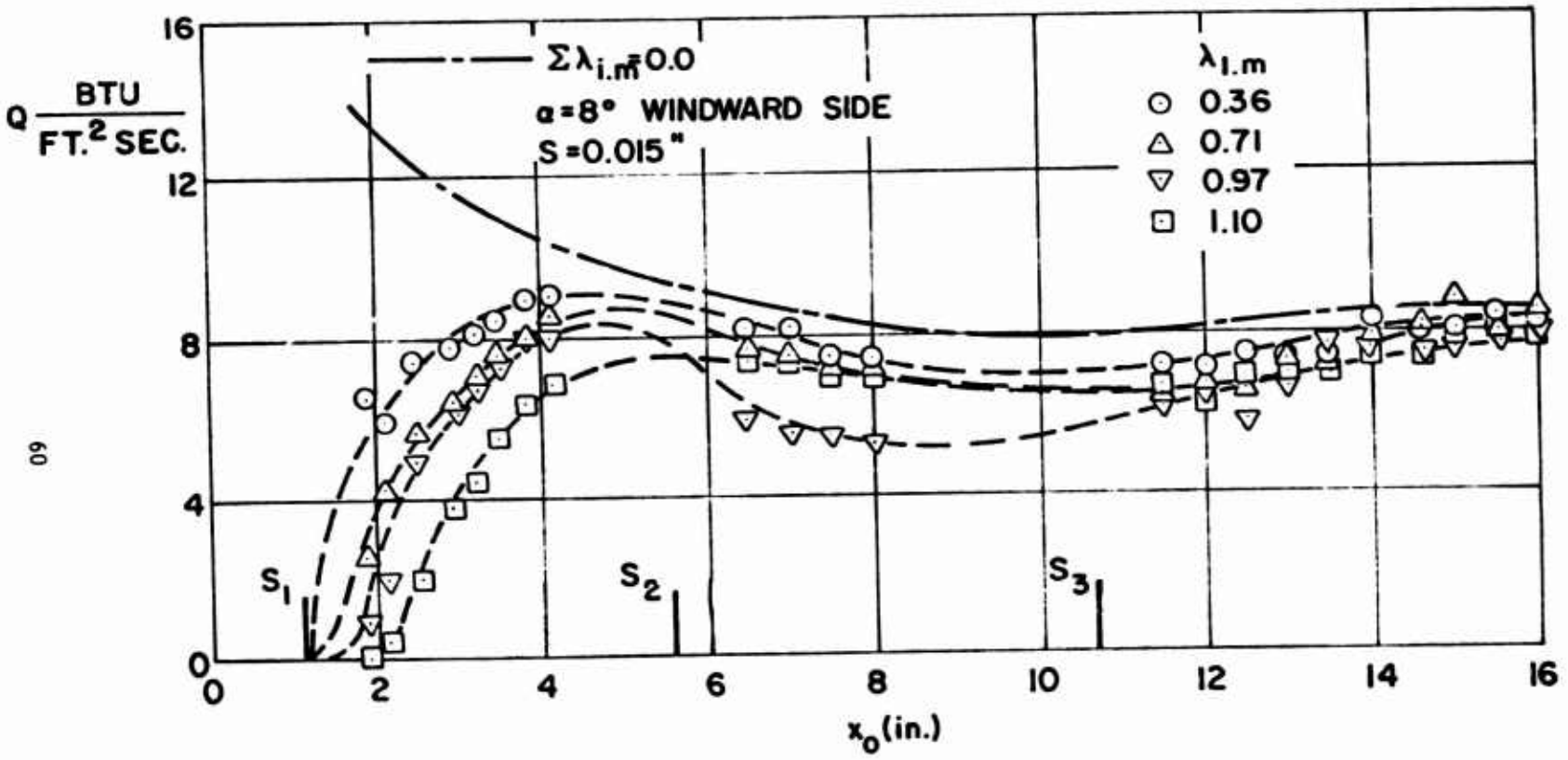

Fig. 25 Distributions of the surface heat transfer rate, 1st slot downstream injection, s = 0.015 in., α = 8°, windward side

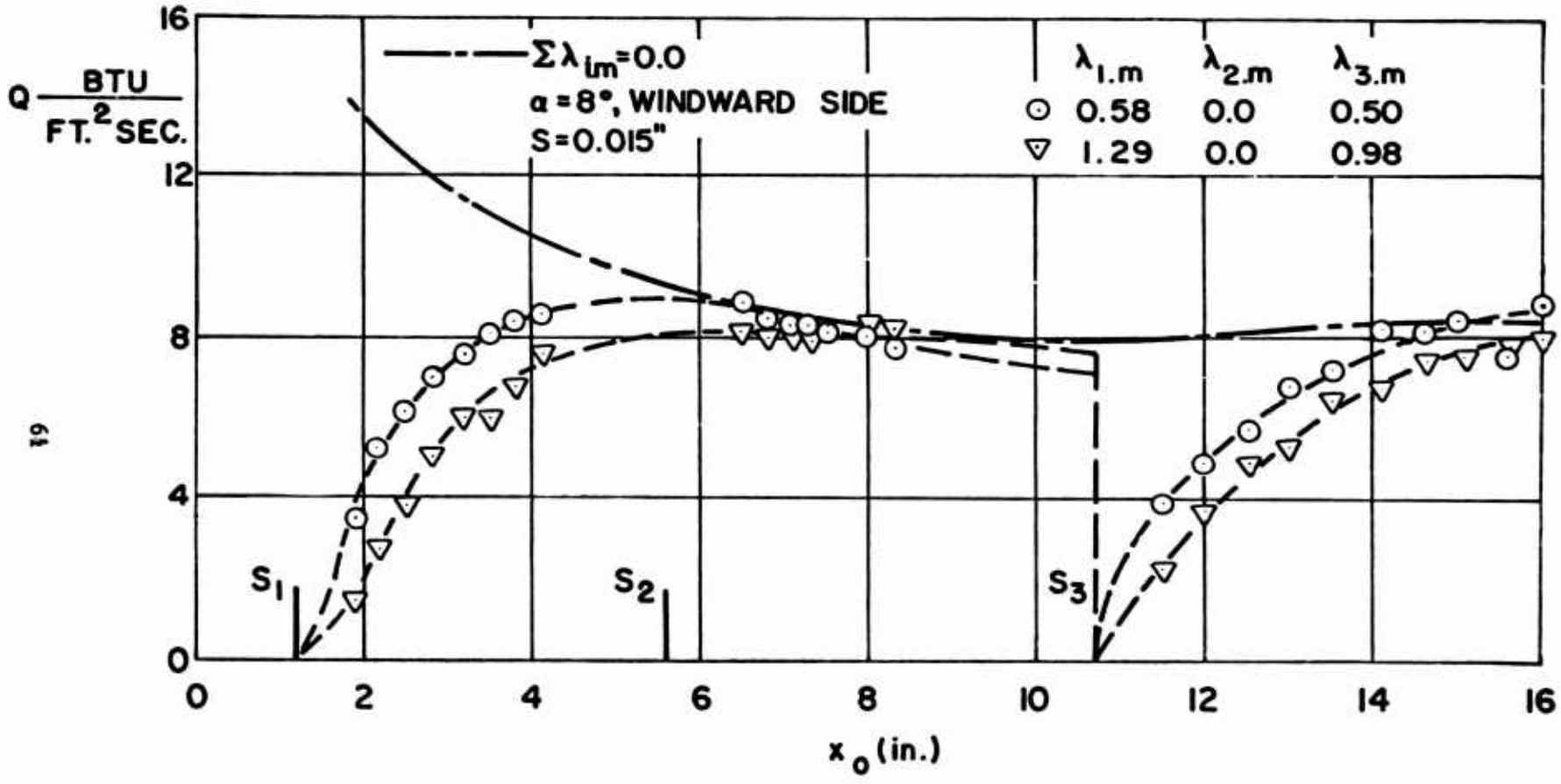

Fig. 26 Distributions of the surface heat transfer rate, 1st and 3rd slot downstream injection, s = 0.015 in., $\alpha = 8^{\circ}$, windward side

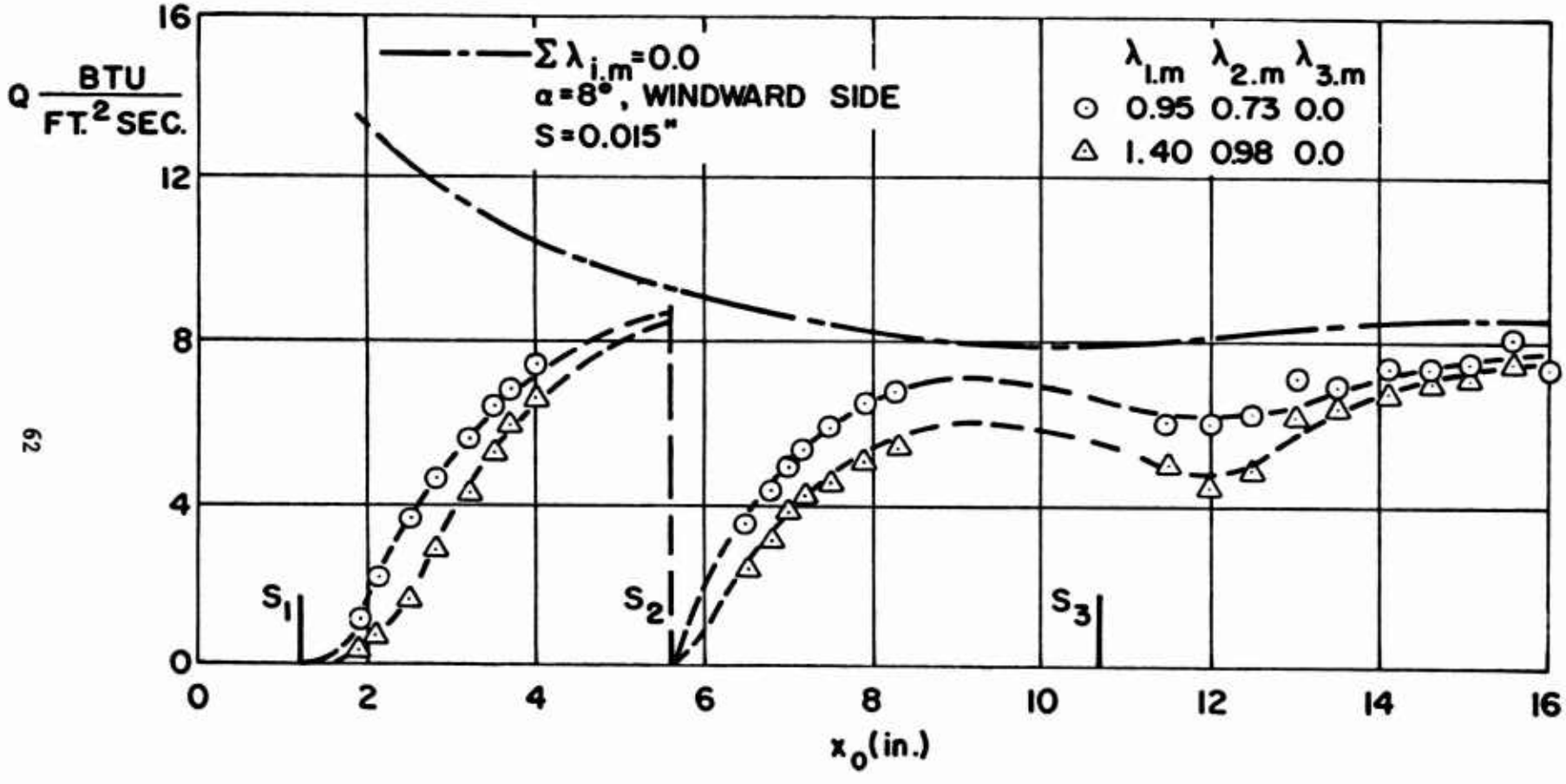

Fig. 27 Distributions of the surface heat transfer rate, 1st and 2nd slot downstream injection, $s = 0.015$ in., $\alpha = 8^{\circ}$, windward side

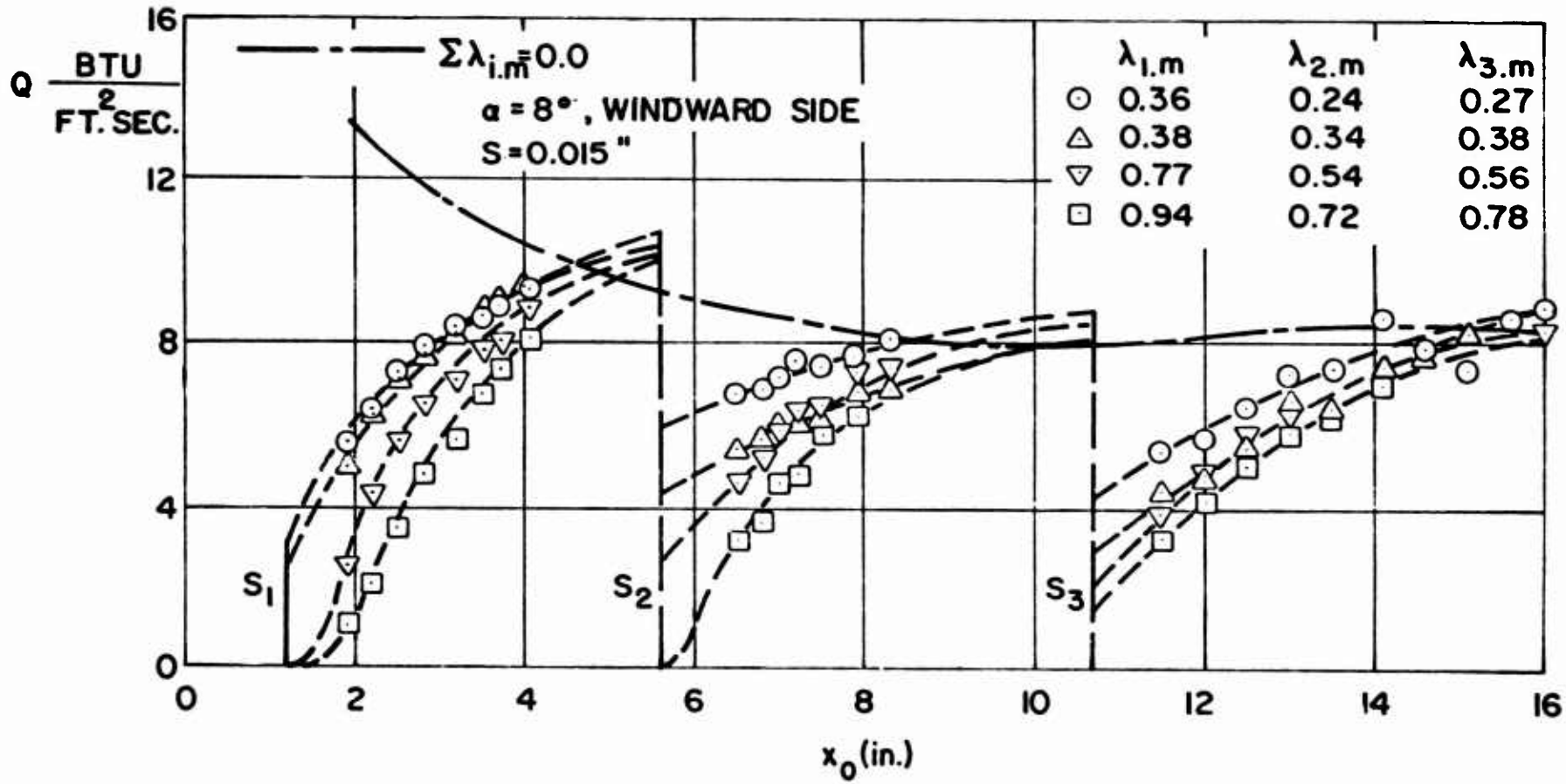

Fig. 28 Distributions of the surface heat transfer rate, 3 slot downstream injection, s = 0.015 in., $\alpha = 8^{o}$, windward side

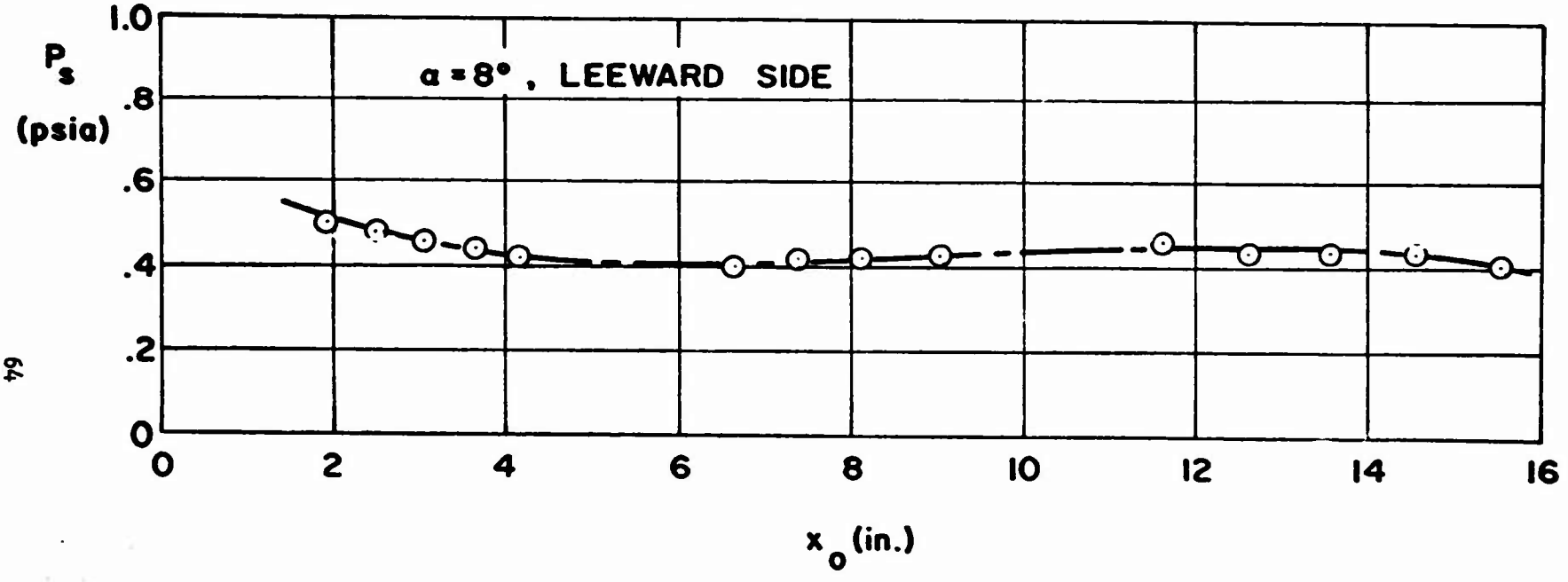

Fig. 29 Distributions of the surface pressure on the leeward side at $\alpha = 8^{\circ}$

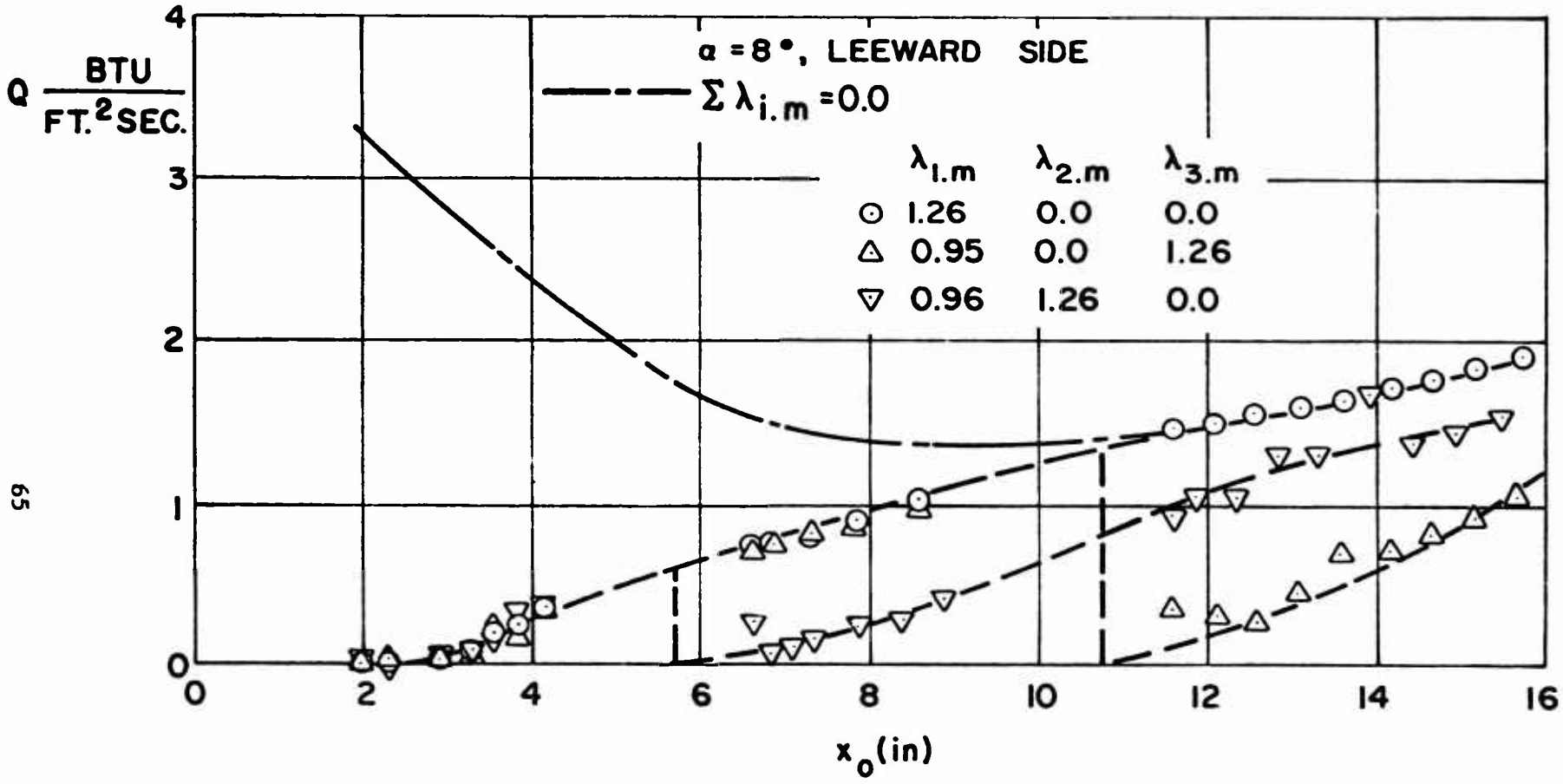

Fig. 30 Distributions of the surface heat transfer rate on the leeward side, α = 8o

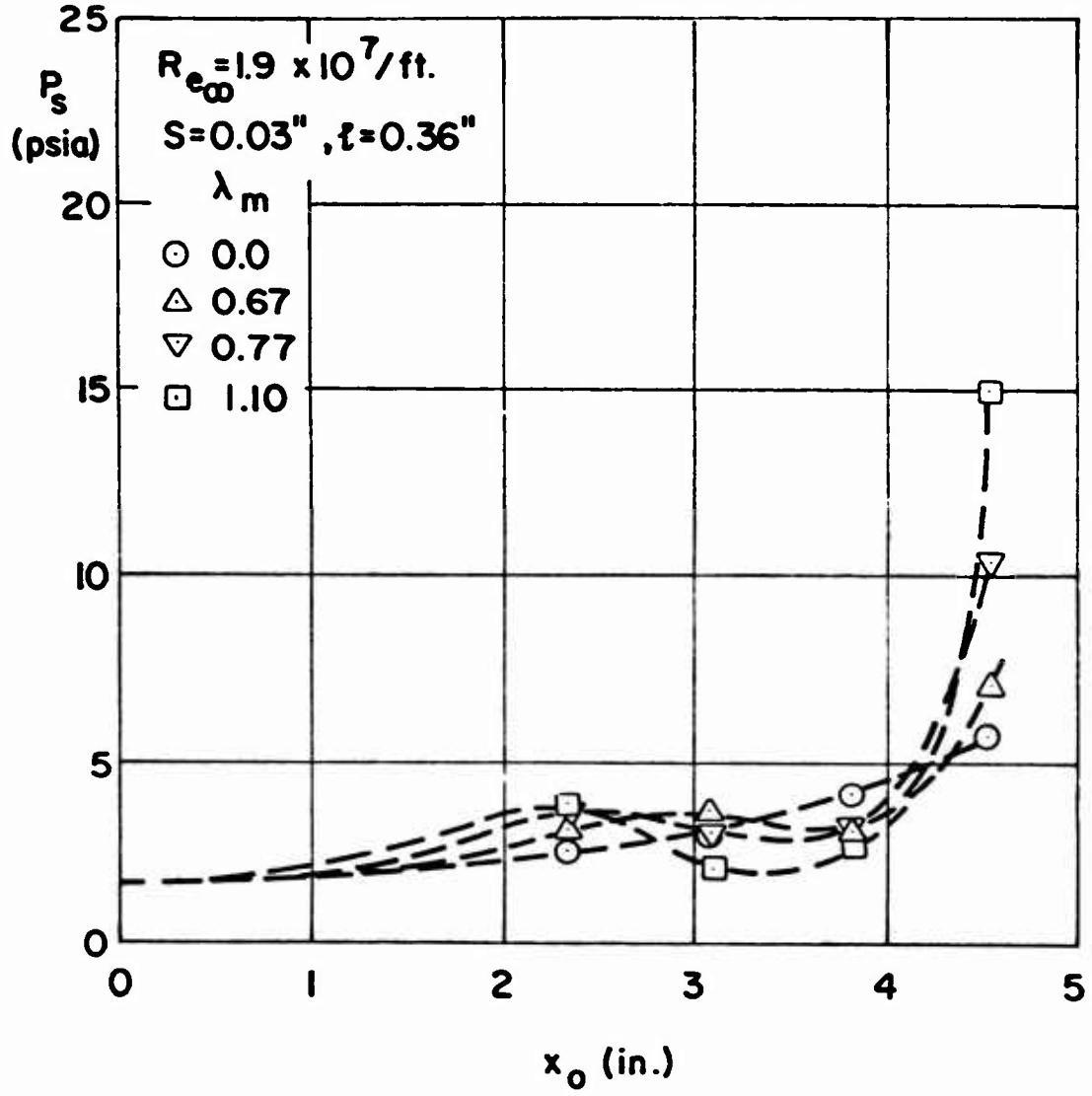

Fig. 31 Distributions of the surface pressure of the upstream injection

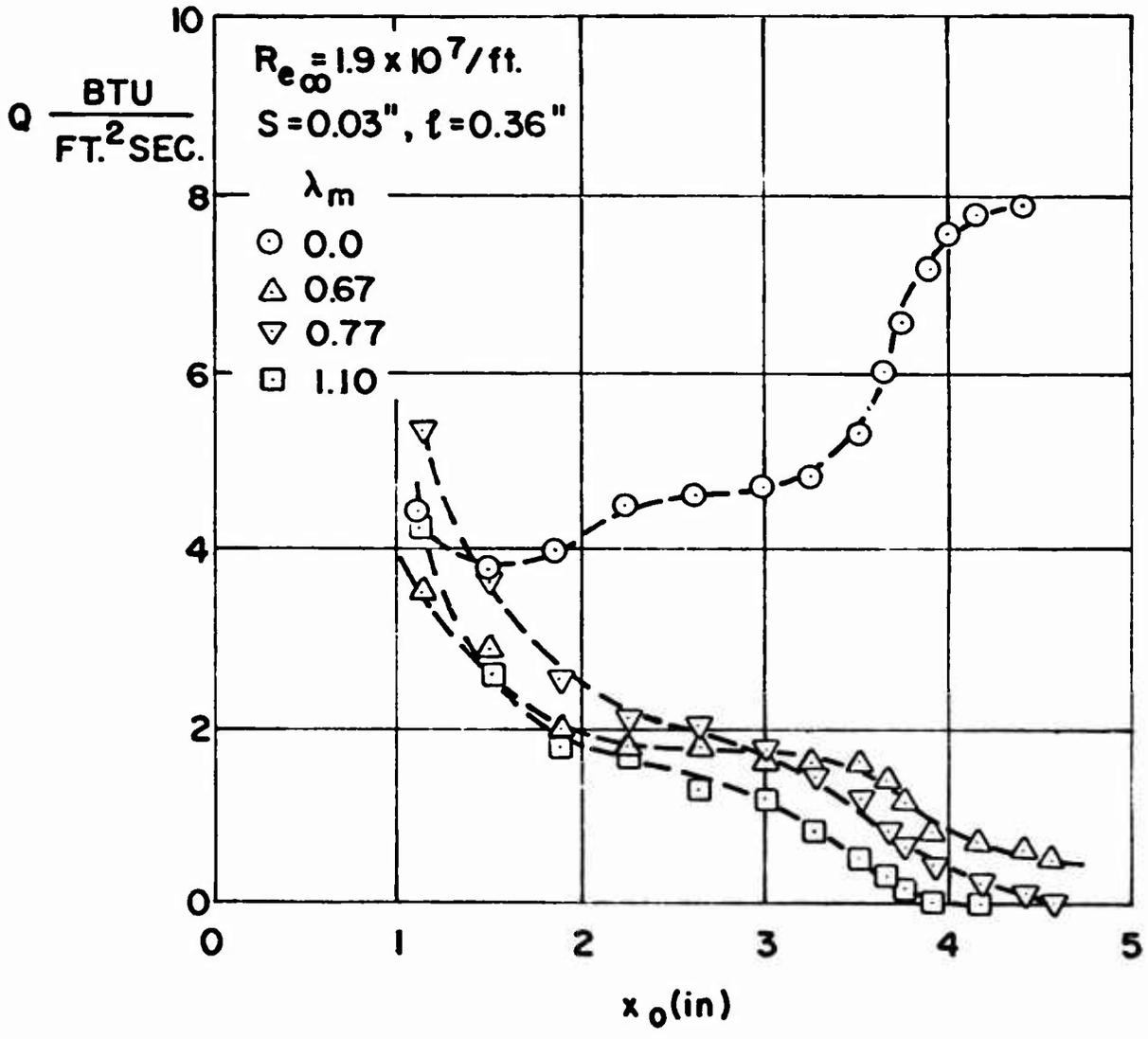

Fig. 32 Distributions of the surface heat transfer rate of the upstream injection

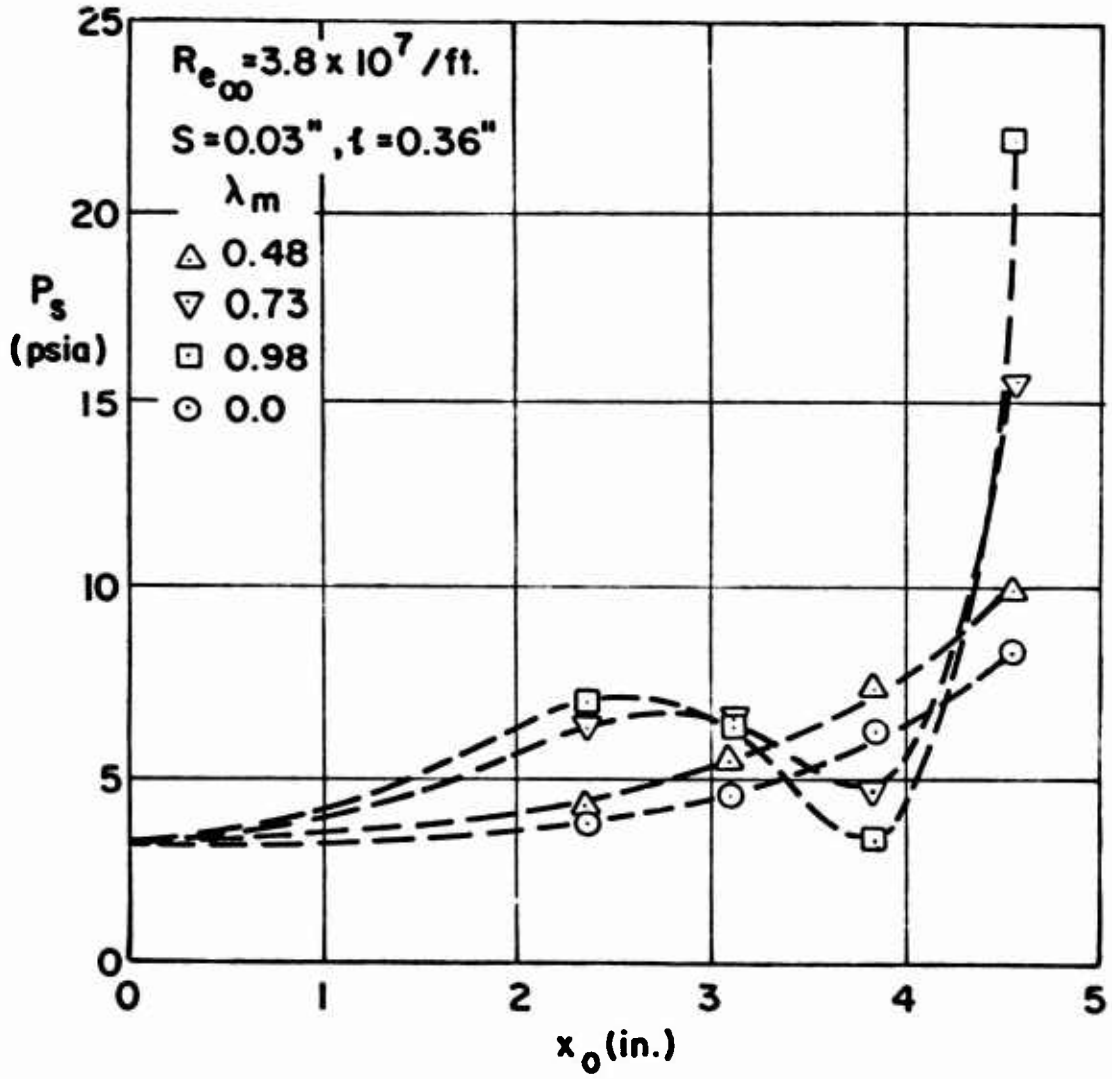

Fig. 33 Distributions of the surface pressure of the upstream injection

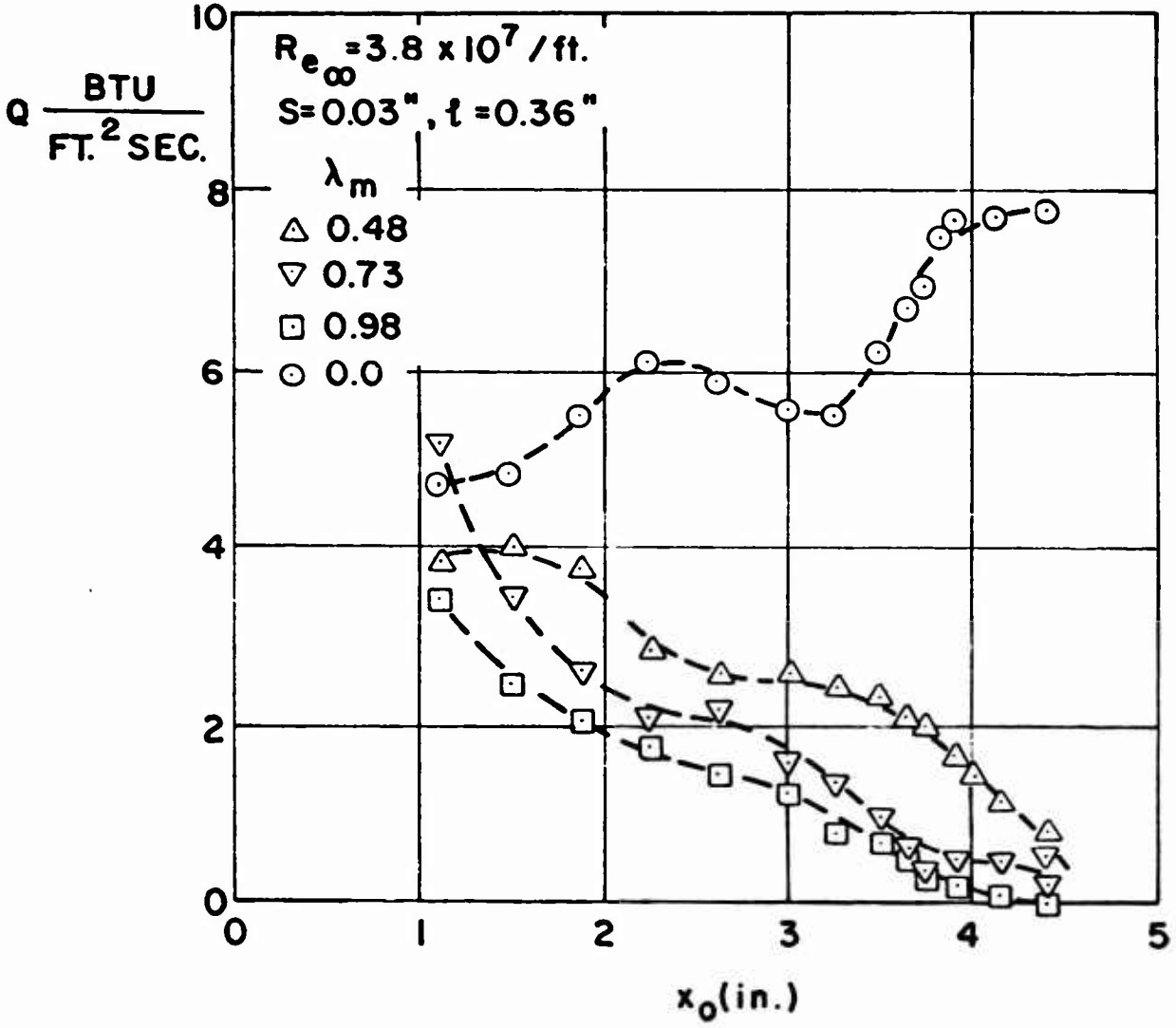

Fig. 34 Distributions of the surface heat transfer rate of the upstream injection

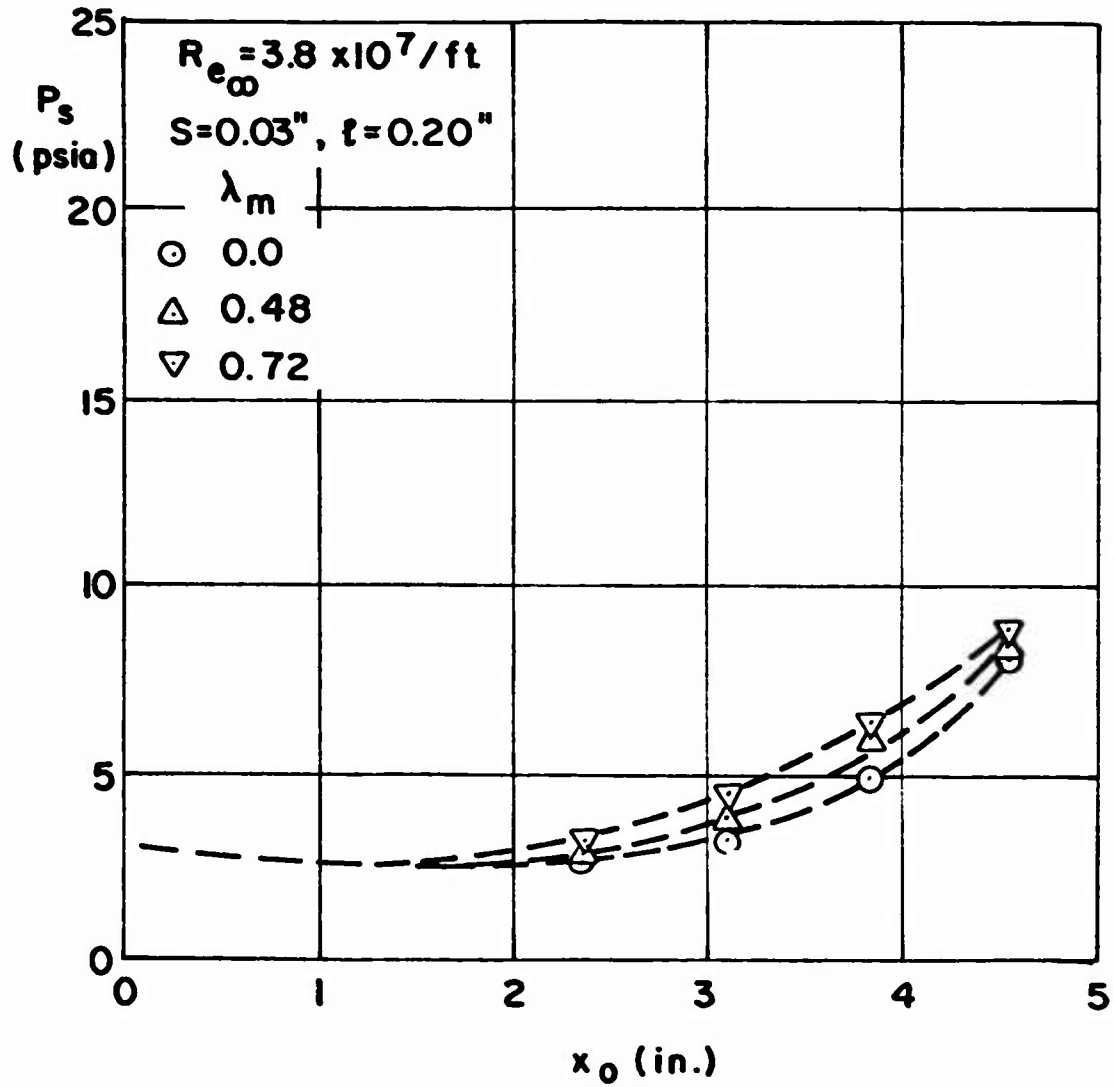

Fig. 35 Distributions of the surface pressure of the upstream injection

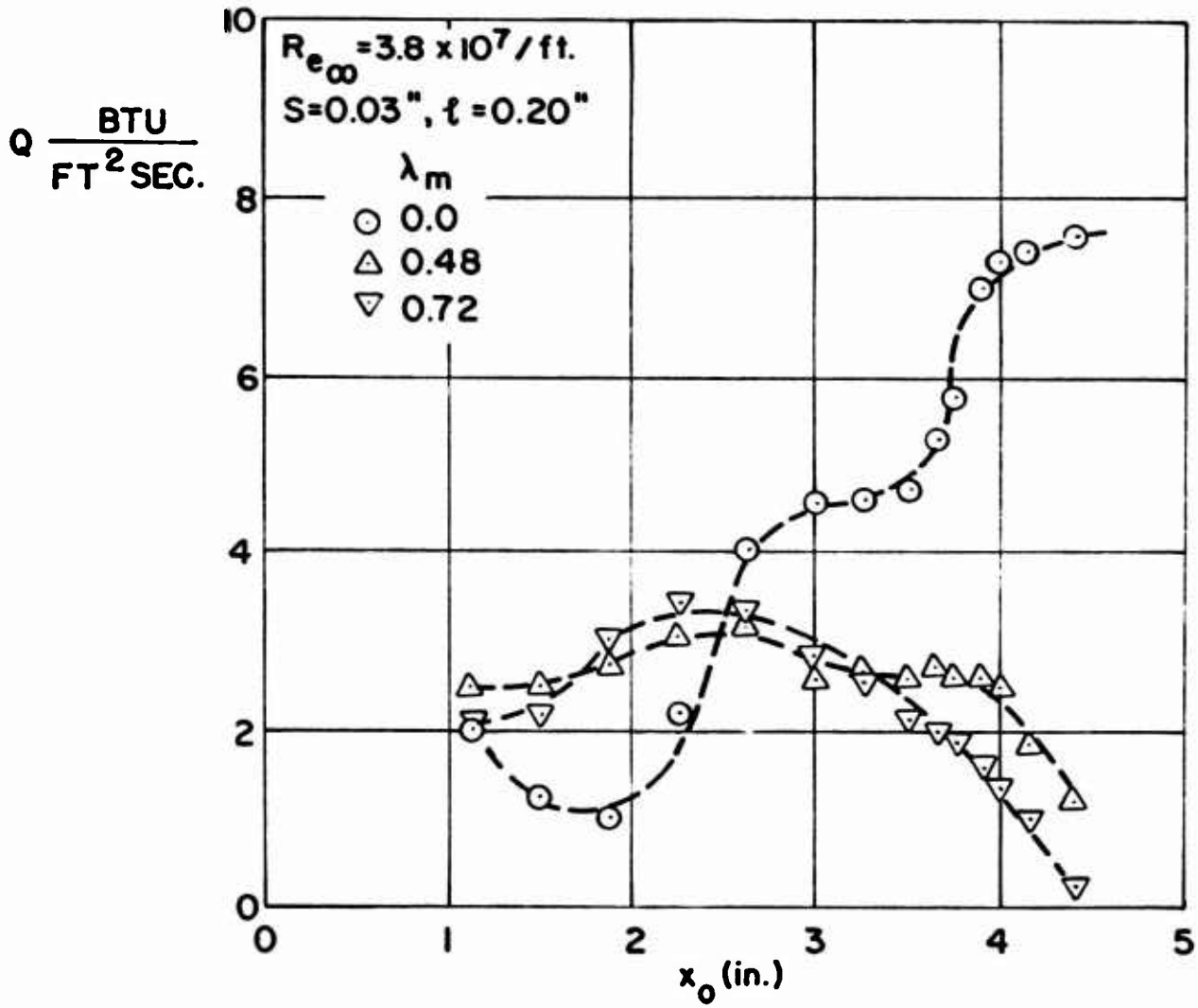

Fig. 36 Distributions of the surface heat transfer rate of the upstream injection

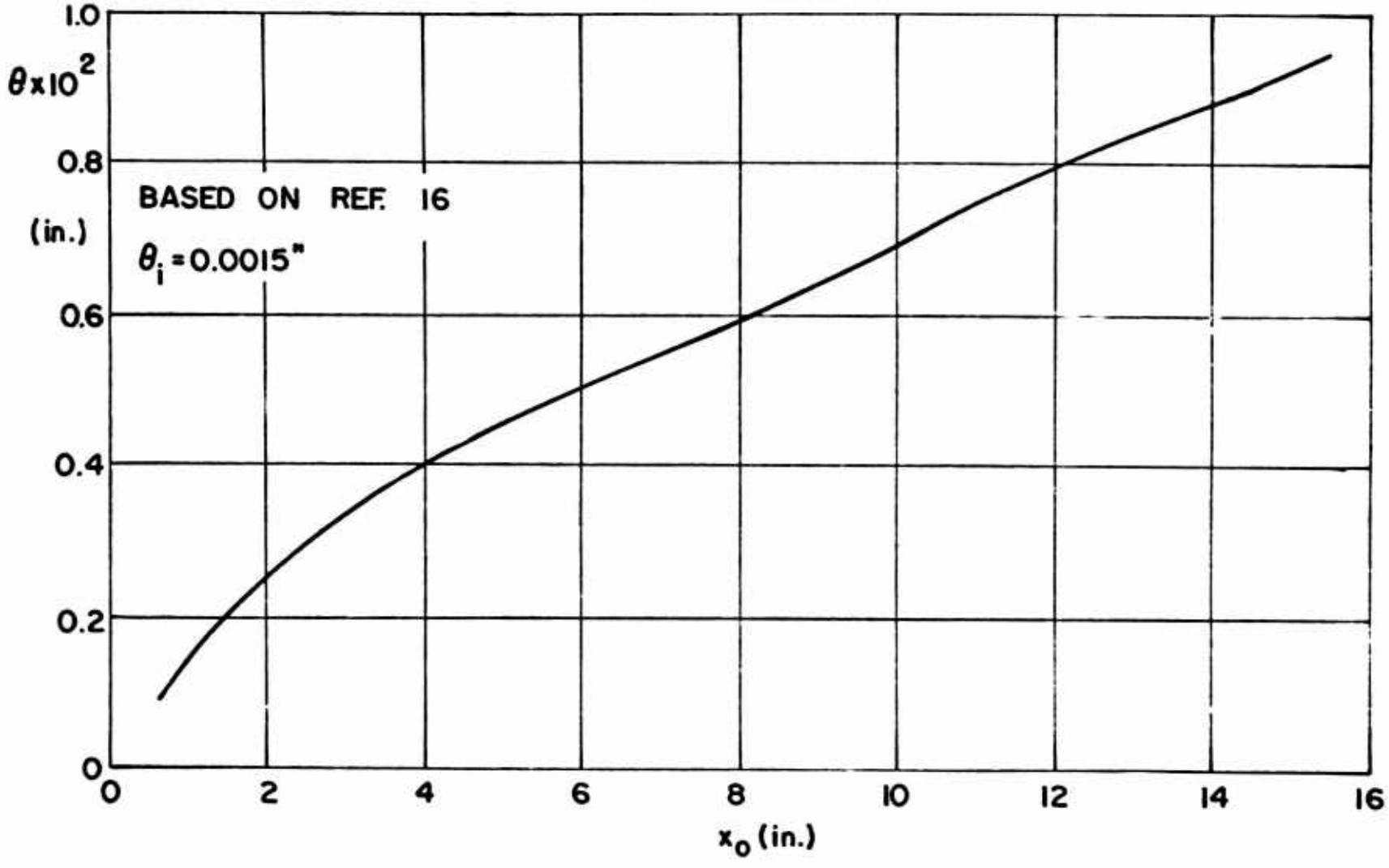

Fig. 37 Boundary layer momentum thickness along the surface of the blunt nosed cone, $\alpha = 0^{o}$, without slot injection

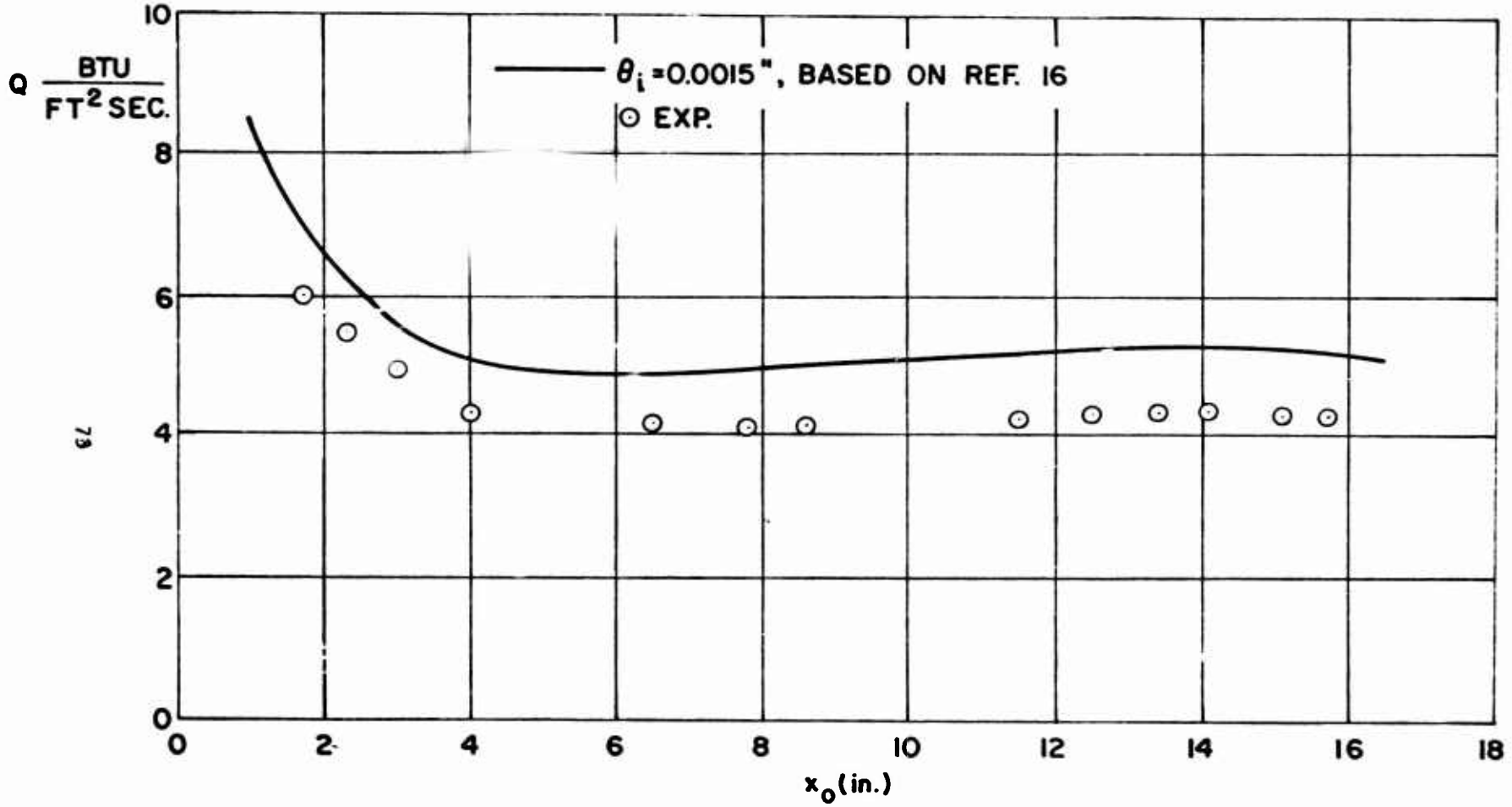

Fig. 38 Comparison of the surface heat transfer rates between experiment and theory, without downstream injection

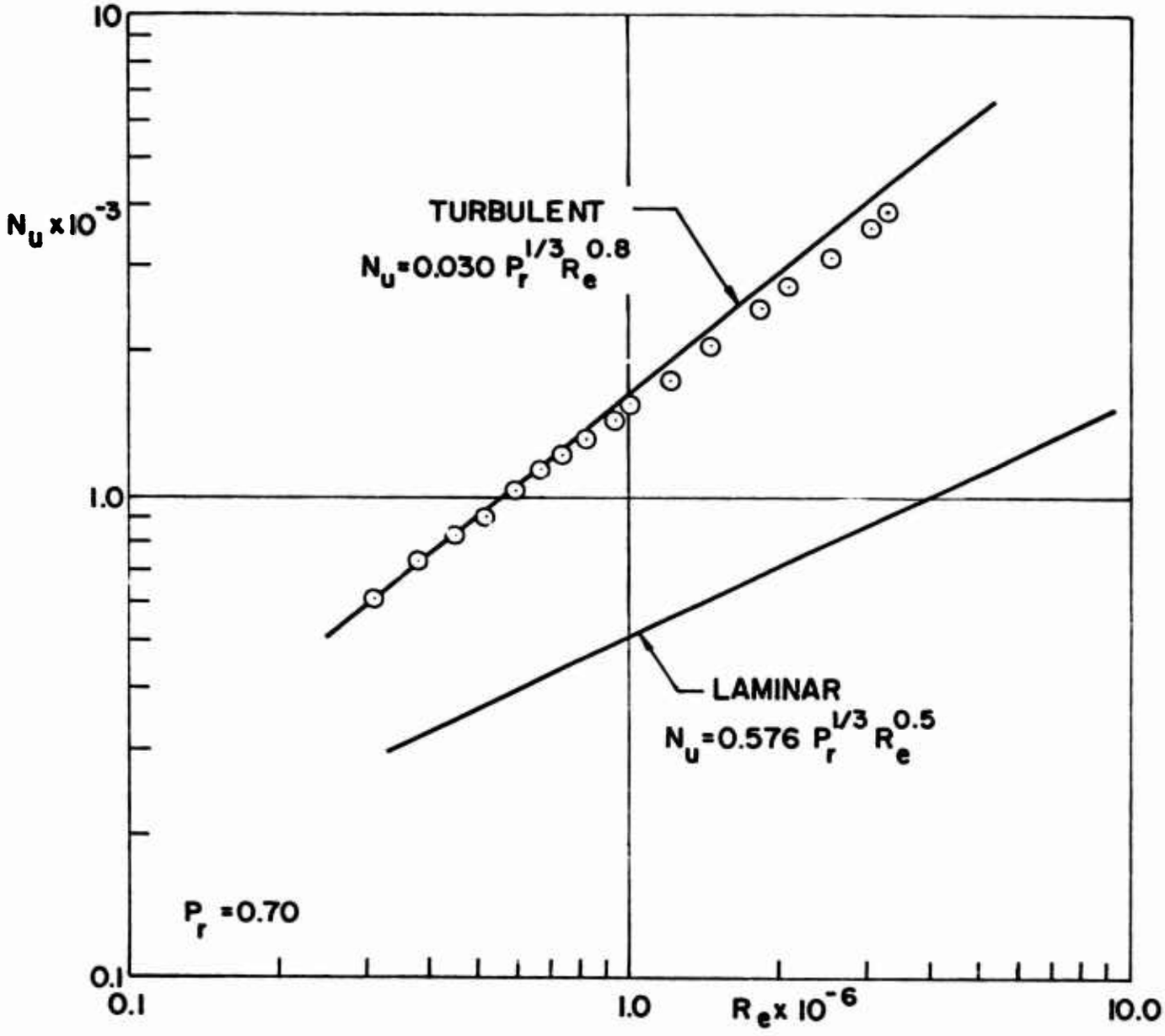

Fig. 39 Nusselt number Reynolds number relation between experiment and FPRE Method, with downstream injection

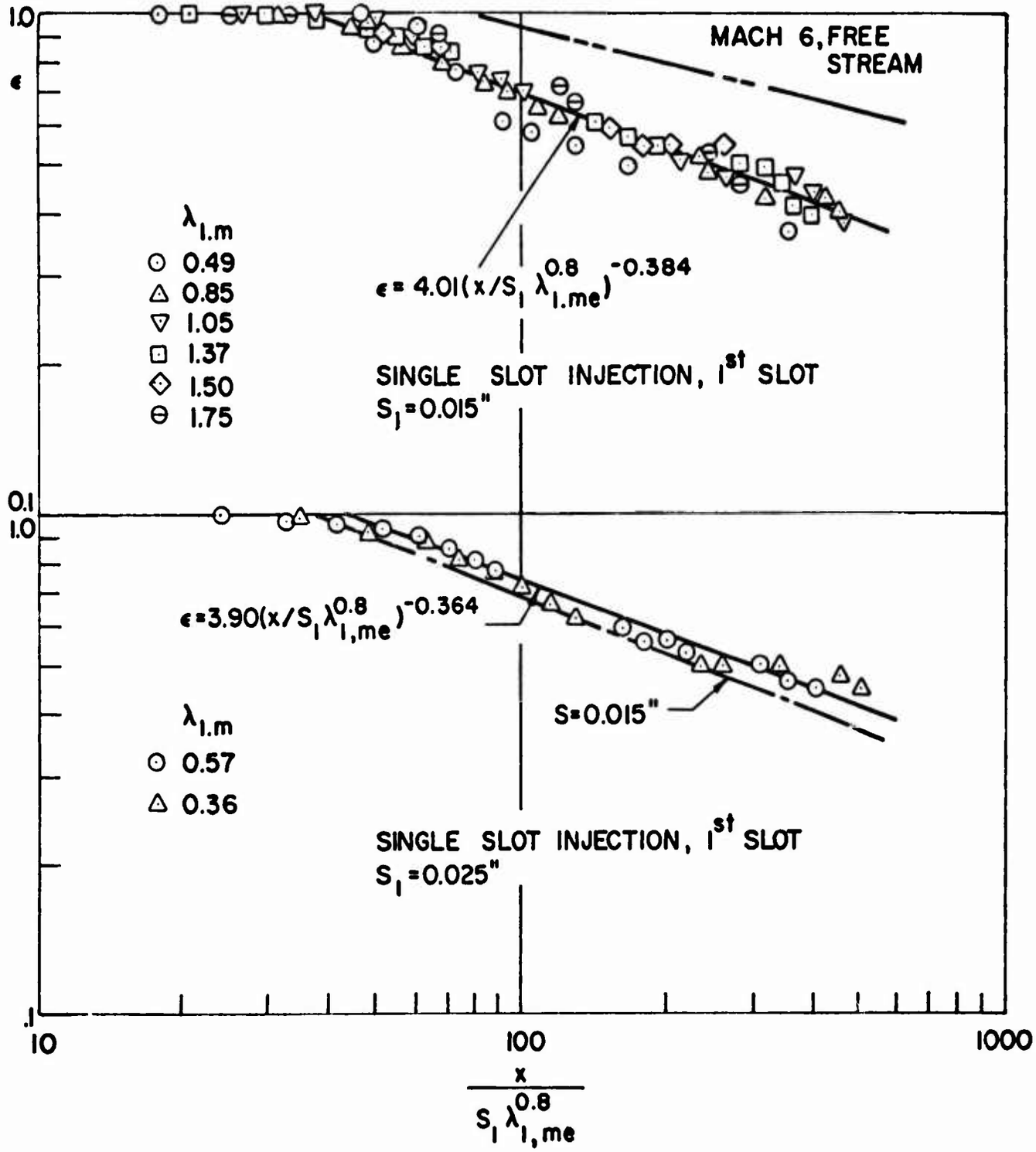

Fig. 40 Correlations of the experimental film cooling effectiveness due to 1st slot downstream injection, $\alpha = 0^{o}$

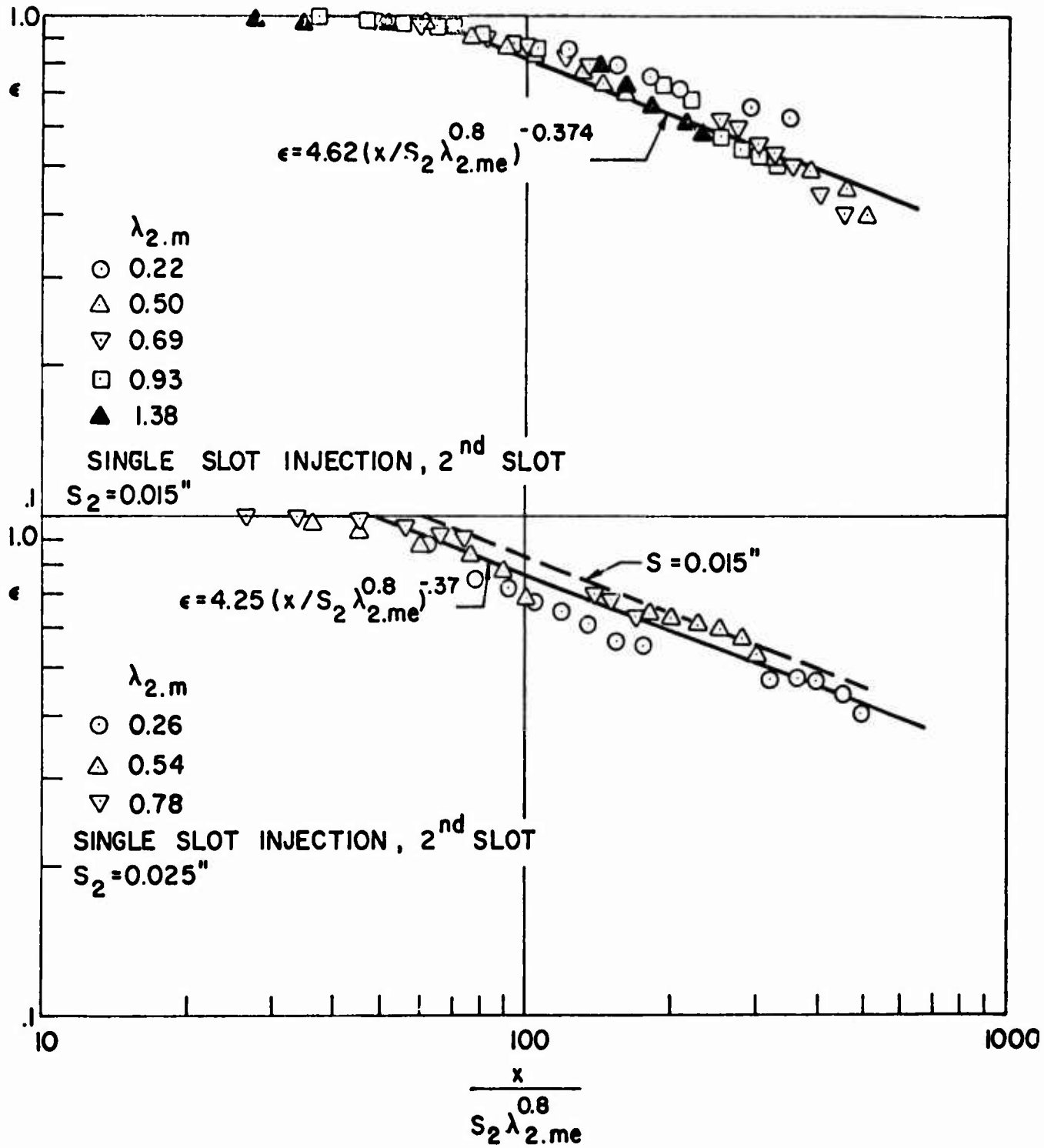

Fig. 41 Correlations of the experimental film cooling effectiveness due to 2nd slot downstream injection, $\alpha = 0^{\circ}$

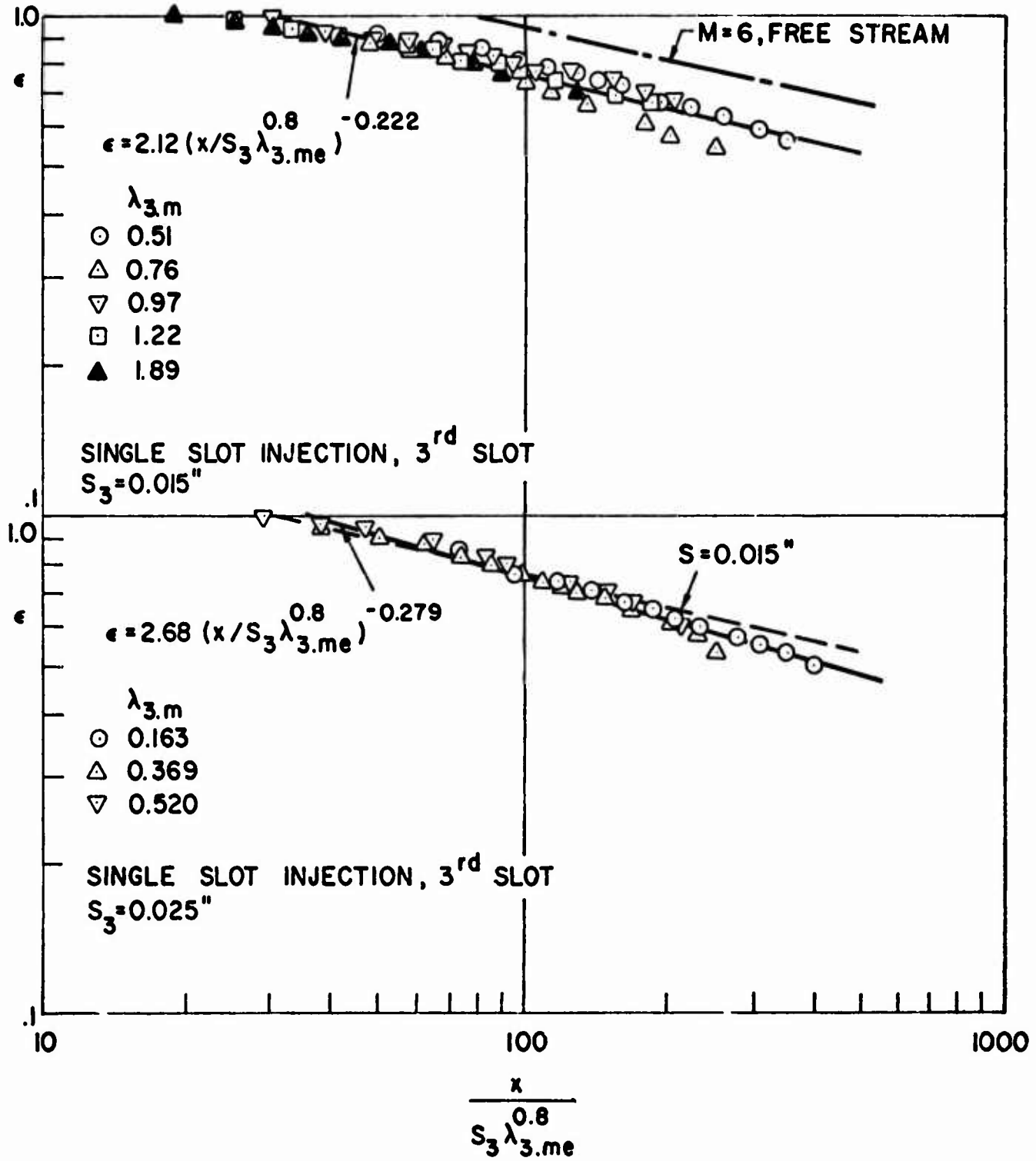

Fig. 42 Correlations of the experimental film cooling effectiveness due to 3rd slot downstream injection $\alpha = 0^{\circ}$

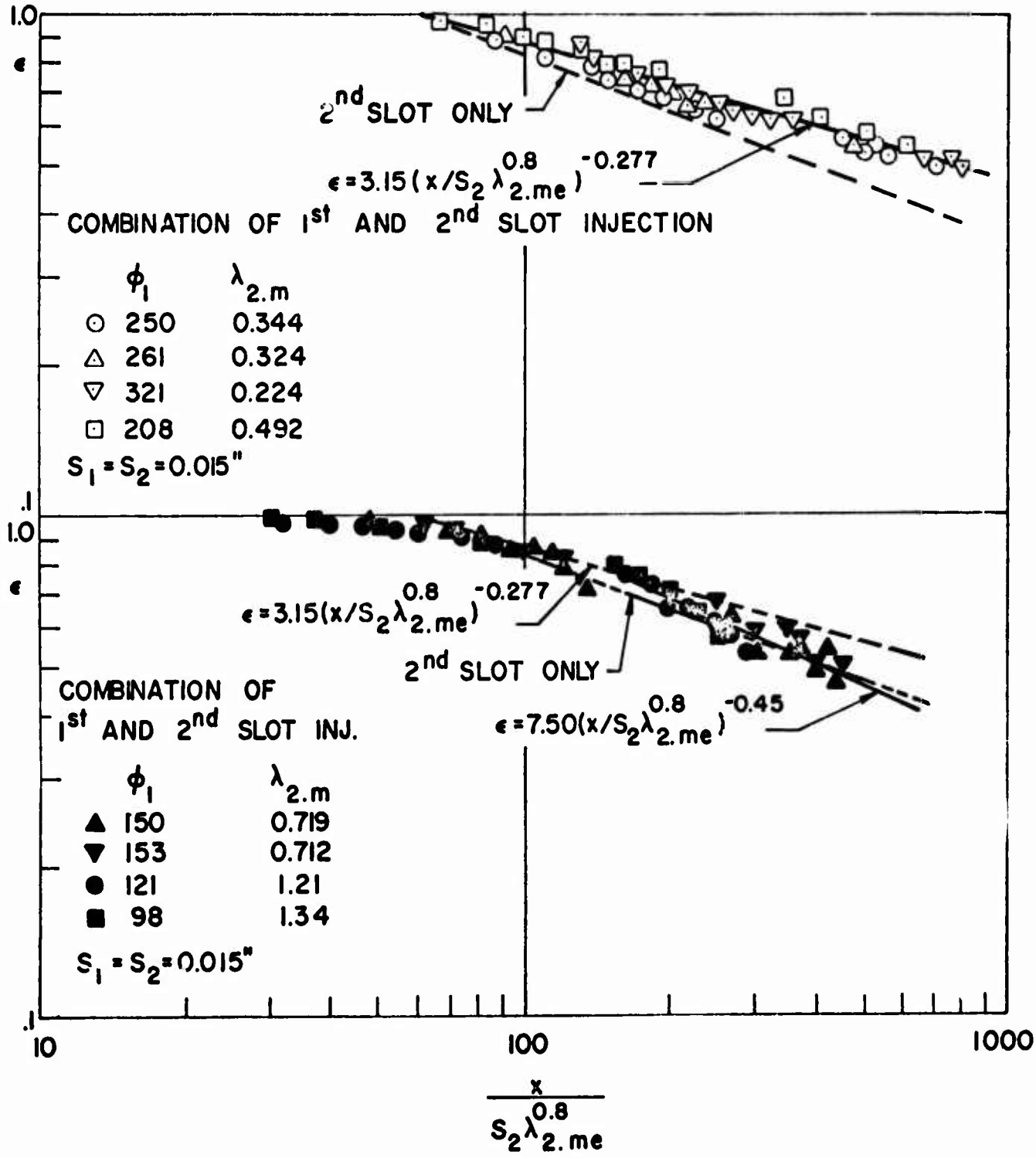

Fig. 43 Correlations of experimental film cooling effectiveness due to 1st and 2nd slot downstream injection, $\alpha = 0^{\circ}$

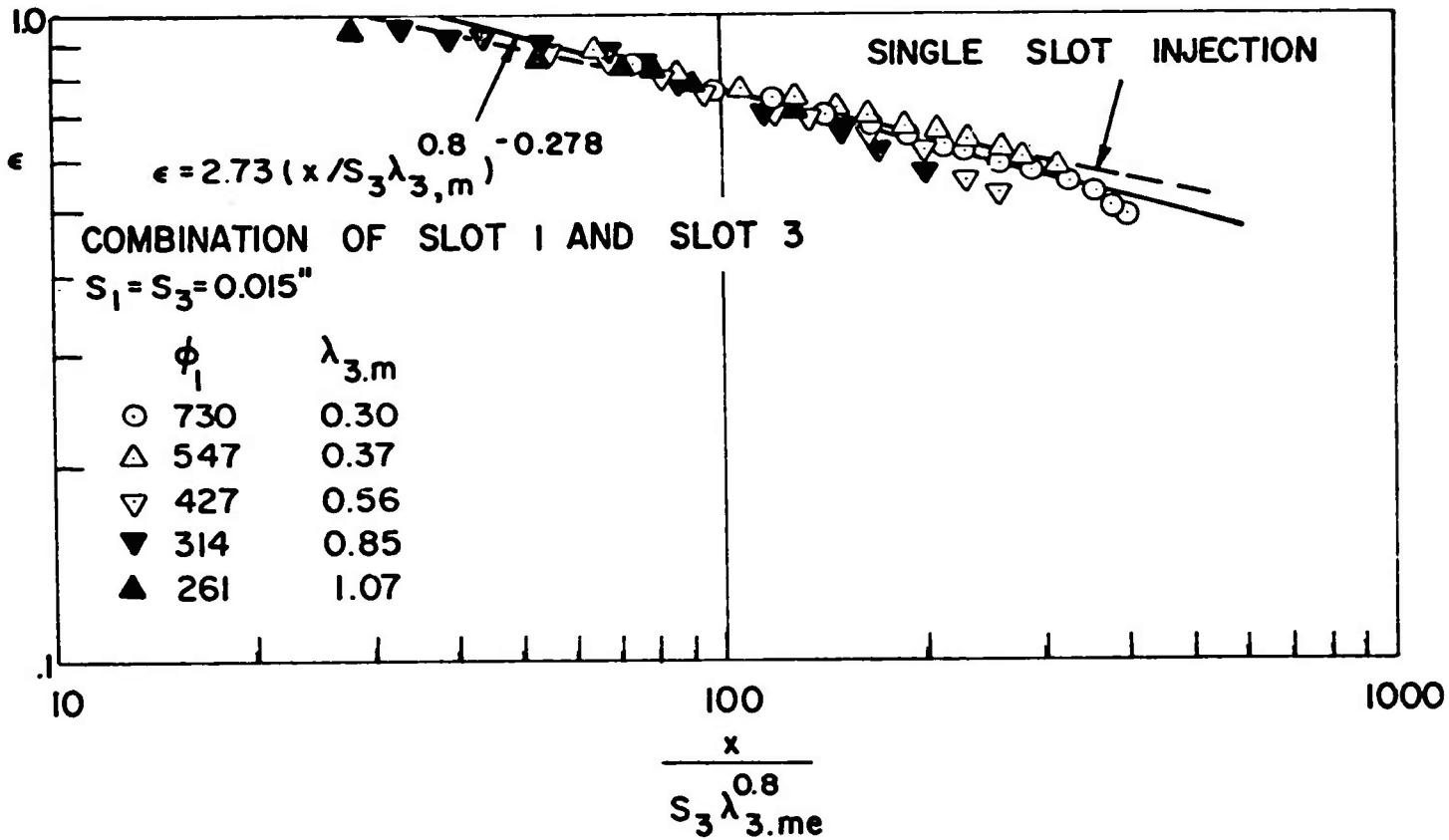

Fig. 44 Correlations of the experimental film cooling effectiveness due to the 1st and 3rd slot downstream injection, $\alpha = 0^{\circ}$

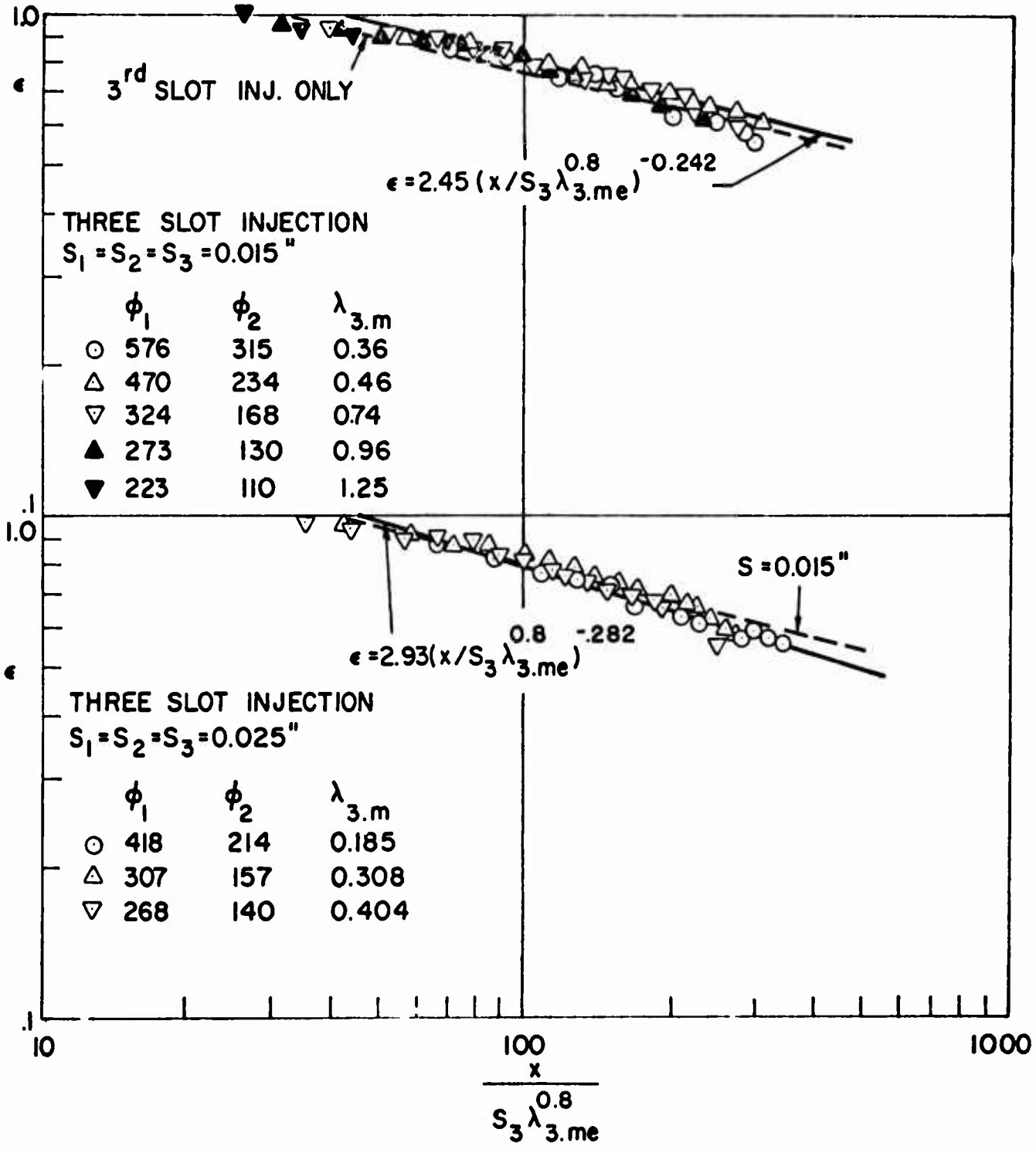

Fig. 45 Correlations of the experimental film cooling effectiveness due to three slot downstream injection, $\alpha = 0^o$

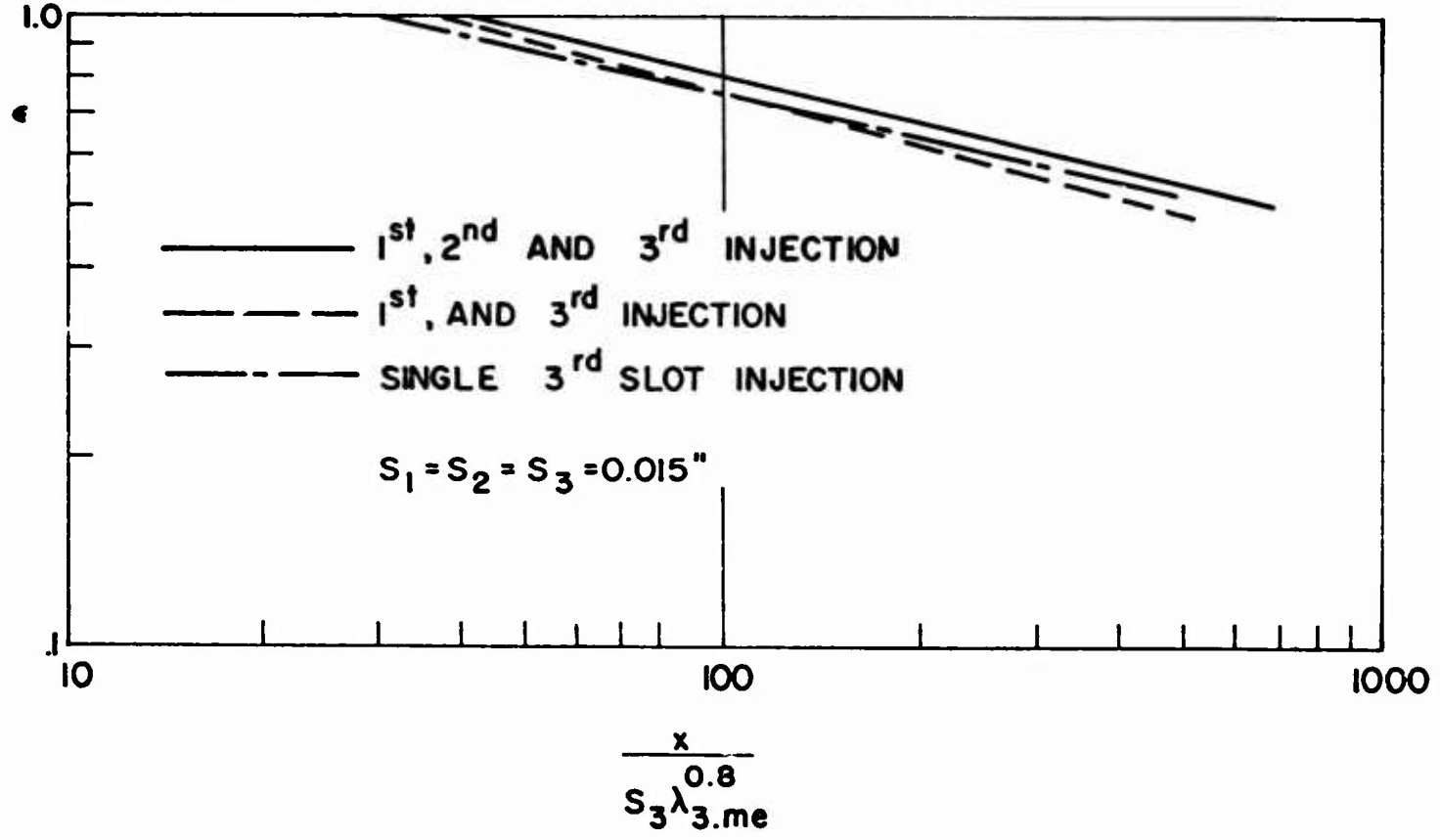

Fig. 46 Comparison of the effectiveness correlation among single and multiple slot downstream injection, $\alpha = 0^{\circ}$

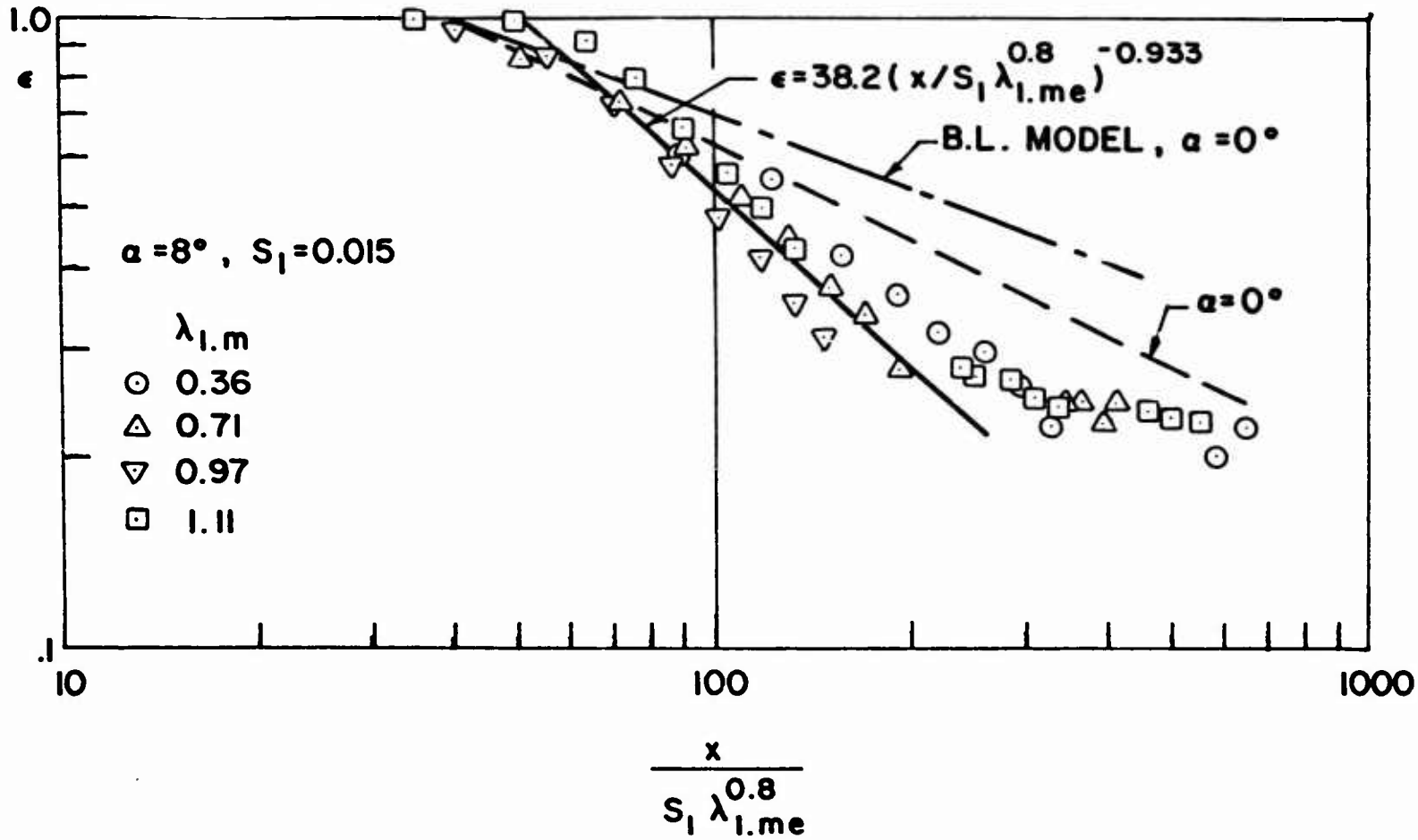

Fig. 47 Correlation of the experimental film cooling effectiveness, 1st slot downstream injection, $\alpha = 8^{\circ}$, windward side

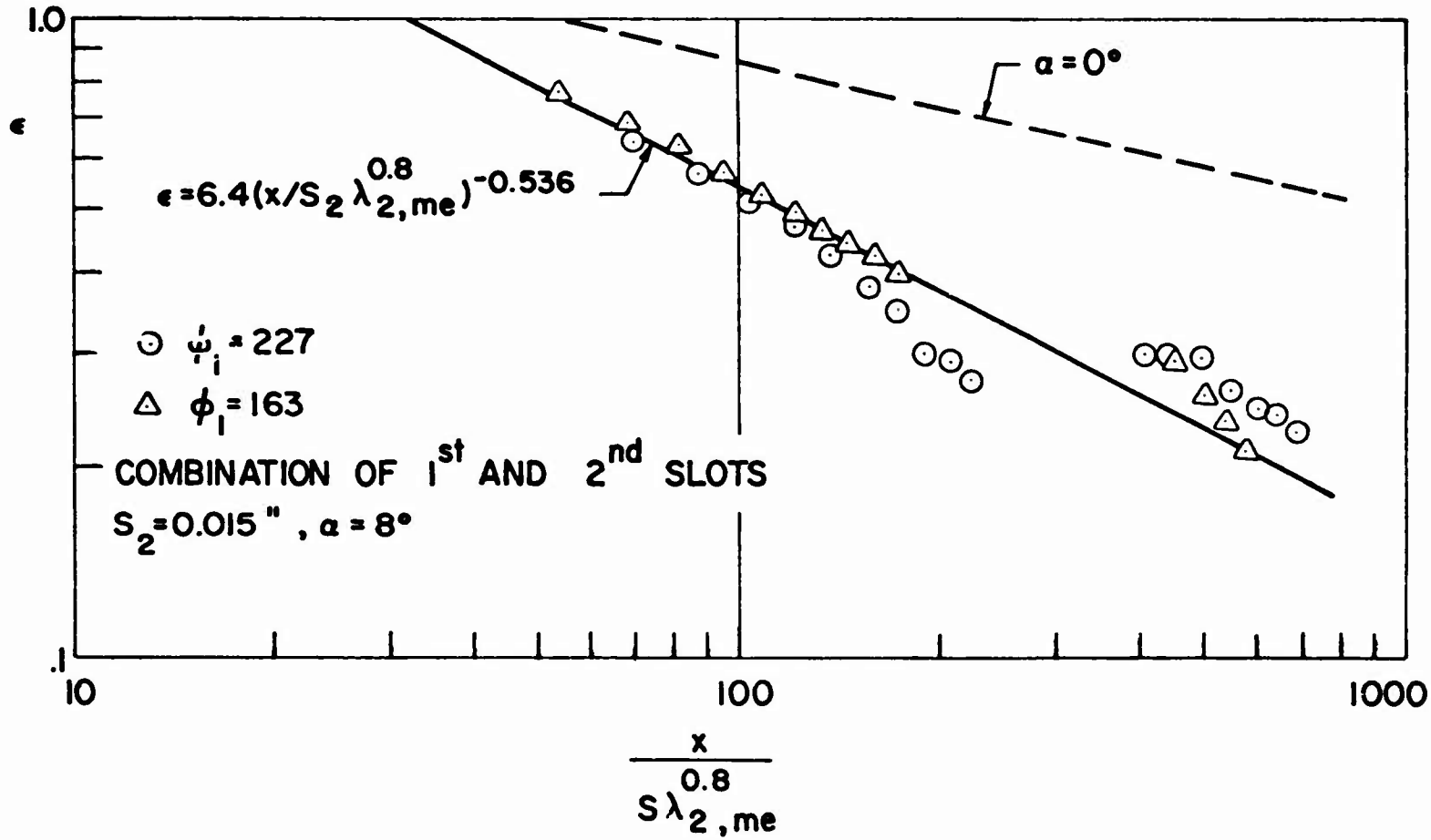

Fig. 48 Correlation of the experimental film cooling effectiveness, 1st and 2nd slot downstream injection, $\alpha = 8^{\circ}$, windward side

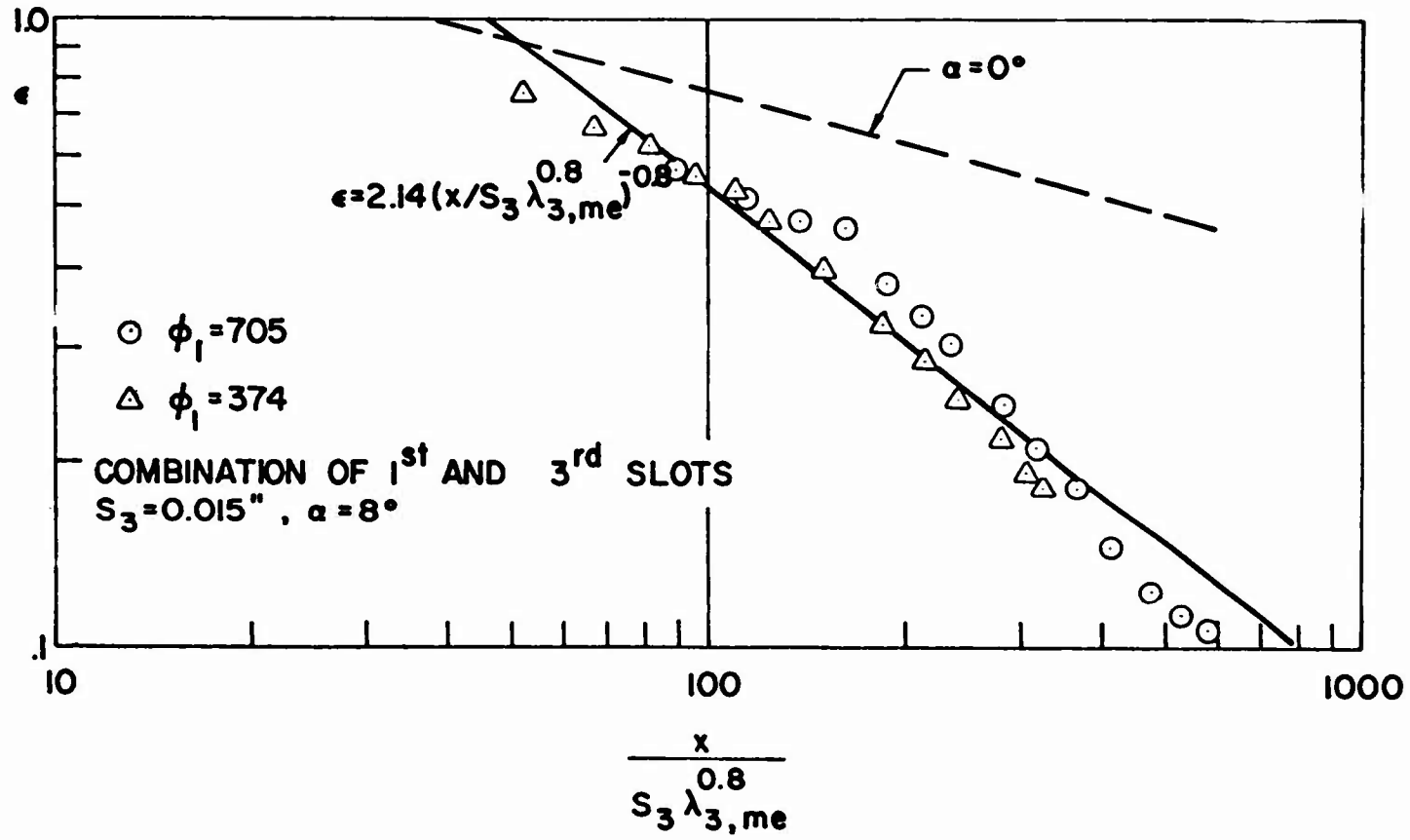

Fig. 49 Correlations of the experimental film cooling effectiveness, 1st and 3rd slot downstream injection, $\alpha = 8^{\circ}$, windward side

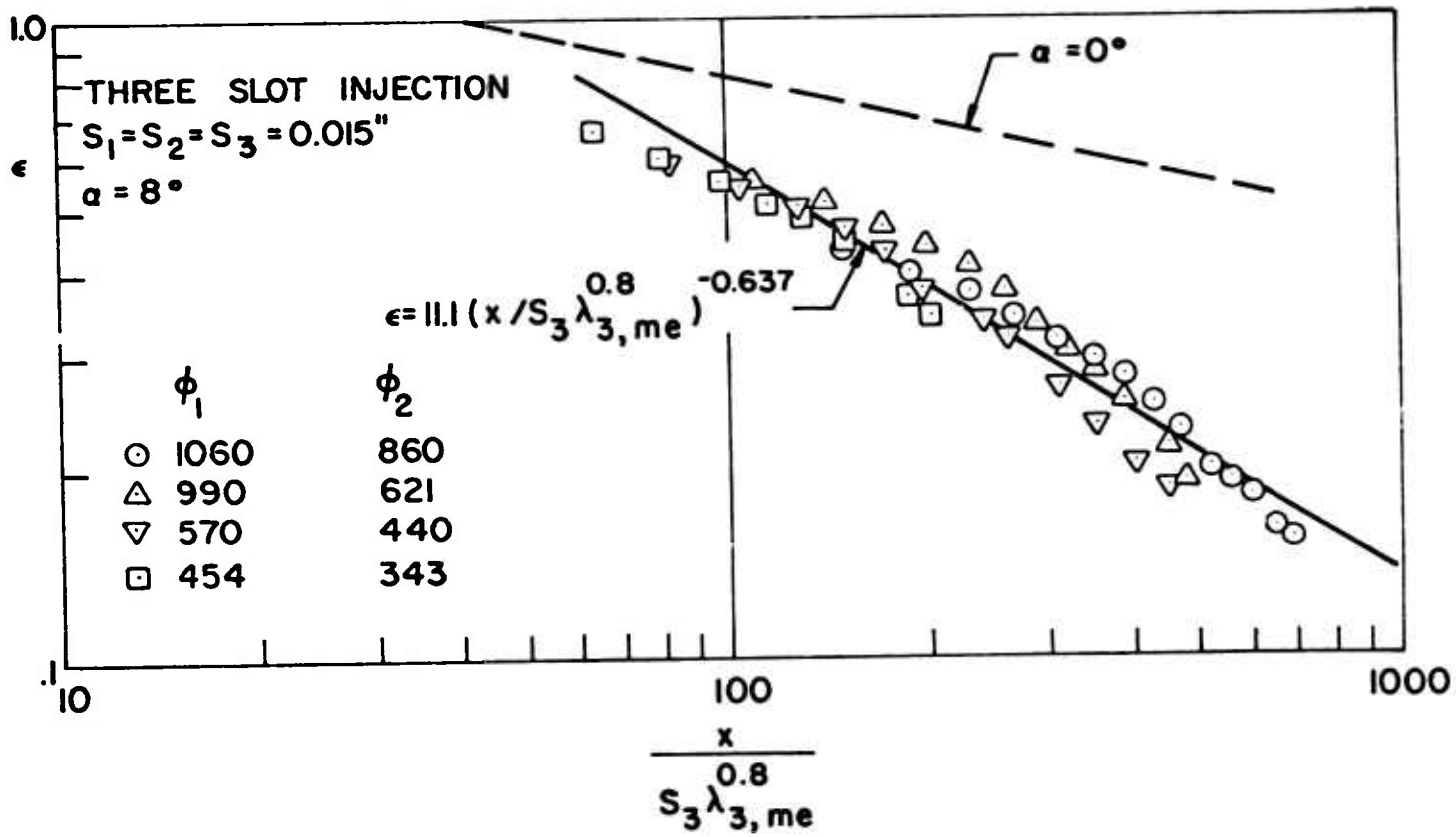

Fig. 50 Correlation of the experimental film cooling effectiveness, 3 slot downstream injection, $\alpha = 8^{\circ}$, windward side

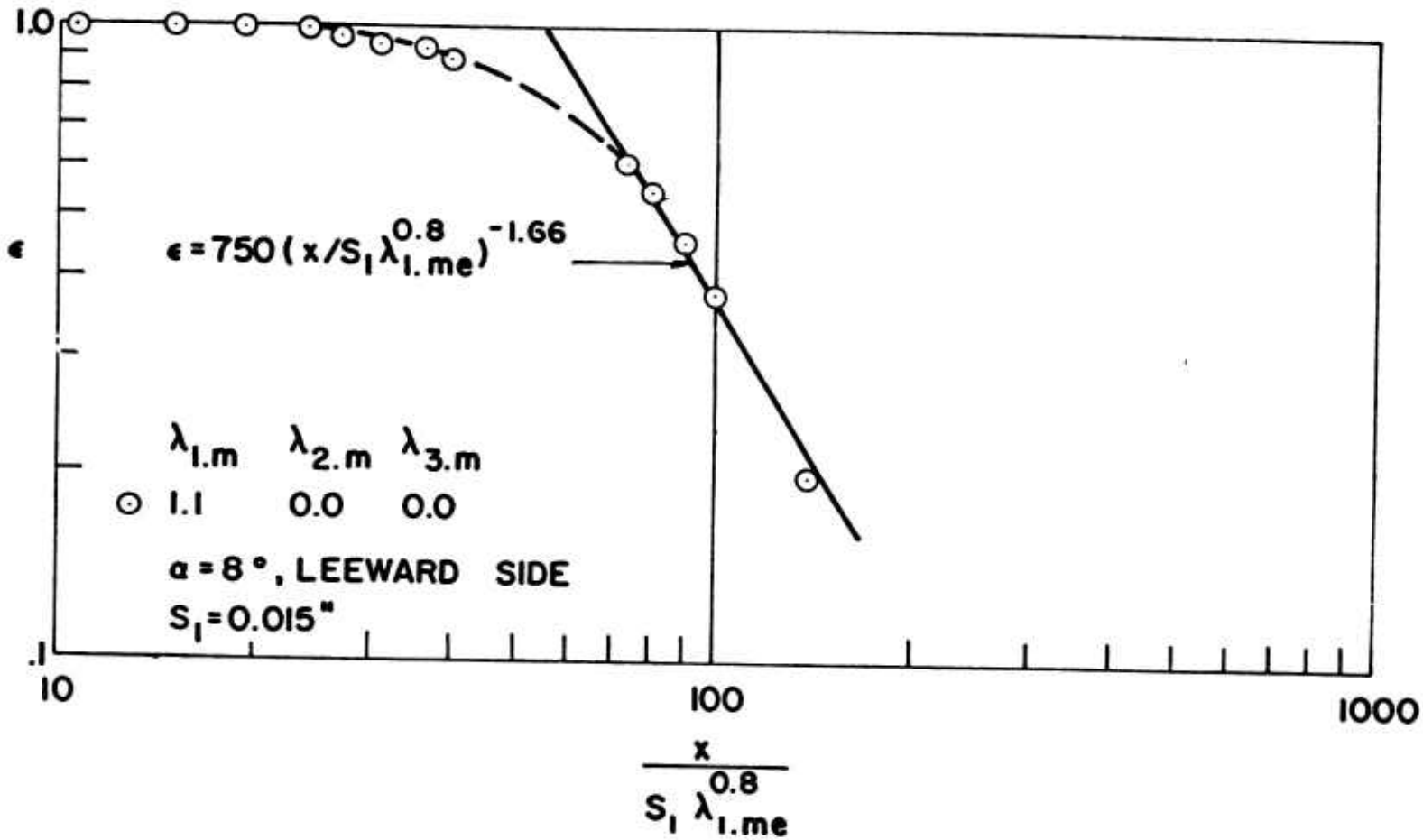

Fig. 51 Correlation of the experimental film cooling effectiveness, lst slot downstream injection $\alpha = 8^{o}$, leeward side

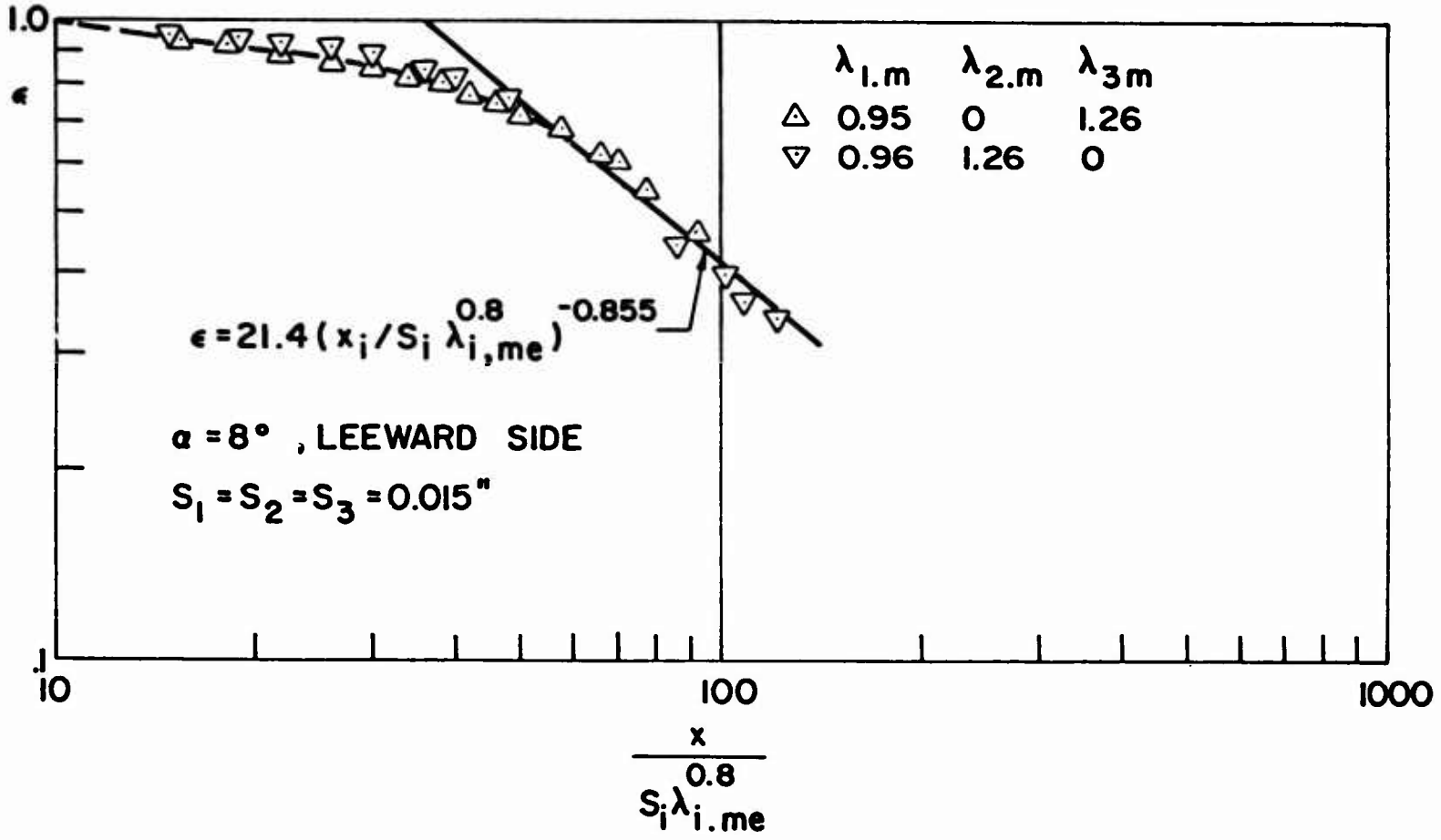

Fig. 52 Correlation of the experimental film cooling effectiveness, 2 slot downstream injection, $\alpha = 8^{\circ}$ leeward side

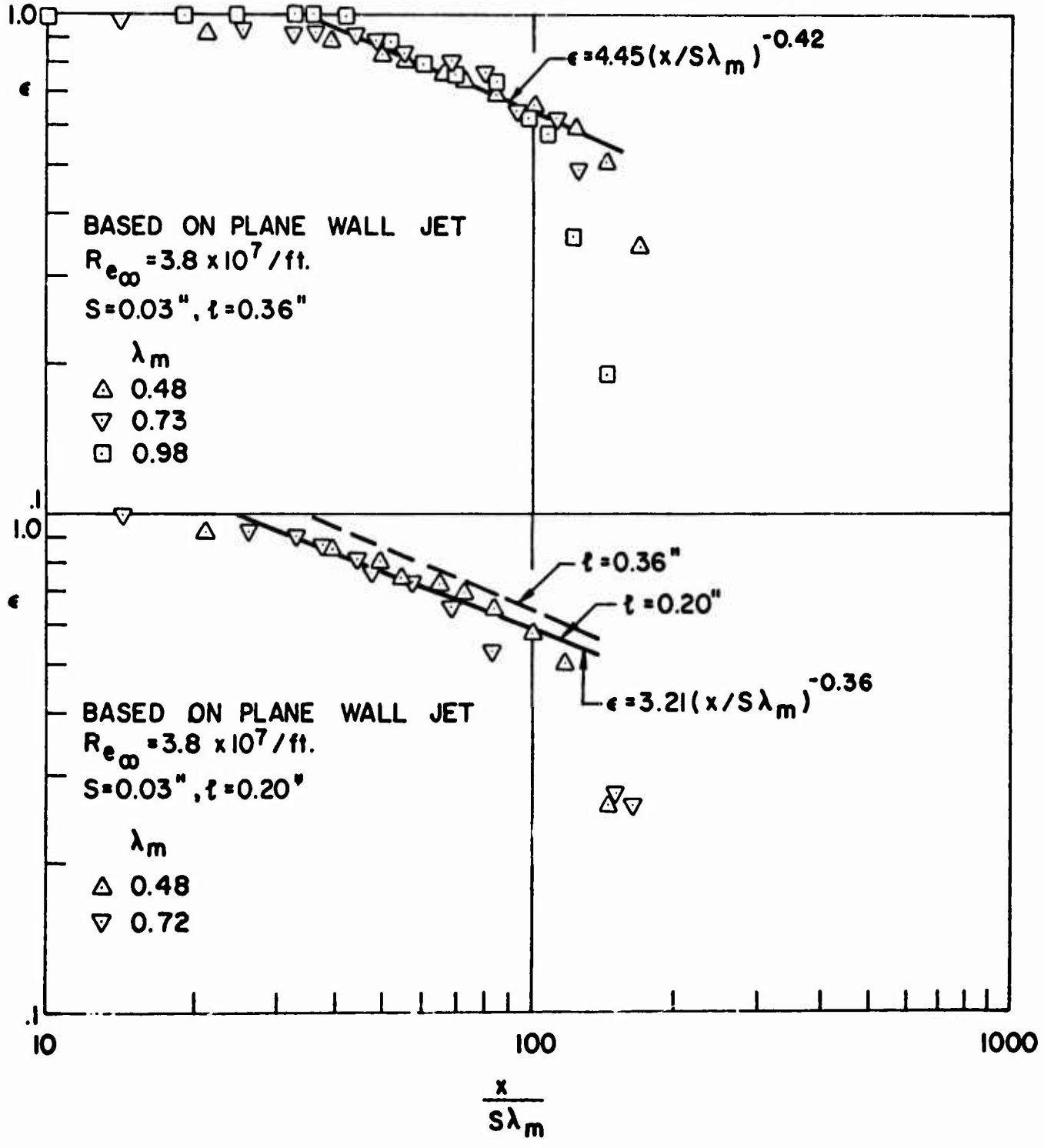

Fig. 53 Correlation of the experimental film cooling effectiveness, upstream injection, plane wall jet theory

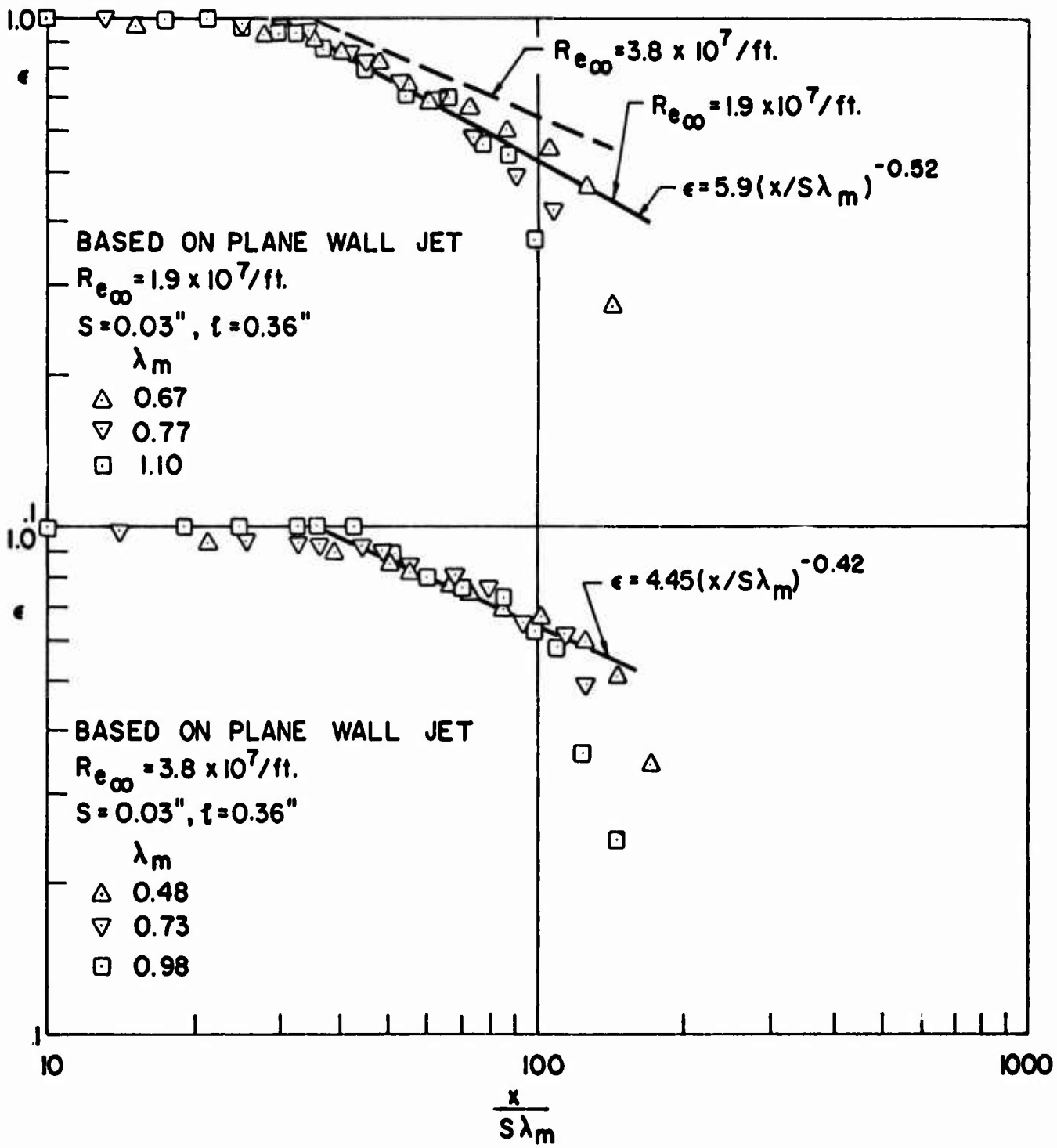

Fig. 54 Correlations of the experimental film cooling effectiveness, upstream injection, plane wall jet theory

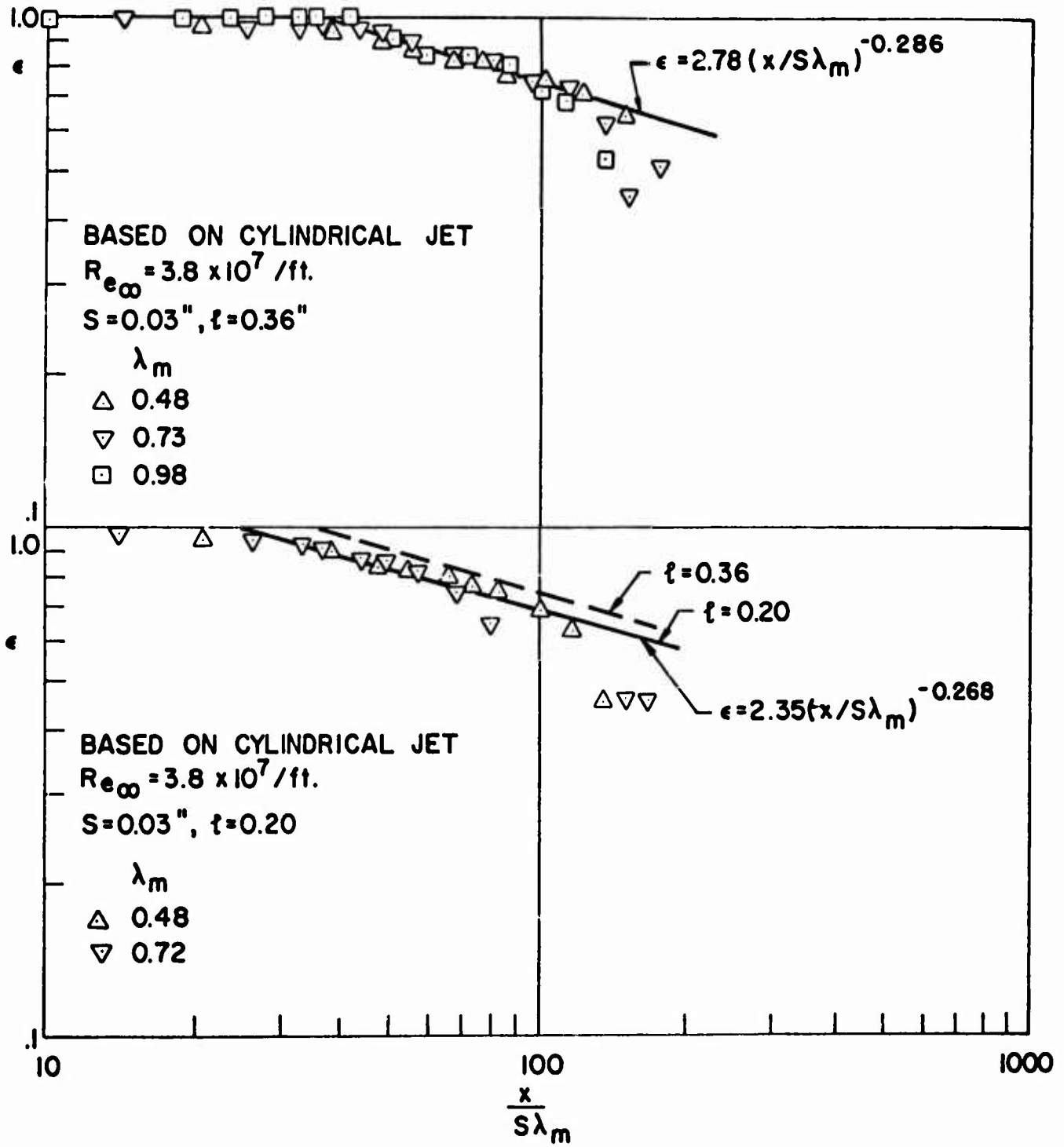

Fig. 55 Correlation of the experimental film cooling effectiveness, upstream injection, cylindrical jet theory

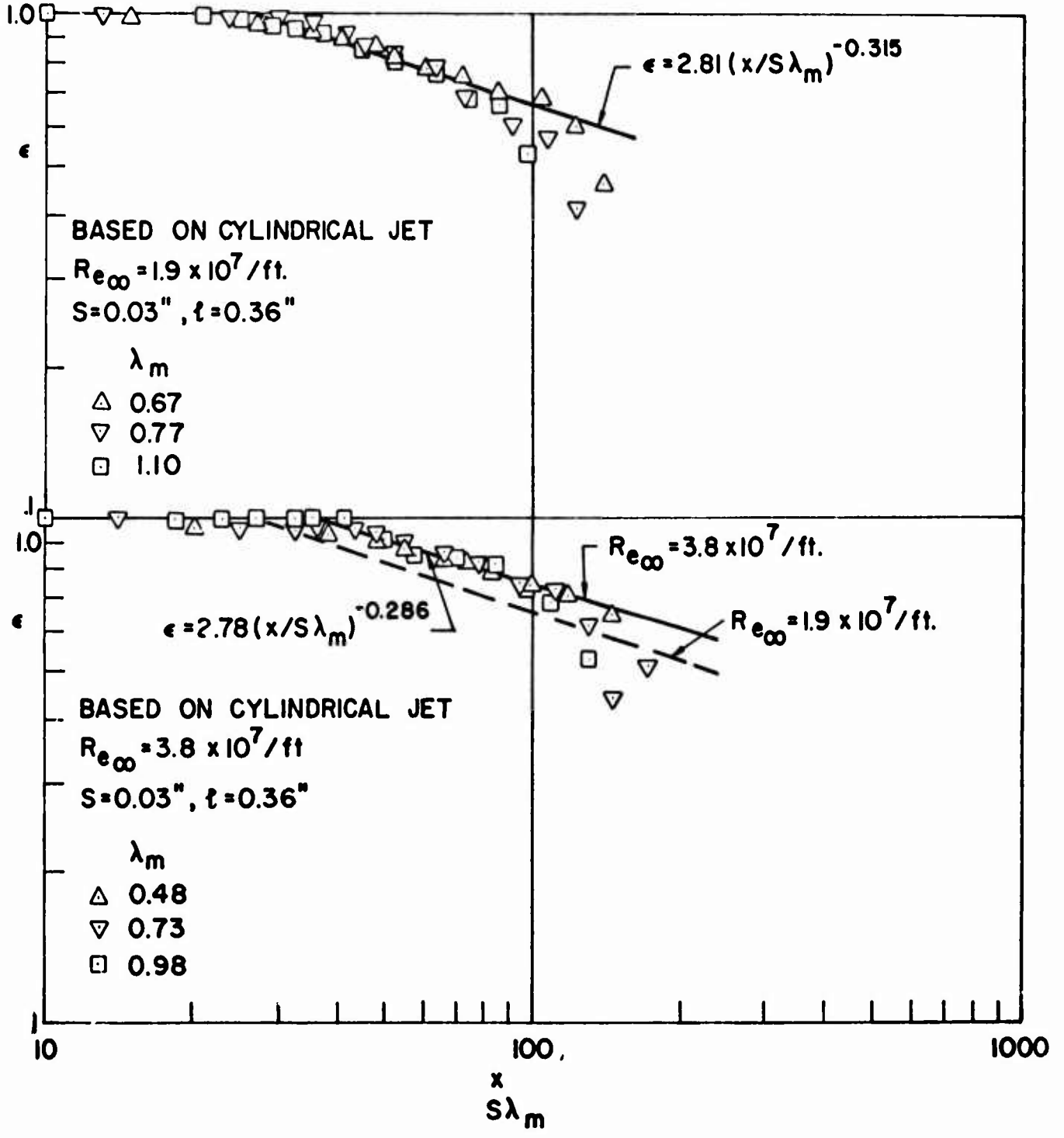

Fig. 56 Correlation of the experimental film cooling effectiveness, upstream injection, cylindrical jet theory

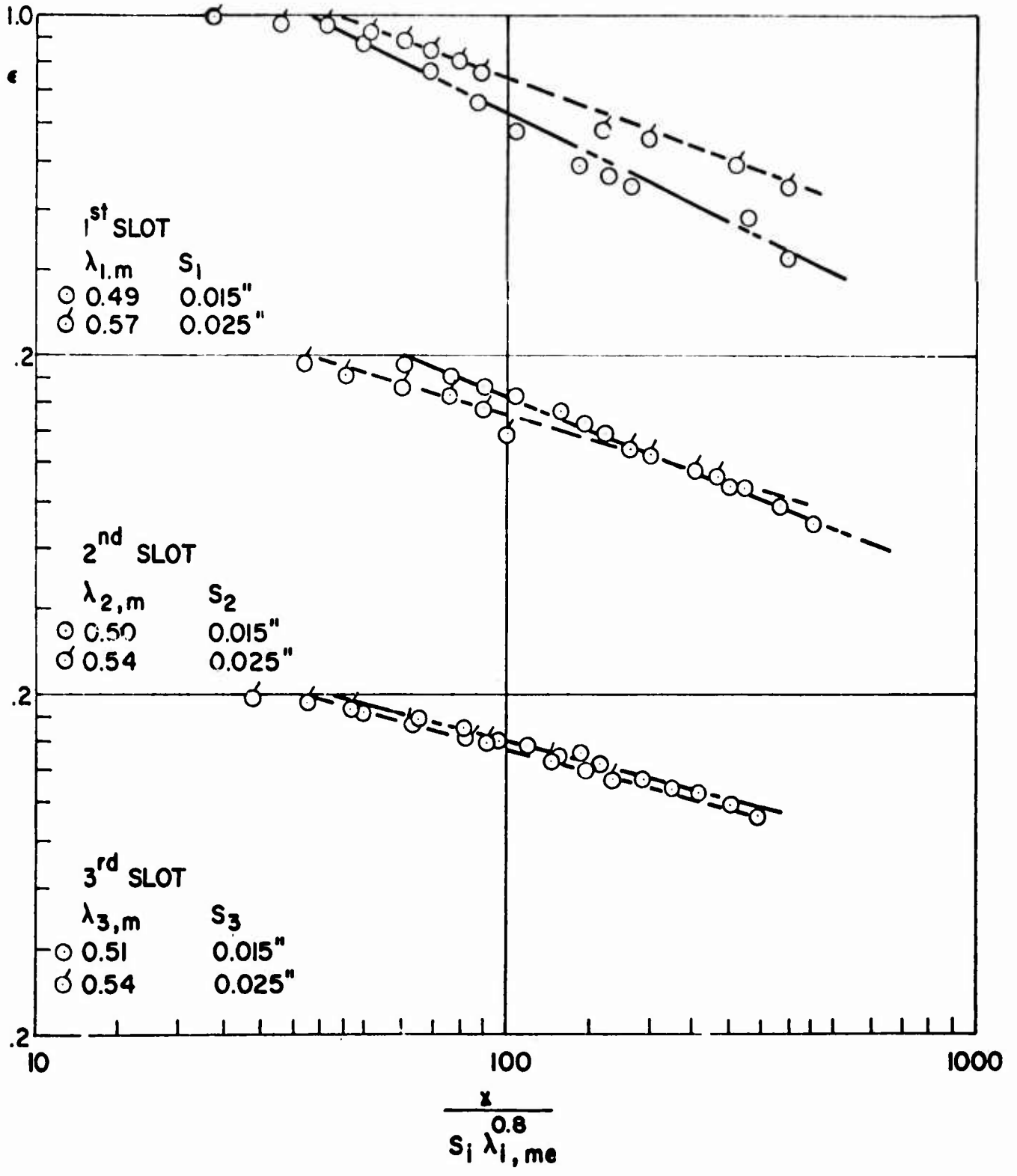

Fig. 57 Effect of the slot heights to the downstream film cooling effectiveness

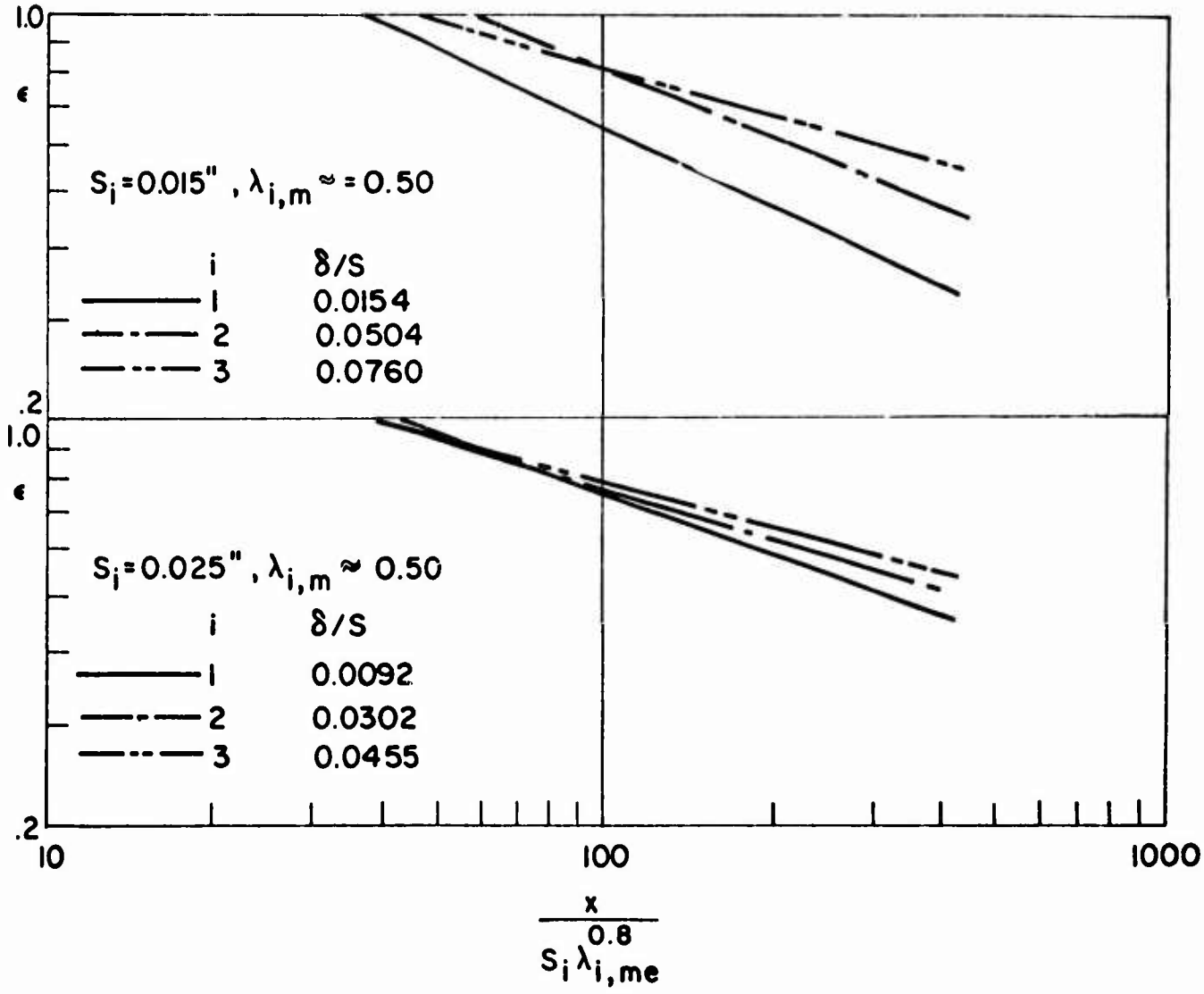

Fig. 58 Effect of the boundary layer thickness at the injection slot to the film cooling effectiveness

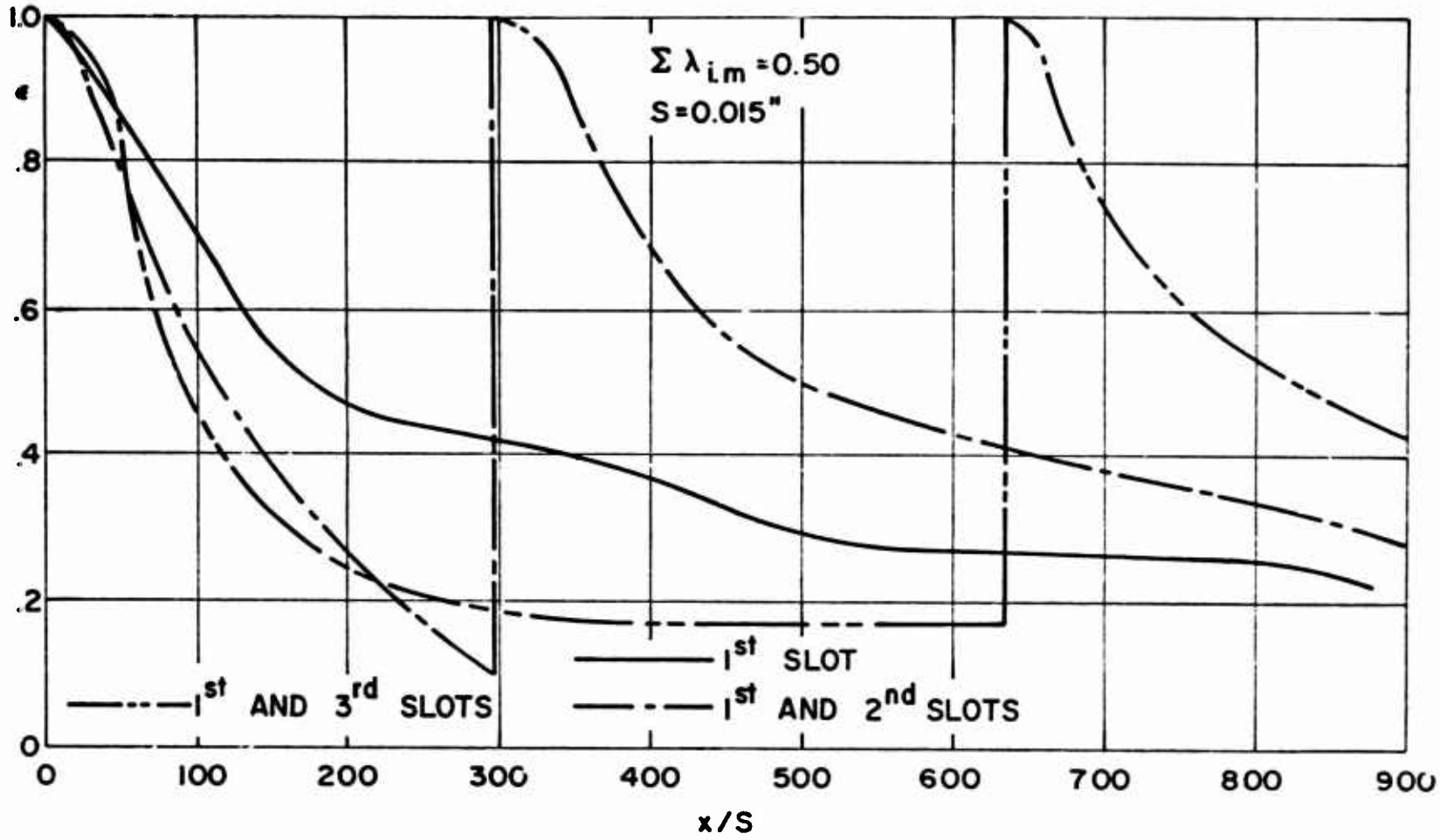

Fig. 59 Comparison of effectiveness between single and multiple slot downstream injection with the same injection mass flow rate

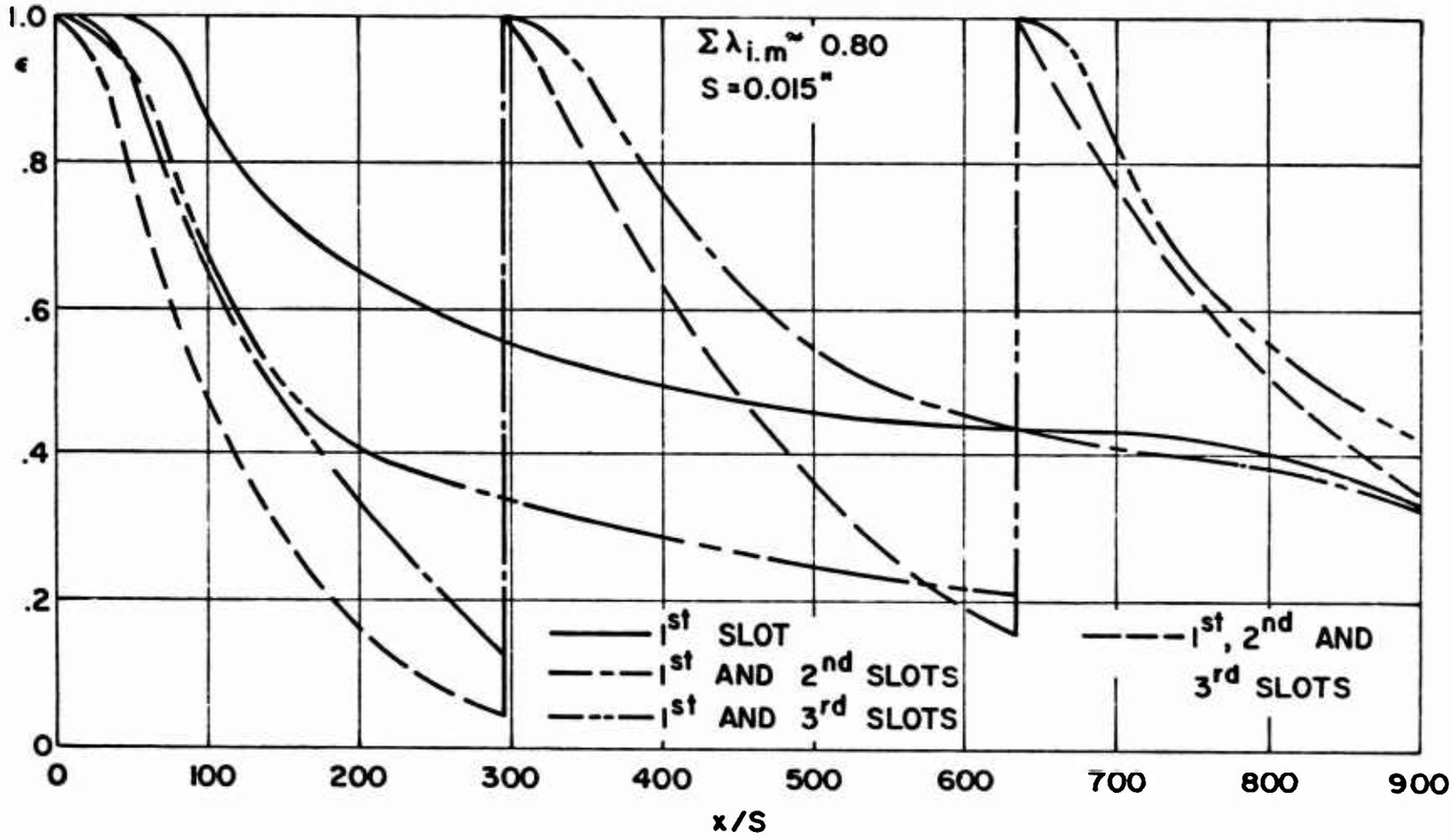

Fig. 60 Comparison of effectiveness between single and multiple slot downstream injection with the same injection mass flow rate

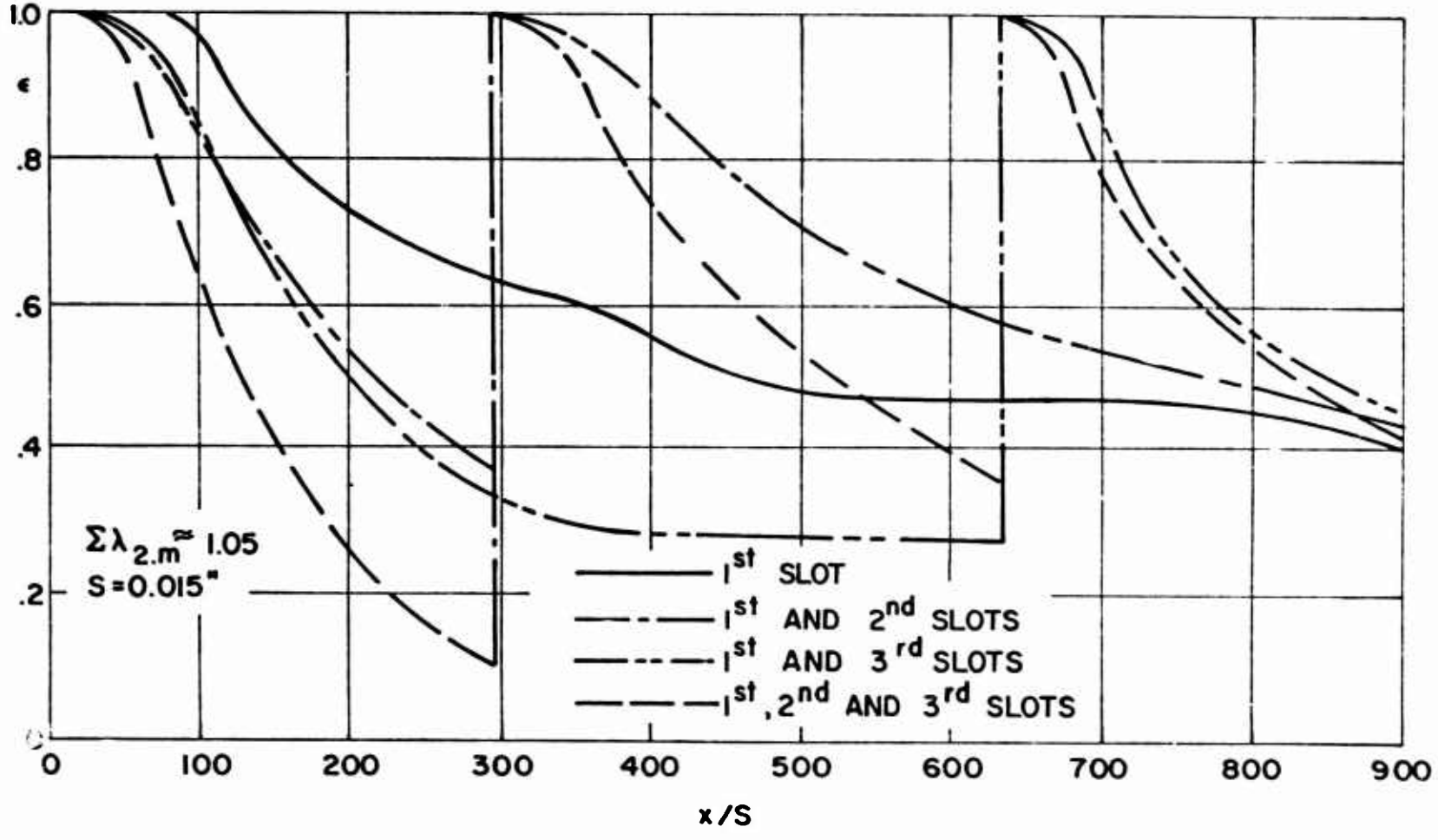

Fig. 61 Comparison of effectiveness between single and multiple slot downstream injection with the same injection mass flow rate

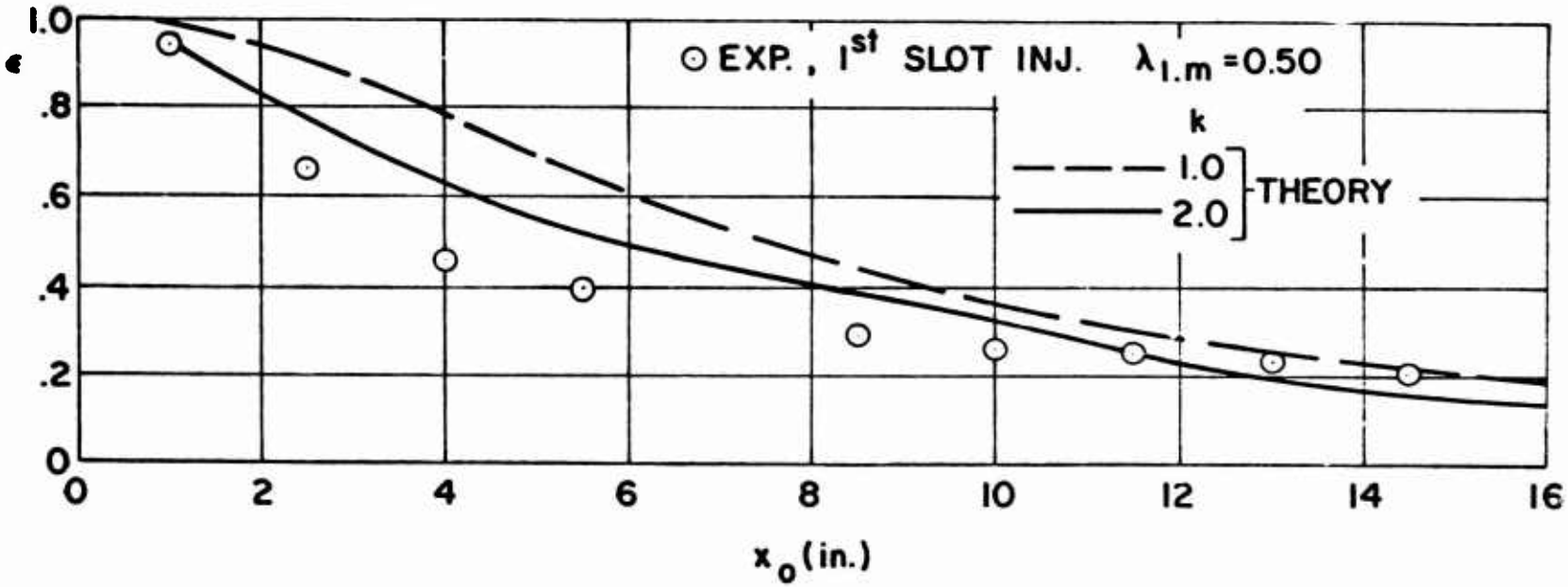

Fig. 62 Comparison of the downstream injection effectiveness between theory and experiment, $\alpha = 0^{\circ}$, 1st slot injection

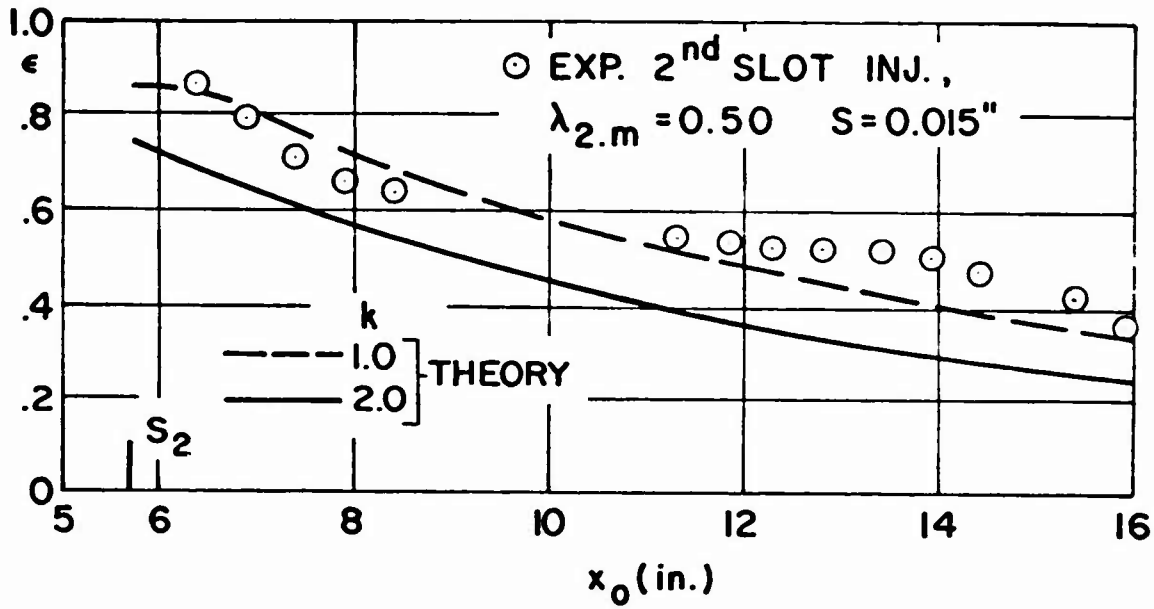

Fig. 63 Comparison of the downstream injection effectiveness between theory and experiment, $\alpha = 0^{\circ}$, 2nd slot injection

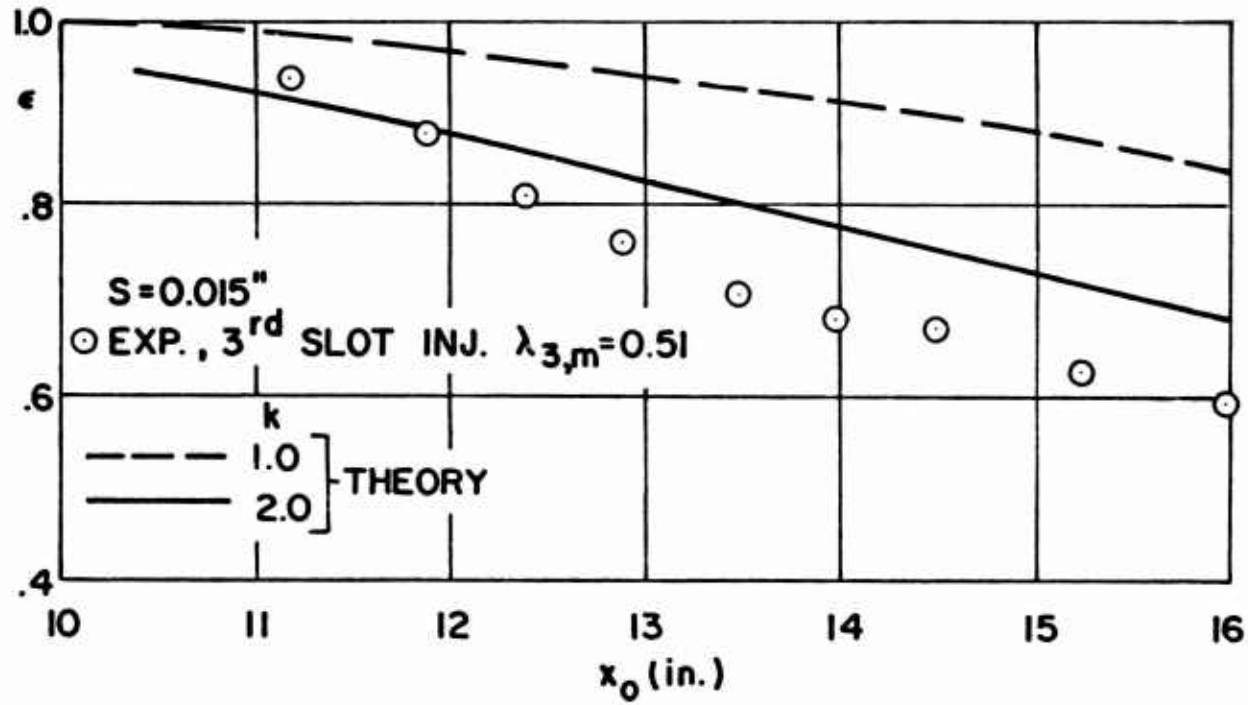

Fig. 64 Comparison of the downstream injection effectiveness between approximate theory and experiment, $\alpha = 0^{\circ}$, 3rd slot injection

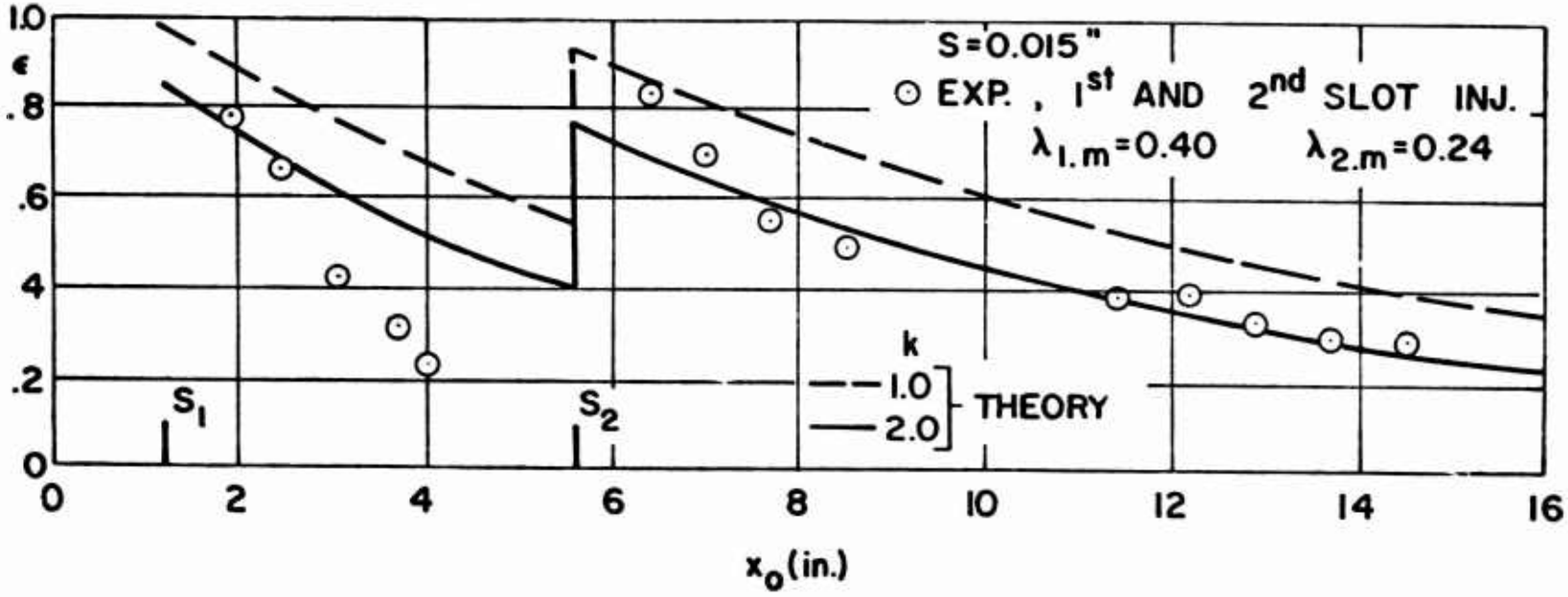

Fig. 65 Comparison of the downstream injection effectiveness between theory and experiment, $\alpha = 0^{\circ}$, 1st and 2nd slot injection

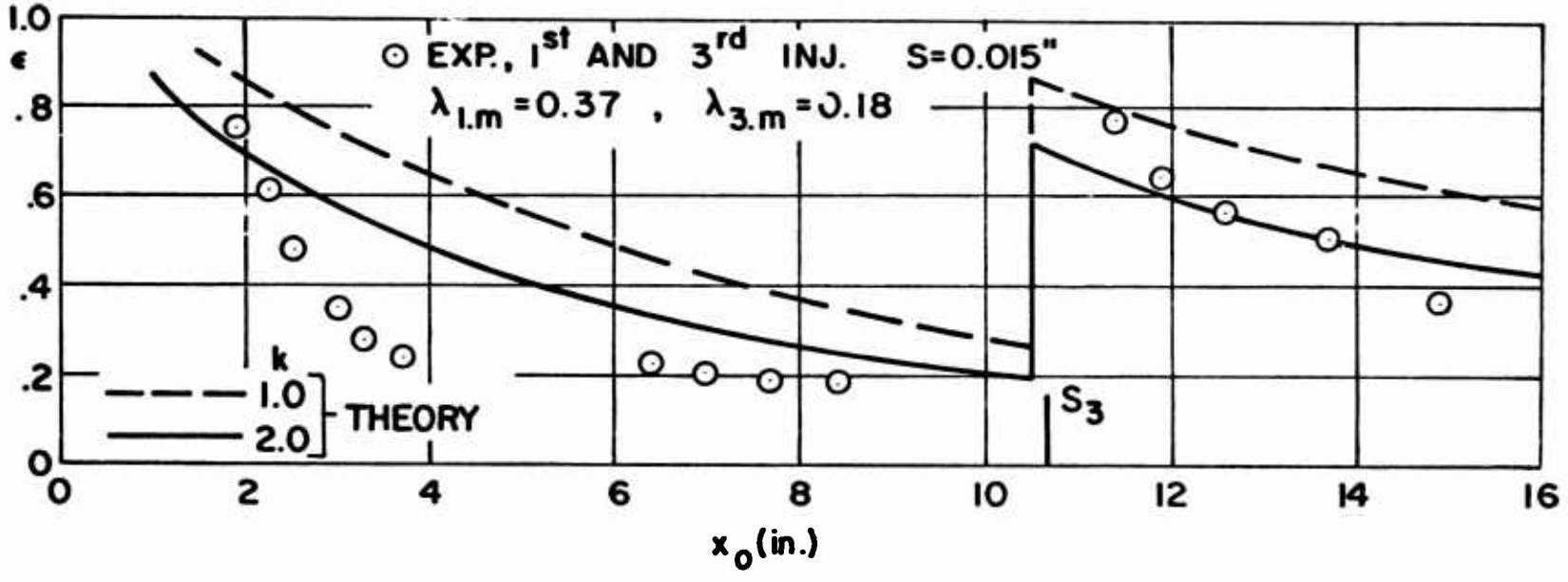

Fig. 66 Comparison of the downstream injection effectiveness between approximate theory and experiment, $\alpha = 0^{\circ}$, 1st and 3rd slot injection

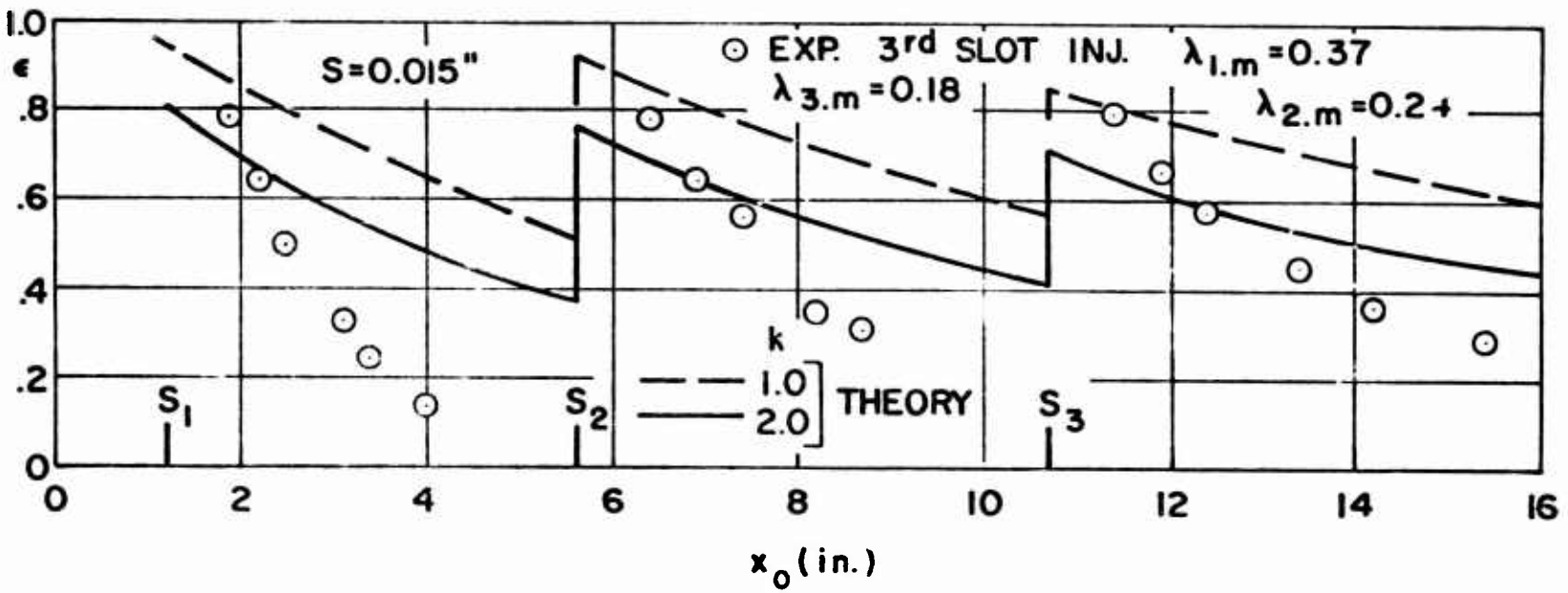

Fig. 67 Comparison of the downstream injection effectiveness between approximate theory and experiment, $\alpha = 0^{\circ}$, three slot injection

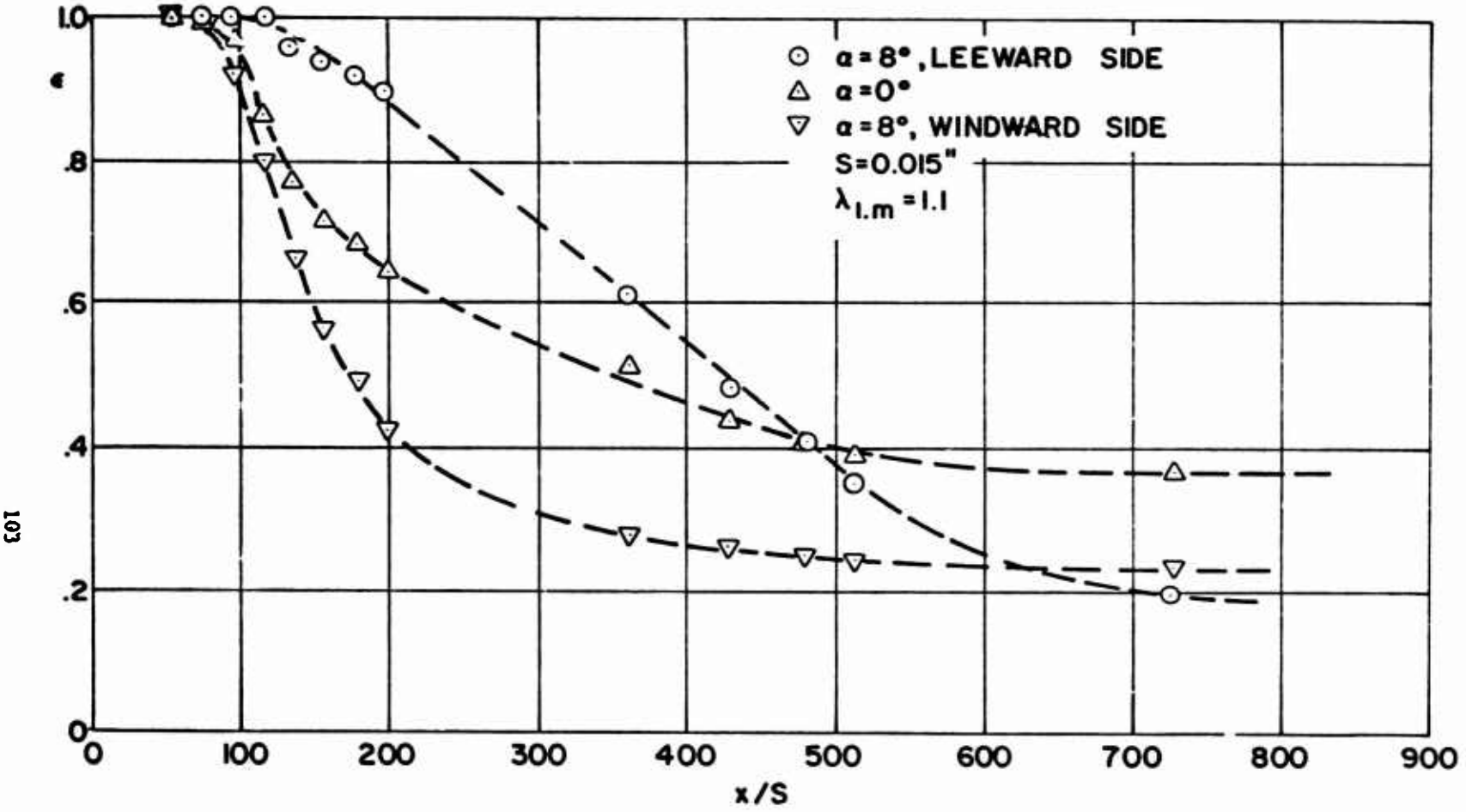

Fig. 68 Comparison of the effectiveness due to 1st slot downstream injection, with and without angle of attack

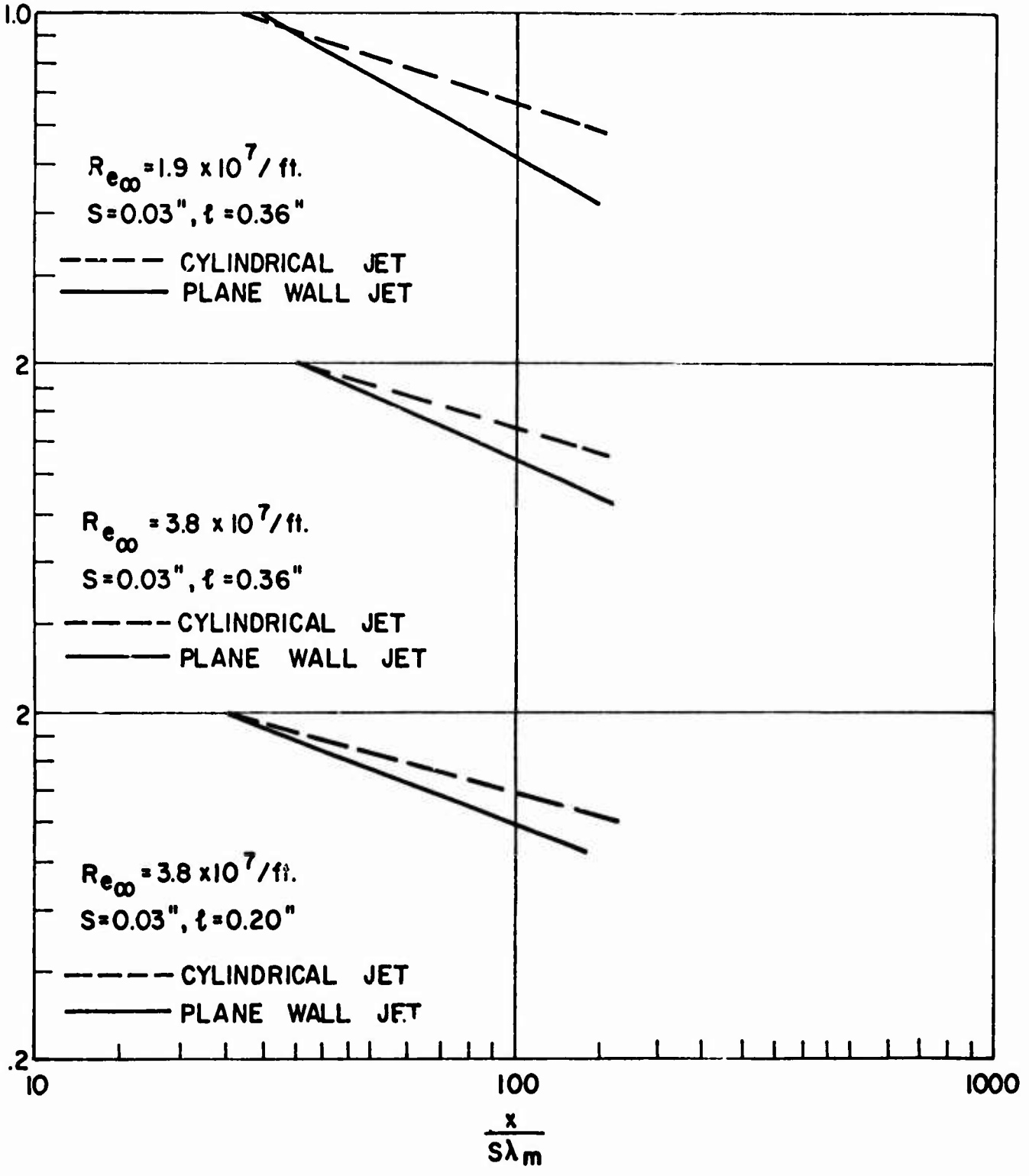

Fig. 69 Comparison of the upstream injection film cooling effectiveness correlations between plane wall jet and cylindrical jet

REFERENCES

1. Hatch, J.E. and Papell, S.S., "Use of a Theoretical Flow Model to Correlate Data for Film Cooling or Heating an Adiabatic Wall by Tangential Injection of Gases of Different Fluid Properties," NASA TN D-130, 1959.

2. Seban, R.A., "Heat Transfer and Effectiveness for a Turbulent Boundary Layer with Tangential Fluid Injection," Journal of Heat Transfer, Vol. 82, pp. 303-312, 1960

3. Papell, S.S. and Trout, A.M., "Experimental Investigation of Air Film Cooling Applied to an Adiabatic Wall by Means of An Axially Discharging Slot," NASA TN D-9, 1959.

4. Hartnett, J.P., Birkebak, R.C., and Eckert, E.R.G., "Velocity Distributions, Temperature Distributions, Effectiveness and Heat Transfer for Air Injected through a Tangential Slot into a Turbulent Boundary Layer," Journal of Heat Transfer, Vol. 83, pp. 293-306, 1961

5. Chin, J.H. et al., "Film Cooling with Multiple Slots and Louvers," Journal of Heat Transfer, Vol. 83, pp. 281-292, 1961.

6. Jubasz, A.J. and Marek, C.J., "Combustor Liner Film Cooling in the Presence of High Free Stream Turbulence," NASA TN D-6360, 1971.

7. Parthasarathy, K. and Zakkay, V., "An Experimental Investigation of Turbulent Slot Injection at Mach 6," AIAA Journal, Vol. 8, No. 7, pp. 1302-1307, July 1970.

8. Miyazawa, M., "An Experimental Investigation of Film Cooling at Mach 6," Masters Thesis, New York University.

9. Cary, A.M. and Hefner, J.N., "Film Cooling Effectiveness and Skin Friction in Hypersonic Turbulent Flow," AIAA Journal, Vol. 10, pp. 1188-1193, 1973.

10. Zakkay, V., Wang, C.R., and Miyazawa, M., "Effect of Adverse Pressure Gradient on Film Cooling Effectiveness," NYU Contract Report, 1972.

11. Fox, H. and Hoydysh, W.G., "An Experimental and Analytical Investigation of Multiple Slot Cooling," NYU Contract Report.

12. Piva, R., "Leading Edge Cooling by Upstream Injection," NASA CR-111965, 1971.

13. Gorman, R., "Shock Generators in the Hypersonic Turbulent Boundary Layer," ARL 67-0186, AD 661992, New York University, September 1967.

14. Manian, V.S., McDonald, T.W., and Besant, R.W., "Heat Transfer Measurements in Cylindrical Wall Jets," Int. Journal of Heat Mass Transfer, Vol. 12, pp. 673-679, 1969.

15. Seban, R.A. and Back, L.H., "Velocity and Temperature Profile in a Wall Jet," Int. Journal of Heat Mass Transfer, Vol. 3, pp. 255-265, 1961.

16. Reshotko, E. and Tucker, M., "Approximate Calculation of the Compressible Turbulent Boundary Layer with Heat Transfer and Arbitrary Pressure Gradient," NACA TN-4154, December 1957.

17. Stollery, J.L. and El-Ehwany, A.A.M., "A Note on the Use of Boundary Layer Model for Correlating Film Cooling Data," Int. Journal of Heat Mass Transfer, Vol. 8, pp. 55-65, 1965.

18. Persh, J. and Lee, R., "Tabulation of Compressible Turbulent Boundary Layer Parameters," NAVORD Report 4282, May 1956.

19. Zakkay, V. and Callahan, C.J., "Laminar, Transitional, and Turbulent Heat Transfer to a Cone-Cylinder-Flare Body at Mach 8," Journal of the Aerospace Science, Vol. 29, No. 12, pp. 1403-1420, December 1962.

20. Kleinstein, G., "An Approximate Analysis of the Slot Injection of a Gas in Laminar Flow," Quarterly of Applied Mathematics; also ARL Report 51, AD# 257808, 1961.

21. Fox. H. and Libby, P.A., "Helium Injection into the Boundary Layer at an Axisymmetric Stagnation Point," Journal of the Aerospace Sciences, Vol. 29, No. 8, pp. 921-933, 1962.

22. Seban, R.A., "Effects of Initial Boundary Layer Thickness on a Tangential Injection Slot," Transaction of ASME, Series C; Journal of Heat Transfer, Vol. 82, pp. 392-393, November 1960.

23. Klaimon, J.H., "Bow Shock Correlation for Slightly Blunted Cones," Journal of the Aerospace Sciences, Vol. 1, No. 2, 1963.